

PIPELINE INTEGRITY FOR GROUND MOVEMENT HAZARDS

***USE OF PIPELINE GEOMETRY MONITORING
TO ASSESS PIPELINE CONDITION***

Report to:

United States Department of Transportation
Pipeline and Hazardous Materials Safety Administration
Office of Pipeline Safety

By:

James D. Hart & Nasir Zulfiqar
SSD, Inc.
6119 Ridgeview Court, Suite 400
Reno, Nevada, 89519
Phone: 775-770-1126
Email: info@ssdinc.com

Carl H. Popelar
Popelar Mechanics
602 Stone Wood Dr.
San Antonio, TX 78216
Phone: 210-402-1580
Email: cpopelar@earthlink.net

December 3, 2008

EXECUTIVE SUMMARY

Large lateral or transverse movements of buried pipelines in regions of unstable soil or natural hazards, including settlement, landslides, fault creep, earthquake ground displacement, frost heave, thaw settlement, long wall mining subsidence, other subterranean and subsea phenomena, etc., can induce significant strains in addition to those experienced by the pipeline under normal operating conditions. Design codes offer little in the way of guidance for evaluating the state of strain induced in the pipeline from such movements and typical codified analysis procedures, usually based upon elastic behavior and infinitesimal strains, are of limited use. Current practice for making a structural integrity assessment of a laterally displaced pipeline based upon evaluating only the induced flexural strain is often non-conservative because the induced longitudinal extensional strain can be on the same order magnitude as the flexural strain.

Specialized in-line inspection (ILI) tools, often referred to as geometry pigs, are used to map the centerline of a pipeline. Geometry pigs are capable of measuring the pipe's centerline orientation (pitch and azimuth) and odometer distance from which the northing, easting and elevation coordinates and the vertical, horizontal and resultant curvature and the induced flexural strains can be deduced. Heretofore, no method exists for deducing from geometry pig measurements the induced extensional strain which must be superimposed upon the flexural strain and operating strain to establish the total strain demand. The objective of the research reported herein is to develop and assess the efficacy of a method for estimating the longitudinal or axial, extensional and flexural strains in a pipeline deformed by lateral ground displacement directly from ILI data or other measurements of pipeline displacement, and provide a basis for optimizing the design of *in-situ* geo-hazard monitoring programs and targeted ILI.

In the research reported herein, an algorithm is developed for deducing the longitudinal or axial strain from geometry pig measurements of a laterally displaced pipeline. The development is limited to those lateral displacements of the pipeline that results in a predominantly transverse loading; i.e., the induced transverse component of the loading is much greater than its axial component. The emphasis is upon evaluating inelastic straining that accompanies large lateral displacement of the pipeline. The induced extensional strain is found to vary linearly with the change in curvature of the pipeline. The validity of the approach is established through favorable comparisons of the predictions for the extensional strains with those determined from buried pipeline finite element simulations of various displaced pipe configurations, pipe geometries and loading amplitudes. Since the algorithm relies only upon measurements of the geometry of the displaced pipeline, it is independent of the pipe's and soil's material properties, pipe-soil interaction and the loading conditions.

The efficacy of the algorithm is demonstrated by performing a large matrix of finite element simulations of displaced pipelines of different geometries subjected to block subsidence, landslides intersecting the pipeline at varying angles, fault crossings at different angles and different loading states, and comparing the analytical strains with the strains deduced from "digital pig" measurements of the curvature of deformed pipeline. In this regard the finite element simulations serve the role of surrogate geometry pig measurements. These comparisons are used to establish the resolution of the change in curvature measurement required of a geometry pig to produce a reliable estimate for the longitudinal strain in a displaced pipeline. An error analysis is also performed to establish the relative error as a function of the curvature measurement gage length, a characteristic feature length and the abruptness of the displaced shape of the pipeline. A corollary of this analysis is an improved estimate for the strain when measurements of the curvature are established for two different gage lengths.

A discussion of measurement considerations for incorporating the developed technology into pipeline geometry measurement tool data processing is presented. Emphasis is placed upon in-line methods of measurements since it appears that this method holds the promise for measuring the centerline curvature

of the pipeline with sufficient resolution. Critical to establishing the curvature is the gage length over which numerical differentiation of the pipeline orientation is performed—too large of a gage length underestimates the curvature. Establishing a reliable estimate for the curvature is further complicated by noise in the geometry pig data signals resulting from pipeline irregularities, girth welds, etc. Various means for filtering the signal and the potential pitfalls are discussed. For example, one way that is often used to smooth out the data is to select a curvature calculation gage length that is several multiples of the pipe diameter (longer than the characteristic length of the noise features), provided that the gage length does not degrade the accuracy of the curvature measurement. Therefore, care must be exercised when selecting an appropriate gage length and it may even be appropriate to evaluate the curvature using two different gage lengths. A baseline survey of the “as built” pipeline is required since the algorithm is based upon changes in geometry of the pipeline. The baseline survey can also be used to identify and eliminate measurement noise traceable to pipeline irregularities. Interfacing the axial strain algorithm with the monitoring technologies of geometry pig vendors is discussed.

TABLE OF CONTENTS

	Page
EXECUTIVE SUMMARY	i
LIST OF TABLES	iv
LIST OF FIGURES	v
1. INTRODUCTION	1
2. AXIAL STRAIN DEVELOPMENT	2
3. VALIDATION OF EXTENSIONAL STRAIN ALGORITHM.....	4
3.1 Introduction	4
3.2 Preliminary Validation of the Strain Algorithm	4
3.3 Validation of the Strain Algorithm Considering “Pigged” Curvature Measures.....	6
3.4 Preliminary Evaluation of the Strain Algorithm on Pipeline Configurations Containing Bends.....	9
3.5 Evaluation of Strain Algorithm	9
4. MEASUREMENT CONSIDERATIONS.....	13
4.1 Overview and Categorization of Existing Pipe Geometry Monitoring Technology	13
4.2 Discussion of In-Line Methods	13
4.3 Interface Axial Strain Algorithm with Monitoring Technology.....	16
4.4 Assessment of Measurement Error.....	17
4.4.1 Theoretical Error Analysis.....	17
4.4.2 Evaluation of Improved Strain Calculations	21
4.5 Discussion of Noise in Geometry Pig Data	23
4.6 Importance of a Baseline Survey.....	24
4.7 Survey to Survey Comparisons	24
5. CONCLUSIONS.....	26
6. RECOMMENDED FURTHER RESEARCH	28
7. REFERENCES	29

LIST OF TABLES

		Page
Table 3.1	Pipe-Soil Interaction Analysis Cases and Results - NPS8 Pipe.....	31
Table 3.2	Pipe-Soil Interaction Analysis Cases and Results - NPS16 Pipe.....	32
Table 3.3	Pipe-Soil Interaction Analysis Cases and Results - NPS24 Pipe.....	34
Table 3.4	Pipe-Soil Interaction Analysis Cases and Results - NPS36 Pipe.....	35
Table 3.5	Pipe-Soil Interaction Analysis Cases and Results NPS48 Pipe.....	36
Table 3.6	Pipe-Soil Interaction Analysis Cases and Results - NPS10 Pipe.....	37

LIST OF FIGURES

		Page
Figure 3.1	Pipe Strain Profiles for State A: 4' of Subsidence over 100' Long Block Profile, D=16", 6' of Sand Cover.....	39
Figure 3.2	Pipe Strain Profiles for State B: 7' of Subsidence over 100' Long Block Profile, D=16", 6' of Sand Cover.....	39
Figure 3.3	Pipe Strain Profiles for State A: 6' of Right Lateral Fault Offset Beta=90 deg, D=16", 6' of Sand Cover	40
Figure 3.4	Pipe Strain Profiles for State B: 9' of Right Lateral Fault Offset Beta=90 deg, D=16", 6' of Sand Cover	40
Figure 3.5	Plan View of Pipeline Crossing a Horizontal Landslide: Schematic Illustration of Different Crossing Angles	41
Figure 3.6	Plan View of Pipelines Crossing a Right Lateral, Strike-Slip Fault Schematic Illustration of Effect of Pipeline Fault Crossing Angle β	42
Figure 3.7	Overview of Digital Pigging Concept	43
Figure 3.8	First Pass Calculations to Compute Profile of Pig Pitch Angle $\theta(S)$ Based on Elevation Change (ΔY) Over Length of Pig	43
Figure 3.9	Second Pass Calculations to Compute Profile of Vertical Curvature $\Psi(S)$ Based on Pitch Angle Change ($\Delta\theta$) Over Gage Length	44
Figure 3.10(a)	8-inch Pipe: Comparison of Governing Normalized Strains - State A.....	45
Figure 3.10(b)	8-inch Pipe: Comparison of Governing Normalized Strains - State B.....	45
Figure 3.11(a)	16-inch Pipe: Comparison of Governing Normalized Strains - State A.....	46
Figure 3.11(b)	16-inch Pipe: Comparison of Governing Normalized Strains - State B.....	46
Figure 3.12(a)	24-inch Pipe: Comparison of Governing Normalized Strains - State A.....	47
Figure 3.12(b)	24-inch Pipe: Comparison of Governing Normalized Strains - State B.....	47
Figure 3.13(a)	36-inch Pipe: Comparison of Governing Normalized Strains - State A.....	48
Figure 3.13(b)	36-inch Pipe: Comparison of Governing Normalized Strains - State B.....	48
Figure 3.14(a)	48-inch Pipe: Comparison of Governing Normalized Strains - State A.....	49
Figure 3.14(b)	48-inch Pipe: Comparison of Governing Normalized Strains - State B.....	49
Figure 3.15(a)	NPS 8 Cases, Exact vs. Deduced with $L_{gage} = L_{pig}$	50

LIST OF FIGURES (Continued)

	Page
Figure 3.15(b) NPS 8 Cases, Exact vs. Deduced with $L_{gage} = 3D$	50
Figure 3.16(a) NPS 16 Cases, Exact vs. Deduced with $L_{gage} = L_{pig}$	51
Figure 3.16(b) NPS 16 Cases, Exact vs. Deduced with $L_{gage} = 3D$	51
Figure 3.17(a) NPS 24 Cases, Exact vs. Deduced with $L_{gage} = L_{pig}$	52
Figure 3.17(b) NPS 24 Cases, Exact vs. Deduced with $L_{gage} = 3D$	52
Figure 3.18(a) NPS 36 Cases, Exact vs. Deduced with $L_{gage} = L_{pig}$	53
Figure 3.18(b) NPS 36 Cases, Exact vs. Deduced with $L_{gage} = 3D$	53
Figure 3.19(a) NPS 48 Cases, Exact vs. Deduced with $L_{gage} = L_{pig}$	54
Figure 3.19(b) NPS 48 Cases, Exact vs. Deduced with $L_{gage} = 3D$	54
Figure 3.20(a) Slope of Regression Line with Zero Intercept, State A	55
Figure 3.20(b) Slope of Regression Line with Zero Intercept, State B	55
Figure 3.21 Feature Length vs. Pipe Diameter	56
Figure 4.1(a) Extensional Strain Profiles for State B: 9' of Right Lateral Fault Offset Beta=90 deg, D=16", 6' of Sand Cover – (Zoomed View).....	57
Figure 4.1(b) Extensional Strain Profiles for State B: 9' of Right Lateral Fault Offset Beta=90 deg, D=16", 6' of Sand Cover	57
Figure 4.2(a) 8-inch Pipe: Comparison of Governing Normalized Strains - State A.....	58
Figure 4.2(b) 8-inch Pipe: Comparison of Governing Normalized Strains - State B.....	58
Figure 4.3(a) 16-inch Pipe: Comparison of Governing Normalized Strains - State A.....	59
Figure 4.3(b) 16-inch Pipe: Comparison of Governing Normalized Strains - State B.....	59
Figure 4.4(a) 24-inch Pipe: Comparison of Governing Normalized Strains - State A.....	60
Figure 4.4(b) 24-inch Pipe: Comparison of Governing Normalized Strains - State B.....	60
Figure 4.5(a) 36-inch Pipe: Comparison of Governing Normalized Strains - State A.....	61
Figure 4.5(b) 36-inch Pipe: Comparison of Governing Normalized Strains - State B.....	61
Figure 4.6(a) 48-inch Pipe: Comparison of Governing Normalized Strains - State A.....	62

LIST OF FIGURES (Continued)

		Page
Figure 4.6(b)	48-inch Pipe: Comparison of Governing Normalized Strains - State A.....	62
Figure 4.7(a)	Exact Strain Versus Improved Strain State A.....	63
Figure 4.7(b)	Exact Strain Versus Improved Strain State B.....	63
Figure 4.8(a)	Slope of Regression Line with Zero Intercept, State A.....	64
Figure 4.8(b)	Slope of Regression Line with Zero Intercept, State B.....	64
Figure 4.9(a)	Properties of Noise (Unfiltered Minus Filtered) Signal in NPS 48 Pipeline.....	65
Figure 4.9(b)	Properties of Noise (Unfiltered Minus Filtered) Signal in NPS 48 Pipeline.....	65
Figure 4.9(c)	Properties of Noise (Unfiltered Minus Filtered) Signal in NPS 48 Pipeline.....	65
Figure 4.10(a)	Properties of Noise (Unfiltered Minus Filtered) Signal in NPS 10 Pipeline.....	66
Figure 4.10(b)	Properties of Noise (Unfiltered Minus Filtered) Signal in NPS 10 Pipeline.....	66
Figure 4.10(c)	Properties of Noise (Unfiltered Minus Filtered) Signal in NPS 10 Pipeline.....	66

1. INTRODUCTION

Strains induced in buried pipelines from large transverse or lateral movements associated with unstable soil regions or resulting from natural hazards can be significant when acting in concert with normal operating conditions; e.g., due to internal pressure, temperature differential, etc. Such movements that result in large lengths of a pipeline being displaced from its original position include landslides, settlement, fault creep, earthquake ground displacement, insufficient cover (buoyancy), frost heave, thaw settlement, subsidence due to long wall mining or other subterranean operations, etc. Proper evaluation of the pipeline straining produced by large transverse movements of pipes is an important consideration within the pipeline industry for safe, uninterrupted operation of its pipelines. Modern pipeline design codes provide little guidance with respect to procedures for evaluating pipelines subjected to significant levels of pipeline displacement and typical “codified” analysis methods, which are based on the assumptions of elastic behavior and infinitesimal strains, are of limited use for these applications.

The geometry of pipelines located in potential ground movement zones is often inspected using specialized in-line inspection (ILI) tools, sometimes referred to as geometry pigs. The more sophisticated geometry tools include high accuracy strap-down inertial navigation systems, odometers, calipers and girth weld locators. These geometry pigs are capable of providing pipe centerline northing, easting and elevation coordinates, pitch, azimuth, and vertical, horizontal and resultant pipeline curvature profiles that are adequate for deducing the induced longitudinal flexural strain. Heretofore, no method is available for deducing the accompanying extensional strain which under some conditions can be of the same order of magnitude as the flexural strain. The deduced flexural and extensional strains can be superimposed on estimates of the operating strains to establish the total longitudinal strain demand, which can be compared with the strain capacity of the pipe material to quantify the structural integrity of the displaced pipeline or to establish an *in-situ* margin of safety. Such a determination is essential for making an informed decision about the necessity for remedial action and/or continued geometry monitoring. It is noteworthy that the current practice of making a structural integrity assessment of a laterally displaced pipeline based only upon the induced flexural strain can be non-conservative.

The objective of the research reported herein is to develop and assess the efficacy of a method for estimating the longitudinal or axial extensional and flexural strains in a pipeline deformed by lateral ground displacement directly from ILI data or other measurements of pipeline displacement, and provide a basis for optimizing the design of *in-situ* geo-hazard monitoring programs and targeted ILI.

In the following, the technology for deducing the longitudinal extensional and flexural strains from geometry pig measurements of a laterally displaced pipeline is presented. An estimate for the axial or longitudinal extensional strain induced in a laterally displaced pipeline is developed. The development is limited to loadings that are predominantly transverse to the pipe’s axis. The emphasis is placed upon inelastic straining wherein the extensional strain is coupled with the change in curvature as a consequence of the shift of the neutral axis resulting from plastic deformation. The validity of the approach is established by the favorable comparisons of the predictions of induced extensional strains with those determined in buried pipeline finite element simulations for various displaced pipe configurations, pipe geometries and loading amplitudes.

Digital pig analyses of a large matrix of buried pipeline finite element simulations are conducted and the actual analytical strains are compared with the deduced strains from the digital pig “measurements” to establish the requisite resolution of geometry pig measurements. An error analysis is also performed to establish the relative error as a function of curvature measurement gage length, and the feature length and abruptness of the displaced shape of the pipeline. Further discussions on interfacing the axial extensional strain with monitoring technologies are presented.

2. AXIAL STRAIN DEVELOPMENT

Central to the development of a method for estimating the axial and flexural strains is the measurement; e.g., as might be accomplished with a geometry-pig, of the variation of the northing, easting and elevation coordinates, pitch, azimuth, or curvature of the displaced pipeline as function of position along the pipeline. In this development the displacement of the pipeline is assumed to be confined to a plane; e.g., the x - y plane or the principle plane of curvature. The pipeline is considered to be initially straight or if it is not, the initial strains produced by any deviation from the straight configuration are taken to be much smaller than the strain change induced by the subsequent pipeline displacement.

The most highly strained fibers in the pipe's cross section are the ones furthest from the neutral axis and whose total longitudinal or axial strain ε can be expressed as:

$$\varepsilon = \varepsilon_e \pm \varepsilon_f \quad (2.1)$$

where ε_e is the extensional strain and ε_f is the maximum flexural strain given by:

$$\varepsilon_f = D|\Psi|/2; \quad (2.2)$$

in which D is the pipe diameter and Ψ is the change in curvature of the pipeline. Since the curvature is assumed to be measured directly or derivable from geometry pig data, the development of an estimate for the total longitudinal strain rests with the determination of an effective means for evaluating the extensional strain from ILI measurement data.

If the loading in the region of the laterally displaced pipeline is predominately transverse; i.e., the work done by the axial frictional forces in this region is negligible compared to the work done by the transverse loading, it can be readily shown via the principle of virtual work that the axial force in this region is a constant. Clearly, in the regions adjacent to the laterally displaced pipeline, soil frictional forces restrain the axial motion of the pipe and are not negligible, and the axial force is not constant. However, the maximum straining occurs in/near the displaced region and this is the area of interest and the focus of attention in the following investigation. For linear elastic behavior the implication of a constant axial force is that the extensional strain is also constant and the extensional strain and the flexural strain are uncoupled. The extensional strain can be established, for example, from measurement of the change of length of a pipe joint of known initial length and the flexural strain is derivable from measurements leading to the change in curvature per Equation (2.2).

While the elastic strain can be readily estimated from ILI measurements, the more pressing problem is estimating the inelastic longitudinal strain accompanying larger permanent ground displacement (PGD). Unlike the case of elastic behavior, the problem is further complicated by the fact that the interaction of the bending moment and the axial force causes the neutral axis to shift as the pipeline plastically deforms. As a consequence, the extensional strain is inevitably coupled with the change of curvature.

Assuming that; (a) plane cross sections remain plane during the lateral displacement, (b) the lateral displacement is sufficient to produce moderate plastic strains; e.g., on the order of a few percent, (c) that the pipe material can be modeled as an elastic-perfectly plastic material, and (d) the magnitude of the total longitudinal strain ε is large compared to the yield strain, it can be shown that to first order, the axial strain is simply expressed as:

$$\varepsilon_e = D|\Psi|/\pi + c; \quad |\varepsilon| \gg \varepsilon_y \quad (2.3)$$

where ε_y is the yield strain. The constant of integration c is determined such that ε_e equals the measured extensional strain in the straight length of the pipe joint adjacent to the displaced region of the pipeline; e.g., by measuring the change in length of an adjacent pipe joint from its known initial length. It is interesting that the yield properties of the material do not explicitly appear in Equation (2.3). This is because the yield strain has been incorporated into the constant of integration c .

In the development of Equation (2.3) the extensional strain is assumed to be tensile and is assigned a positive sign. However, there are ground movement scenarios which induce compressive (negative) strains in the pipe not only in the displaced region, but also in the regions adjacent to the displaced region in which case the constant of integration c assumes a negative value. Therefore, in order to handle both tensile and compressive extensional strains, it is convenient to rewrite Equation (2.3) as:

$$\varepsilon_e = \text{sign}(c)D|\Psi|/\pi + c \quad (2.4)$$

It is clear from Equations (2.1) through (2.4) that an estimate for the total longitudinal strain depends upon measurement of the curvature of the displaced pipe; e.g., via a geometry pig. The deduction of the longitudinal strain from curvature measurements using these equations in conjunction with the operational strains provides an estimate for the total strain demand that can be compared with the strain capacity to facilitate a rational basis for determining whether or not remedial action is necessary and establishing an *in-situ* margin of safety.

3. VALIDATION OF EXTENSIONAL STRAIN ALGORITHM

3.1 Introduction

A series of buried pipeline deformation analyses was undertaken for the purpose of providing a rational basis for validating and evaluating the efficacy of the extensional strain estimate in Equation (2.4). The analyses were performed using the PIPLIN computer program (see Reference [1]), which is a special-purpose finite element program developed for deformation analysis of buried and above-ground pipeline systems. The program considers several nonlinear aspects of pipeline behavior, including pipe steel plasticity, large-displacement effects, and nonlinear soil support. For the purposes of this work, the PIPLIN predicted strains and curvatures were taken as the “exact” results. The PIPLIN results were used in three different ways:

- (1) The PIPLIN computed top/bottom fiber strains were taken as the “exact” strains for comparison with the deduced strains computed using the extensional strain algorithm.
- (2) The PIPLIN nodal curvature profiles were used directly in the algorithm-deduced strain calculations embodied in Equations (2.2) and (2.4).
- (3) The PIPLIN deflected shapes were processed using a “digital pig” which mimics the measurements made by geometry pigs to develop pigged curvature profiles—the “digital pig” data play the role of surrogate geometry pig data. The pigged curvature profiles were then used in the algorithm-deduced strain calculations embodied in Equations (2.2) and (2.4). The digital pigging step is important because a geometry pig measures pipe orientation over a finite “pig length” and the curvature profiles developed from geometry pig orientation profiles are based on numerically differentiating over a finite “gauge length”. Pig length and gauge length effects become especially important when evaluating relatively short pipeline deformation features.

3.2 Preliminary Validation of the Strain Algorithm

Preliminary pipe-soil interaction analyses were carried out for two different permanent ground displacement (PGD) scenarios: vertical subsidence over abrupt block settlement profiles and right lateral movement at a pipeline-fault crossing with a crossing angle of 90°. The abruptness of the imposed ground displacement profiles is characterized by 100% of the ground movement occurring over a distance of 1 foot. These analyses considered a 16-inch diameter by 0.375-inch thick X60 gas pipeline with an internal pressure of 725 psi. The pipeline is assumed to be buried with a uniform cover depth of 6 feet in a cohesionless sand material with an *in-situ* density of 120 pcf and a soil friction angle of 35°. The pipe is assumed to have a coal tar external coating. Bilinear (elastic-perfectly plastic) pipe-soil springs were developed for these models based on industry standard procedures (e.g., see References [2] and [3]). An isotropic X60 pipe steel stress-strain relationship is assumed. Pipe plasticity effects are considered for biaxial stress conditions using the von Mises yield criterion with multi-linear kinematic hardening [4]. The pipeline model mesh is refined to provide a grid of 1-foot long pipe elements that extend well beyond the region where significant bending deformation and transverse pipe-soil spring engagement occurs.

In each analysis, the pipeline is first pressurized and then subjected to the PGD profile which is imposed through the base of the pipe-soil springs using PIPLIN’s settlement profile option. For all cases, the analysis results were checked to verify that the length of the boundary sections of the model extended beyond the location of the longitudinal virtual anchor. The ground movement profile is imposed in small steps and the nonlinear solution is established using an event-to-event solution strategy for obtaining the resulting pipe-soil deformation state at selected levels of imposed displacement. The pipe output state includes the along-the-pipe distribution of the pipe axial force, bending moment, curvature, compression

and tension stresses and strains at the pipe nodes, as well as the forces and deformations in the pipe-soil springs. The key results from these analyses are the extreme fiber total axial strains, the pipeline curvature and the pipe centerline extensional strain.

For the vertical subsidence analysis case, the length of the settlement span was selected to be 100 feet. For this model, the output state was provided in Excel format for two different subsidence levels; namely; State A at 4 feet of subsidence and State B at 7 feet of subsidence. Note that at approximately 7 feet of imposed settlement, the pipeline “bridged” through the uplift pipe-soil springs such that additional settlement did not change the pipe state. For the right lateral fault crossing analysis case, the output state was also provided in Excel format for two levels of fault offset; specifically, State A at 6 feet of fault offset and State B at 9 feet of fault offset.

The evaluation of the efficacy of the algorithm developed in Chapter 2 for deducing the total axial strain distribution from curvature measurement used the PIPLIN analyses described above to provide realistic surrogate curvature measurements. The PIPLIN nodal curvatures, together with an estimate for the extensional strain in the pipe joint adjacent to the region of displaced pipe serve as inputs to Equations (2.2) and (2.4) for estimating the flexural and extensional strains, respectively. The algorithm-deduced strains are compared with those computed directly from PIPLIN to establish the efficacy of the algorithm.

Figures 3.1 and 3.2 depict the PIPLIN computed longitudinal extensional strain, and strains in the top and bottom fibers of the pipe for vertical block subsidence magnitudes of 4 feet (State A) and 7 feet (State B), respectively, over a distance of 100 feet for the subject 16-inch diameter pipe configuration. Also shown in these figures are the corresponding algorithm-deduced strains using the PIPLIN nodal curvatures as surrogate measured curvatures. While the deduced extensional strains have nearly the same distribution as the PIPLIN strains, they overestimate the PIPLIN strains for States A and B. However, the overestimate is less for State B than State A where the plastic deformations in the former state are greater; i.e., the overestimate of the extensional strain provided by Equation (2.4) decreases with increasing plastic straining for this case. The estimated total strains at the top fibers exceed those provided by the PIPLIN analysis whereas the algorithm underestimates the magnitude of strains in the bottom fibers. These differences are a direct consequence of Equation (2.4) overestimating the extensional strain. Since it is the magnitude of the maximum longitudinal strain that is of concern in a structural integrity assessment, that the algorithm underestimates the bottom fiber strain is of academic interest only.

The right lateral fault crossing displacement scenario was selected to provide a more challenging test of the efficacy of the algorithm. Figures 3.3 and 3.4 show the PIPLIN computed longitudinal extensional strain, and the total strains in the top and bottom fibers of the pipe for a right lateral fault crossing at fault offsets of 6 feet (State A) and 9 feet (State B), respectively, for the subject 16-inch diameter configuration. The corresponding algorithm strains deduced from the surrogate PIPLIN nodal curvatures are also shown in these figures. Once again, Equation (2.4) overestimates the extensional strain. The strain distributions deduced from the algorithm differ slightly from those established by PIPLIN. The overestimate of the extensional strain, also witnessed in the above subsidence comparisons, is responsible for overestimating the top fiber strain and underestimating the magnitude of the bottom fiber strain.

In general, these comparisons are considered very favorable and appear to improve with increasing plastic straining. The algorithm provides a conservative (over) estimate for the maximum tensile strain which will have the more onerous impact on the structural integrity of the displaced pipeline. The very favorable comparisons and the simplicity of the algorithm attest to its potential usefulness for estimating the total longitudinal strains in a displaced pipeline from ILI data.

It is also worth noting that Figures 3.1 through 3.4 exhibit rather steep curvature gradients near the extremities of the lateral ground movement. These steep gradients are symptomatic of intense reactive forces there. How these gradients impact the establishment of the pipeline curvature from geometry pig measurements is discussed in the following chapter. It should be noted that the assumption of a Winkler soil foundation, wherein each of the individual pipe-soil springs is completely independent of the adjacent pipe-soil springs, likely results in an overestimate of the transverse force and curvature gradients since there *can* be interaction of the soil along the pipe (e.g., continuum behavior, arch action).

3.3 Validation of the Strain Algorithm Considering “Pigged” Curvature Measures

The preliminary validation cases described in Section 3.2 used the PIPLIN computed nodal curvatures in the algorithm-deduced strain calculations embodied in Equations (2.2) and (2.4). These deduced strains were then compared to the “exact” strains computed directly by PIPLIN. In this section, these same comparisons are performed but additional comparisons are used to evaluate the algorithm based on “pigged” measures of the pipeline geometry. The PIPLIN deflected shapes are processed using a “digital pig” which mimics the measurements made by geometry pigs to develop “pigged” curvature profiles which are then used in the algorithm-deduced strain calculations. The digital pigging step is important because a geometry pig measures pipe orientation over a finite “pig length” and the curvature profiles developed from geometry pig orientation profiles are based on numerically differentiating the orientation data over a finite “gauge length”. Pig length and gauge length effects can be especially important when evaluating relatively short pipeline deformation features.

Additional PIPLIN analyses were performed for a wide range of pipe diameters and ground movements for further evaluating the deduced strain algorithm of Equations (2.2) and (2.4) and to assess the influence of the gauge length on the deduced strain when inferring the curvature from “digitally pigged” measurements--the digitally pigged measurements being surrogate geometry pig measurements. The columns on the left side of Tables 3.1 through 3.5 summarize the matrix of pipe-soil interaction analysis cases in terms of the analysis case number, the pipe diameter, wall thickness, internal pressure, cover depth, and the ground movement profile and its amplitude.

Three different types of ground movement profiles have been considered herein, namely; block vertical subsidence profiles, horizontal landslides, and right lateral fault crossings. The vertical subsidence cases considered downward settlement over abrupt block settlement profiles. The horizontal landslide movements considered abrupt block landslide profiles with different crossing angles as illustrated schematically in Figure 3.5. For the right lateral pipeline fault crossings, a range of different fault crossing angles “ β ” was considered. As shown schematically in Figure 3.6, β values $\geq 90^\circ$ result in a net longitudinal tension in the pipe while β values $< 90^\circ$ result in a net longitudinal compression. The majority of the ground displacement profiles considered herein utilized very abrupt transitions from zero ground displacement to 100% ground displacement (typical “guillotine” transition ramps of 1-foot were assumed). Abrupt transitions of this sort are conservative from a pipe-soil interaction analysis perspective but they may be unrealistically short. In order to investigate the effect of the transition length, additional cases were analyzed to consider progressively less abrupt transitions. For each diameter, the following ground displacement cases were analyzed:

- (1) A 200-foot long block subsidence profile with a 1-foot long transition from zero to maximum ground displacement.
- (2) A 100-foot long block subsidence profile with a 1-foot long transition from zero to maximum ground displacement.
- (3) Supplementary vertical subsidence cases to consider less abrupt linear ramp subsidence profiles with transitions from zero to maximum ground displacement occurring over linear ramp distances

of 20 and 40 feet. For the 8-inch through 36-inch diameter pipe cases, the subsidence span length is 100 feet, while for the 48-inch pipe cases, the subsidence span length is 200 feet.

- (4) A 100-foot long block horizontal landslide profile with a 1-foot long transition from zero to maximum ground displacement crossing the pipeline at an angle of 90° .
- (5) A 100-foot long block horizontal landslide profile with a 1-foot long transition from zero to maximum ground displacement crossing the pipeline at an angle of 45° .
- (6) Right lateral fault crossing profiles for fault crossing angles " β " of 70° , 80° , 90° , 100° and 110° .
- (7) Supplementary right lateral fault crossing cases to consider less abrupt fault displacement profiles over linear "ramp distances" of 20 and 40 feet. For 8-inch and 16-inch pipes, the additional cases were run for $\beta=90^\circ$; for 24-inch pipe, these additional cases were run for $\beta=110^\circ$ and for 36-inch and 48-inch pipes, the additional cases were run for $\beta=100^\circ$.

For the 16-inch pipe, in addition to the cases described above, several added cases were considered:

- (1) For the scenario that considered a 100-foot long block vertical subsidence profile, the additional less abrupt cases considered the cosine type landslide displacement functions described in Reference [5] again with exponent values of $n = 20, 10$ and 4 , and for W_s of 100 feet. Note that when W_s equals 100 feet, for $n = 20, 10$ and 4 the full landslide displacement is imposed over a distances of about $0.21 \cdot W_s$, $0.29 \cdot W_s$ and $0.4 \cdot W_s$, respectively, so the corresponding effective "ramp distances" for these cases are about 21, 29 and 40 feet.
- (2) For the scenarios that considered a 100-foot long block transverse landslide profile crossing the pipeline at an angle of 45° , the additional less abrupt cases considered the cosine type landslide displacement functions described in Reference [5] with exponent values of $n = 20, 10$ and 4 for W_s of 100 feet. Note that when W_s equals 100 feet, for $n = 20, 10$ and 4 the full landslide displacement is imposed over a distances of about $0.21 \cdot W_s$, $0.29 \cdot W_s$ and $0.4 \cdot W_s$, respectively, so the corresponding effective ramp distances for these cases are about 21, 29 and 40 feet, respectively.
- (3) For the scenarios that considered a 100-foot long block transverse landslide profile crossing the pipeline, additional cases were used to evaluate crossing angles of 30° , 15° , 7.5° , and 0° . These cases used the abrupt guillotine over a ramp distance of 1 foot.
- (4) For the 45° crossing angle the additional less abrupt cases considered the cosine type landslide displacement functions described in Reference [5] with exponent values of $n = 20, 10$ and 4 for W_s of 100 feet. Note that when W_s equals 100 feet, for $n = 20, 10$ and 4 the full landslide displacement is imposed over a distances of about $0.21 \cdot W_s$, $0.29 \cdot W_s$ and $0.4 \cdot W_s$, respectively, so the corresponding effective ramp distances for these cases are about 21, 29 and 40 feet, respectively.
- (5) For the right lateral fault crossing scenarios with a crossing angle of $\beta=80^\circ$, the additional less abrupt cases consider the cosine type fault displacement functions described in Reference [5] with an exponent of $n = 10$ for W_f values of 30, 40, 50 and 70 feet. Note that for $n = 10$, the full fault displacement is imposed over a distance of about $0.57 \cdot W_f$ so the effective "ramp distances" for these cases are about 17, 23, 29 and 40 feet.

Because the deduced strains in practice will be developed based on geometry pig data, it is desirable that the PIPLIN results be "mapped" into the corresponding profiles of geometry pig "signals". Consideration of digital pig curvatures is important because geometry pigs measure the pipe orientation over a finite pig length (L_{pig}) and the curvatures computed from the geometry pig orientation are then computed over a finite gage length (L_{gage}). In order to accomplish this mapping, the concept of a "digital pig" was applied to the PIPLIN deflected shapes. As illustrated schematically in Figures 3.7 through 3.9, the digital pig calculations are performed as a post-processing operation on the PIPLIN deflected shape for the output

state of interest. A first-pass calculation loop is used to compute the orientation angle “ $\theta_{pig}(S)$ ” at the current station “ S ” (i.e., this is the pitch angle for vertical profiles and the azimuth angle for horizontal profiles) over the length of the pig (L_{pig}) as shown in Figure 3.8. A second-pass calculation loop is then used to compute the curvature of the deflected pipe $\Psi(S)$ at the current station over a user-selected gage length (L_{gage}) as shown schematically in Figure 3.9. For more information on digital pigging, see Reference [6]. The pig lengths and curvature gage lengths used for the calculations were selected based on previous project experience and discussions with geometry pig vendors. For all cases, curvature gage lengths of L_{pig} and $3D$ were considered.

The extreme fiber total longitudinal strains computed by PIPLIN were taken as the “exact” strains for comparison with the total strains deduced from the algorithm (see the “Exact” columns in Tables 3.1 through 3.5). Three different deduced strain profiles were computed; namely, the deduced strains based on the PIPLIN nodal curvature (denoted as “PIPLIN” under the *Deduced Strains From* columns in Tables 3.1 through 3.5) and the deduced strains based on the “digitally pigged” curvatures for gage lengths of L_{pig} and $3D$ (denoted as “ $L_{gage} = 3D$ ” and “ $L_{gage} = L_{pig}$ ” under the *Deduced Strains From* columns in Tables 3.1 through 3.5). Although detailed strain, curvature and orientation angle profile plots were developed for each analysis case, only the maximum governing strains are presented herein. As noted above, the columns on the right side of Tables 3.1 through 3.5 summarize the maximum exact strains, and the maxima for the three different deduced strain measures for imposed displacements at States A and B. In order to provide a consistent characterization of the “feature length” for each ground movement scenario, the rotation/orientation (θ) profile was processed to determine the length of the steepest portion of the rotation which is nominally centered on the “lobe” of the curvature profile containing the maximum or minimum curvature. The feature length was taken as the distance spanning between 20% and 80% of the range between the minimum and maximum rotation values. As shown in Tables 3.1 through 3.5, the feature length was determined for each pipe state of interest.

One useful way to present the deduced axial strains summarized in Tables 3.1 through 3.5 is by the use of bar charts which present the ratio of the deduced strain to the exact strain for each pipe state. Figures 3.10 through 3.14 present the normalized strain bar charts for the 8-inch through 48-inch diameter cases, respectively. In these figures, the red bars represent the ratio of the algorithm strain deduced from the PIPLIN nodal curvatures to the exact strain, the yellow bars represent the ratio of the algorithm strain deduced from the digital pig using $L_{gage}=L_{pig}$ to the exact strain and the green bars represent the ratio of the algorithm strain deduced from the digital pig using $L_{gage}=3D$ to the exact strain. The top and bottom panels in these plots present the results for States A and B, respectively.

Another useful way to present the exact and deduced axial strains summarized in Table 3.1 to Table 3.5 is through the use of scatter diagrams which compare the exact strains to the corresponding deduced strains on a simple x - y plot. Figures 3.15 through 3.19 present such scatter diagrams for the 8-inch diameter (NPS8) through 48-inch diameter (NPS48) cases, respectively. On each of these figures, the top plot (a) compares the exact strains to the deduced strains for $L_{gage}=L_{pig}$ while the bottom plot (b) compares the exact strains to the deduced strains for $L_{gage}=3D$. The dashed line with a 1-to-1 slope represents the line of perfect correlation. The results for States A and B are shown using different symbols. For each state, a least squares fit trend line with a y -intercept of 0 is also presented. The equation for the trends lines (e.g., $y = m \cdot x$) and their regression coefficients R^2 are also shown. A slope (m value) of less than 1.0 indicates that on average, the deduced strain under-predicts the exact strain while a slope of greater than 1.0 indicates that on average, the deduced strain over-predicts the exact strain. Figures 3.20(a) and 3.20(b) present plots of the slope of the regression line for States A and B, respectively, as a function of the pipe diameter for the strains deduced using the PIPLIN curvatures as well as for the strains deduced by digital pigging using $L_{gage}=L_{pig}$ and $L_{gage}=3D$. Figure 3.21 presents a scatter diagram of the feature length versus the pipe diameter.

3.4 Preliminary Evaluation of the Strain Algorithm on Pipeline Configurations Containing Bends

As previously discussed, the deduced strain calculations are based on the assumption that the loading in the region of the laterally displacement pipeline is predominantly transverse. In locations subjected to permanent ground displacements, buried pipeline configurations containing bends will *always* attract combinations of axial and transverse pipe-soil loading, so such configurations are not well aligned with the fundamental assumptions of the deduced strain theory (i.e., pure transverse loading).

In order to investigate the performance of the deduced strain algorithm on pipeline configurations containing bends, pilot analyses were performed on a buried 10.75-inch diameter by 0.594-inch thick pipeline with a 20-foot long vertical riser section between two 90° bends. The configuration consists of a long horizontal run of 10-inch pipe which runs into a 90° sagbend with a bend radius of 75 inches, followed by a 20-foot vertical run into a 90° overbend with a bend radius of 75 inches and another long horizontal run. Two different ground displacement scenarios were considered for this configuration, namely; block vertical settlement on the high side of the riser (which causes bend closing action) and block vertical settlement on the low side of the riser (which causes bend opening action). For both cases, an abrupt guillotine non-settling to settling transition was centered on the riser. The pertinent inputs and results for these cases are summarized in Table 3.6, which has the same format as Tables 3.1 through 3.5.

For the case considering settlement on the high side of the riser, the governing strain location is in the overbend at the top of the riser while for the case considering settlement on the low side of the riser, the governing strain location is in the sagbend at the bottom of the riser. For these pilot cases, the deduced strains based on the PIPLIN curvature change and the pigged curvatures using $L_{gage}=L_{pig}$ and $L_{gage}=3D$ are all *significantly* larger than the exact strains. Based on a review of the detailed results for these cases, a key observation is that the exact extensional strains are negligibly small whereas the deduced extensional strains are quite large. For example, for State B of the case considering subsidence on the high side of the riser, the exact extensional strain at the governing location is approximately 0.08% while the deduced extensional strain based on the PIPLIN curvature change is about 1.51%. Similarly, for State B of the case considering subsidence on the low side of the riser, the exact extensional strain at the governing location is on the order of 0.12% strain while the deduced extensional strain based on the PIPLIN curvature change is about 1.74%. Hence, if the extensional strains for these cases had been neglected, the results would have provided a very close match with the exact results (i.e., the response of the bends is dominated by flexural response, with negligible extensional straining).

Based on these pilot analysis cases, it is apparent that direct application of the deduced strain calculations to ground movement scenarios involving buried pipeline bends is not appropriate. While these analyses do not represent an exhaustive evaluation in terms of the matrix of possible pipe diameters, bend radii, bend angle, etc., based on these results it appears that the extensional strain effects are negligible and can be neglected when estimating the longitudinal strain in bends of this type.

3.5 Evaluation of Strain Algorithm

Based upon the results from the matrix of buried pipe analyses discussed above, several observations can be made as follows.

- (1) As shown in Figures 3.1 through 3.4 from the preliminary validation cases, when the deduced strains are computed based on the PIPLIN nodal curvatures, the deduced strain over-estimates the governing strain (i.e., the tension strain when the gross strain field is tensile or the compression strain when the gross strain field is compressive). This observation holds for the majority of the cases considered. However, the deduced strains computed based on the PIPLIN nodal curvatures tend to underestimate the non-governing strains (e.g., the tension strain when the gross strain field

is compressive or the compression strain when the gross strain field is tensile) because Equation 2.4 overestimates the extensional strain.

- (2) The following trends are observed for the 8-inch diameter pipe cases:
- The deduced strain based on the PIPLIN nodal curvature always over-predicts the governing exact strain.
 - The deduced strain based on digital pigging with $L_{gage}=L_{pig}$ under-predicts the governing exact strain for all but three of the 26 pipe states evaluated.
 - Very little difference is observed between the deduced strains based on digital pigging with $L_{gage}=L_{pig}$ or $L_{gage}=3D$.
 - The deduced strain based on digital pigging with $L_{gage}=L_{pig}$ matches the governing exact strain to within $\pm 10\%$ for 12 of the 26 (46%) pipe states evaluated and to within $\pm 20\%$ for 19 of the 26 (73%) pipe states evaluated.
 - The worst matches between the deduced strain based on digital pigging with $L_{gage}=L_{pig}$ occurred for the 100-foot subsidence cases. The best match occurred for the 100-foot long block landslide crossing the pipe at 90° .
 - The average ratio of the deduced strain based on digital pigging with $L_{gage}=L_{pig}$ to the exact strain was 0.91 for State A and 0.79 for State B. From the scatter diagrams for $L_{gage}=L_{pig}$, the regression line slopes were about 0.78 for State A and about 0.93 for State B.
- (3) The following trends are observed for the 16-inch diameter pipe cases:
- The deduced strain based on the PIPLIN nodal curvature over-predicts the governing exact strain for all but 5 of the 54 pipe states evaluated. The most notable exceptions was for the block landslide crossing the pipeline at an angle of 0° (i.e., the ground movement is parallel to the pipeline and produces a predominantly axial, rather than a transverse loading and, hence, violates a fundamental hypothesis in the development of the algorithm).
 - The deduced strain based on digital pigging with $L_{gage}=L_{pig}$ under-predicts the governing exact strain for 35 of the 54 pipe states evaluated.
 - The deduced strain based on digital pigging with $L_{gage}=L_{pig}$ matches the governing exact strain to within $\pm 10\%$ for 26 of the 54 (48%) pipe states evaluated and to within $\pm 20\%$ for 43 of the 54 (80%) pipe states evaluated.
 - Aside from the block landslide crossing the pipeline at an angle of 0° , the worst matches between the deduced strain based on digital pigging with $L_{gage}=L_{pig}$ occurred for the 200-foot block landslide cases with pipeline crossing of $\leq 15^\circ$. Once again, the loading for such shallow crossings is predominantly axial, is not transverse, and violates an essential hypothesis of the algorithm.
 - The average ratio of the deduced strain based on digital pigging with $L_{gage}=L_{pig}$ to the exact strain was 0.93 for State A and 0.82 for State B. From the scatter diagrams, the regression line slopes were about 0.86 for State A and about 0.98 for State B.
- (4) The following trends are observed for the 24-inch diameter pipe cases:
- The deduced strain based on the PIPLIN nodal curvature over-predicts the governing exact strain for most of the 26 pipe states evaluated. The only exceptions were the fault crossing cases with $\beta \geq 100^\circ$.
 - The deduced strain based on digital pigging with $L_{gage}=L_{pig}$ under-predicts the governing exact strain for all but 8 of the 26 pipe states evaluated.
 - The deduced strain based on digital pigging with $L_{gage}=L_{pig}$ matches the governing exact strain to within $\pm 10\%$ for 13 of the 26 (50%) pipe states evaluated and to within $\pm 20\%$ for 23 of the 26 (88%) states evaluated.

- The worst matches between the deduced strain based on digital pigging with $L_{gage}=L_{pig}$ occurred for the 200 foot subsidence case (over prediction by 23%) and for the fault crossing case for $\beta = 110^\circ$ with a ramp distance of 40 feet. The best match occurred for the 100-foot long block landslide crossing the pipe at 90° and the 100 foot block subsidence with a ramp distance of 40 feet.
 - The average ratio of the deduced strain based on digital pigging with $L_{gage}=L_{pig}$ to the exact strain was 0.89 for State A and 0.83 for State B. From the scatter diagrams for $L_{gage}=L_{pig}$, the regression line slopes were about 0.90 for State A and about 0.95 for State B.
- (5) The following trends are observed for the 36-inch diameter pipe cases:
- The deduced strain based on the PIPLIN nodal curvature over-predicts the governing exact strain for most of the 26 pipe states evaluated. The only exceptions were for State B in the fault crossing case with $\beta = 70^\circ$ and for all of the fault crossing cases with $\beta \geq 100^\circ$.
 - The deduced strain based on digital pigging with $L_{gage}=L_{pig}$ under-predicts the governing exact strain for 12 of the 26 pipe states evaluated.
 - The deduced strain based on digital pigging with $L_{gage}=L_{pig}$ matches the governing exact strain to within $\pm 10\%$ for 8 of the 26 (31%) pipe states evaluated and to within $\pm 20\%$ for 22 of the 26 (85%) states evaluated.
 - The worst matches between the deduced strain based on digital pigging with $L_{gage}=L_{pig}$ occurred for the 100 foot subsidence case with a ramp distance of 40 feet (over prediction by as much as 35%) and for the 100-foot long block landslide crossing the pipe at 45° (over prediction by as much as about 30%). The best match occurred for State B of the 200-foot long block subsidence and both states for the fault crossing case with $\beta = 80^\circ$.
 - The average ratio of the deduced strain based on digital pigging with $L_{gage}=L_{pig}$ to the exact strain was 0.87 for State A and 0.82 for State B. From the scatter diagrams for $L_{gage}=L_{pig}$, the regression line slopes were about 0.97 for State A and about 1.0 for State B.
- (6) The following trends are observed for the 48-inch diameter pipe cases:
- The deduced strain based on the PIPLIN nodal curvature over-predicts the governing exact strain for most of the 26 pipe states evaluated. The only exceptions were for State B in the fault crossing case with $\beta = 70^\circ$ and for all of the fault crossing cases with $\beta \geq 100^\circ$.
 - The deduced strain based on digital pigging with $L_{gage}=L_{pig}$ under-predicts the governing exact strain for all but 8 of the 26 pipe states evaluated.
 - The deduced strain based on digital pigging with $L_{gage}=L_{pig}$ matches the governing exact strain to within $\pm 10\%$ for 11 of the 26 (42%) pipe states evaluated and to within $\pm 20\%$ for 22 of the 26 (85%) states evaluated.
 - The worst matches between the deduced strain based on digital pigging with $L_{gage}=L_{pig}$ occurred for the 100 foot subsidence case (over prediction by over 60%) and for the block landslide crossing the pipe at 45° (over prediction by as much as 42%). The best matches occurred for the State A in the 200-foot long block subsidence cases.
 - The average ratio of the deduced strain based on digital pigging with $L_{gage}=L_{pig}$ to the exact strain was 0.88 for State A and 0.84 for State B. From the scatter diagrams for $L_{gage}=L_{pig}$, the regression line slopes were about 0.93 for State A and about 0.96 for State B.
- (7) When the deduced strains are computed based on the digitally pigged curvatures for a gage length of L_{pig} the deduced strain tends to under-predict the governing strain. The degree of under-prediction increases when the deduced strains are computed using the pigged curvatures for a gage length of $3D$, i.e., the precision of the digitally pigged curvatures decreases with increasing gage length.

- (8) Mapping of the PIPLIN analysis results into “digital pigged” results is important because the pigged rotations can be slightly smaller than the PIPLIN nodal rotations and the pigged curvatures tend to be less than the PIPLIN nodal curvatures, especially for longer gage lengths. This implies that curvatures from geometry pigs should be developed using as short a gage length as possible. However, as will be discussed later in this report, due to the inevitable presence of low amplitude noise in actual pig rotation data, curvature profiles calculated using shorter gage lengths tend to have a high signal-to-noise ratio and it may be necessary to utilize digital filtering (see References [6] and [7]) in order to reduce the noise. A gage length equal to L_{pig} or less is recommended provided that the effect of noise in the geometry pig data can be properly addressed.
- (9) On average, for each diameter the deduced strains tend to be more accurate for State A than for State B. On average, the deduced strains tend to be more accurate for pipe diameters in the range from 24 to 48 inches. The deduced strains are least accurate for the 8-inch diameter cases.
- (10) For the 16-inch diameter pipe case with a block landslide moving along the pipe with no transverse component (i.e., with a crossing angle of zero, Case 22), the deduced strains provide a poor comparison with the exact strains because contrary to the assumption of the loading being primarily transverse in the development of Equation (2.4), the loading for this case is purely axial. For the 16-inch diameter pipe block landslide cases, the accuracy of the deduced strains begins to deteriorate at crossing angles of $\leq 15^\circ$ wherein the axial component of the ground movement begins to become dominant.
- (11) Both components of the total deduced strain i.e., the flexural term from Equation (2.2) and the extensional term from Equation (2.4) depend on the pipeline curvature. Therefore, when the deduced strain is computed from digitally pigged results, the effect of longer gage lengths will influence both of these terms.
- (12) As shown in Figure 3.21, the feature length increases with increasing pipe diameter. For the 8, 16, 24, 36 and 48-inch pipe cases, the average feature lengths are about 4.2, 6.5, 10.0, 10.1 and 11.8 feet, respectively. All of the maximum feature lengths are less than 20 feet or less than half of length of a typical 40-foot pipe joint.

In summary, these comparisons demonstrate the efficacy of the strain algorithm for deducing the magnitude of the maximum longitudinal strain when the loading in the laterally displaced region of the pipeline is predominately transverse. A reliable estimate for the curvature is central to making a faithful deduction of the strain. When the PIPLIN nodal curvature is used, the deduction for the strain, with a couple of exceptions, generally overestimates the magnitude of the maximum exact strain and the amount of the overestimate decreases with increasing plastic straining. It goes without saying that the estimate for the longitudinal strain provided by Equations (2.1) through (2.4) is no better than the estimate for the curvature.

4. MEASUREMENT CONSIDERATIONS

4.1 Overview and Categorization of Existing Pipe Geometry Monitoring Technologies

Several different methods are used to monitor the geometry of below-ground pipelines. For this discussion, the methods are categorized herein as indirect methods, direct external methods and in-line methods. A general overview of these methods is as follows:

- *Indirect methods* make measurements of the geometry of the ground in which the pipeline is buried, not the geometry of the pipeline itself. Indirect methods include: aerial stereoscopy or photogrammetry, conventional surface topography surveys, Light Detection and Ranging (LiDAR), satellite based surveys such as Interferometric Synthetic Aperture Radar (InSAR), GPS surface topography surveys, inclinometers, and extensometers, etc. For buried offshore pipeline applications in relatively shallow water, some operators will conduct periodic side scan sonar surveys of the sea floor topography over a swath containing the pipeline right of way. While indirect methods are useful for identifying locations along a pipeline route where differential ground movement has occurred, they provide only an oblique characterization of how the geometry of the pipeline may have been affected by the ground movement. Hence, indirect methods are not directly applicable for the pipeline strain calculations developed in this report which rely on accurate profiles of the centerline curvature of the pipeline.
- *Direct external methods* make measurements using instruments attached directly to the outside of the pipeline. Direct methods include monitoring rods which are attached to the top of pipe and protrude through the soil cover [8], inclinometers, strain gages (either foil or vibrating wire), and fiber optic sensors, etc. Direct external methods are useful for measuring ground movement-induced changes in the pipeline geometry at discrete locations along the pipeline. In order to provide geometry profiles over the instrumented section of pipeline, some sort of numerical interpolation scheme (e.g., a polynomial fit) is required. Considering the discrete and localized deployment of direct external methods along the pipeline, their utilization with the pipeline strain calculations developed in this report (which rely on accurate curvature profiles) is viewed as impractical.
- *In-line methods* measure the pipeline geometry using an in-line inspection (ILI) device or smart pig that travels through the pipeline with the gas or liquid flow. A wide range of geometry measuring instruments are deployed on ILI tools including odometer wheels, mechanical calipers, accelerometers and gyroscopes. The readings from these instruments are sampled at a rate which provides profiles of closely-spaced values of the measured geometric quantities along the pipe. Because they provide essentially continuous profiles of the along-the-pipe geometry measures, including estimates of the pipeline curvature, smart pigs are viewed as the most promising basis for interfacing with the pipeline strain calculations developed in this report. Note that because this work is focused on pipeline centerline geometry profiles, other ILI technologies such as magnetic flux leakage (MFL) for identifying and sizing corrosion defects and ultrasonic tools (UT) for locating and sizing laminations and other features are not pertinent to this report and are not discussed in detail herein.

4.2 Discussion of In-Line Methods

The primary means of *in situ* pipeline geometry mapping is by the use of instrumented in-line tools (smart pigs). One of the leading ILI tools for monitoring the internal geometry of the pipe and the path of the pipeline centerline is the Geopig [9]. This tool deploys the following instruments:

- An Inertial Measurement Unit (IMU) which includes an orthogonal triad of angle rate gyroscopes and a corresponding orthogonal triad of uniaxial accelerometers. These instruments respond to the motion of the pig as it travels down the pipe along a path that is nominally parallel to the pipeline centerline. The IMU is housed within in a cup or wheel supported canister of the pig.
- Spring loaded mechanical caliper arms which measure the geometry of the pipe bore to capture the inside diameter and to characterize features such as ovality, dents, ripples, wrinkles and buckles. The mechanical calipers are also used to locate the girth welds in the pipeline.
- Odometers to measure the along-the-pipe “chainage” distance travelled by the pig. The odometer data can also be used to compute the instantaneous travel speed of the pig.
- Pressure and temperature gages.

The gyroscopes measure the rate of rotation of the tool with respect to an inertial reference frame. The accelerometers measure both the acceleration due to gravity and the acceleration of the inertial system with respect to the inertial reference frame. When the inertial system is stationary with respect to the earth, the accelerometers measure the gravity vector and the gyroscopes measure the earth rotation vector. This allows for determination of the pre-survey or post-survey orientation of the tool with respect to the local level reference frame, i.e., pitch, yaw, and roll. The orientations of the tool during the survey are obtained primarily by integration of the angle rate gyroscope readings after subtraction of the earth rotation. The inertial data processing develops the profile of the pitch and azimuth orientation of the path travelled by the pig during the survey. The pitch angle describes the tilt angle of the pig with respect to the horizontal plane (nose up is positive) while the yaw (or azimuth) angle describes the angle between the pig travel direction and north (yaw is clockwise negative, azimuth is clockwise positive).

The pitch and azimuth data are numerically integrated with the odometer data to develop profiles of the pipe northing, easting and elevation. These three-dimensional pipeline coordinate profiles are then translated and rotated such that they pass through a client-specified set of tie-points with known coordinates. The tie-points are typically established by GPS positioning at traps, valves, bends or wall thickness changes that are easily identified by the pig. The specified accuracy of the pipe position is typically $1/2000^{\text{th}}$ of the distance between tie points. For a distance between tie points of 3000 m, the allowable error in between the tie points for a single survey can reach 0.75 m (i.e., $3000/2/2000$), which corresponds to up to 1.5 m difference between two surveys.

Based on [9], the Geopig specification for the weld-to-weld distance accuracy is ± 12.5 mm (about ± 0.5 inches). Given this level of accuracy, estimates of centerline extensional strain in a 40 foot long pipe joint based on two subsequent measurements are expected to be accurate to within $\pm 0.1\%$ strain to $\pm 0.2\%$ strain.

The pitch (θ) and azimuth (γ) data are numerically differentiated with respect to the odometer data (S) to develop profiles of the pipe vertical and horizontal curvature. The vertical curvature (Ψ_V) and horizontal curvature (Ψ_H) are taken as the change in pitch and azimuth angles, respectively, over a change in pipe distance along the pipe centerline:

$$\Psi_V = \frac{\Delta\theta}{\Delta S} \quad (4.1)$$

$$\Psi_H = \frac{\Delta\gamma}{\Delta S} \cdot \cos(\theta) \quad (4.2)$$

The resultant curvature (Ψ_R) is:

$$\Psi_R = \sqrt{\Psi_V^2 + \Psi_H^2} \quad (4.3)$$

The vertical, horizontal and resultant bending strains are related to the corresponding curvature terms (assuming that plane sections remain plane) as follows:

$$\varepsilon_V = \Psi_V \cdot \frac{D}{2} \quad (4.4)$$

$$\varepsilon_H = \Psi_H \cdot \frac{D}{2} \quad (4.5)$$

$$\varepsilon_R = \Psi_R \cdot \frac{D}{2} \quad (4.6)$$

In order to reduce noise in the curvature, the curvature is typically computed over a distance ΔS of 3 to 6 pipe diameters. This distance is referred to herein as the gage length L_{gage} . The most efficient curvature calculation is based on a simple finite difference approach. A somewhat smoother curvature profile can be computed using a “regression line” method where the curvature is computed as the slope of a least-squares fit line to the profiles of θ vs. S or γ vs. S over the selected gage length. Several ILI vendors have inertia based geometry pigs (for example BJ Pipeline Inspection Services [9] and ROSEN [10]). Different ILI vendors provide different specifications related to the accuracy of their curvature/bending strain. Most vendors refer to a bending strain or curvature “detection threshold” and use this term interchangeably with accuracy. Although some vendor reports/papers show results providing bending strain accuracies of $\pm 0.005\%$ to $\pm 0.01\%$ strain, the best available directly *specified* bending strain accuracy is $\pm 0.02\%$ strain (which is equivalent to a bend radius of 2500D). In addition to a specified bending strain determination of $\pm 0.02\%$ strain, ROSEN [10] also specifies a curvature determination accuracy of ± 0.0007 radians/meter (which is equivalent to a bend radius of 1400 m). The bending strain accuracy specification cited by some vendors also includes a restriction that the specification only applies, and the strains will only be reported for feature lengths greater than 12 m (about 40 feet) which is the length of a typical pipe joint. This restriction is consistent with the theoretical error analysis presented in Section 4.4.1 which shows that the bending strain accuracy is limited by the physical length of the pig, the curvature calculation gage length, *and* the length of the curvature feature.

Less sophisticated accelerometer-based ILI tools can also be used to obtain information about the pipeline geometry. The main vendor for accelerometer based ILI tool inspections is Weatherford Pipeline & Specialty Services with their SAAM tool i.e., Smart Acquisition Analysis Module [11]. The SAAM unit is installed within a utility/cleaning pig and measures and records the pig’s behavior as it passes through a pipeline. The idea behind the SAAM tool technology is that the dynamic response of the pig to the presence of a feature in the pipeline is used as a measure of that feature. Post-survey interpretation/manipulation of the data is used to develop out-of-straightness (OOS) measurements of the pipeline. The primary geometry measurement device is an accelerometer which samples data at a constant frequency. The accelerometer measurement axis is aligned parallel to the axis of the pig. The measurement output from this accelerometer is basically the component of gravity along the axis of the pig or $g \cdot \sin\theta$ (or just $\sin\theta$ when the acceleration signal is normalized by g) where θ is the pitch angle. Note that the SAAM unit *does not* include an odometer. A pipe distance coordinate is established based on aligning weld “kicks” in the acceleration signal profile to known distances from the pipeline as-built information. The weld kicks are sharp acceleration spikes that are recorded as the pig crosses the weld. To position the acceleration data between known features, a detailed pipe length tally or a mean pipe joint length is used. This manipulation allows a distance value to be assigned to each weld in the pipeline and subsequently to each data sample assuming a constant tool velocity between the known positions. The primary geometry deliverable from a SAAM pig survey is a vertical profile of the pipeline which is based

on integration of the measured inclination data and the interpreted pipe distance data. Prior to performing the elevation profile integration, the weld kicks are removed from the signal. It appears that a short (up to ≈ 5 foot long) section of the inclination data nominally centered on the acceleration spike is replaced by a constant inclination value equal to the average inclination over a joint length centered near the spike. The Weatherford deliverable *does not* include a curvature or bending strain profile but a digital profile of the inclination/pitch from the survey can be provided along with the elevation profile upon client request. The pitch data (θ) can be processed numerically with the pipe distance data (S) to obtain vertical curvature using standard calculation methods (e.g., divided difference or regression line). The accuracy of the resulting curvature is unknown.

4.3 Interface Axial Strain Algorithm with Monitoring Technologies

Geometry pig vendors will typically provide a detailed survey report which includes an overall summary of the pipeline geometry and in some cases a listing of locations where client specified curvature or bending strain thresholds are exceeded. In cases where multiple surveys have been performed, locations where client specified limits on the *changes* in curvature or bending strain are exceeded may also be reported. In addition to a detailed strain report, most vendors will also provide the client with a software package that will allow for viewing and printing user selected profiles of the pipeline geometry survey data at different locations along the alignment. Typical software plots include plan views of the pipeline, along-the-pipe profiles of pipe centerline elevation, pitch and azimuth as well as vertical, horizontal and total curvature or bending strain. Vendor software packages should allow for curvature/bending strain calculations based on a user-specified gage length and should include the capability to filter these profiles for example using low-pass filtering to remove high frequency (short wavelength) noise features. It is also possible to develop plots showing all girth weld locations as well as other pipeline features that are programmed into a client supplied pipeline as-built data base or pipe joint length tally. Overlaying plots of these quantities from multiple surveys is also possible to facilitate survey-to-survey comparisons of various geometry measures. Most vendor software packages also have the capability of exporting user selected sections of the data to external files (e.g., in ASCII or Excel format).

Given the software capabilities available for viewing and processing data from geometry pig surveys, extension of the software to include the deduced total strain calculations embodied in Equations (2.1) through (2.4) should be relatively straightforward. The main requirements are (a) addition of Equation (2.4) to estimate the extensional strain term, (b) determination of the constant of integration c , and (c) the ability to combine the bending and extensional strains using Equation (2.1). The capability to compute improved strains (as discussed later in Section 4.4.2) using curvatures computed using two different gage lengths Equation (4.23) should also be easily programmable. As will be discussed in Section 4.6, a key feature of the deduced total strain calculations presented herein is that they must be applied to the *change* in curvature due to ground movement. Therefore, the vendor software must be able to calculate the difference between the current curvature profile and the curvature profile corresponding to an initial baseline survey of the pipeline.

In order to undertake these modifications, it will be necessary for the user to define/select a section of the pipeline over which the calculations are to be performed. It may be possible to define this “study section” based on preliminary comparisons of the pipeline geometry profiles from different surveys and/or based on knowledge regarding where the pipeline may have encountered a ground displacement event (e.g., using indirect methods such as ground surface surveys, inclinometer data, LiDAR surveys, etc.). For the theoretical analyses presented in this report, the location of the pipeline affected by the ground movement is clearly visible in the pipe elevation or plan view plots when the pipeline initial geometry is completely defined.

Development of the constant of integration “ c ” requires detailed information regarding the pipe joint lengths adjacent to the displaced section of the pipeline. For pipelines where a detailed pipe joint length tally is available or for which an initial as-built ILI geometry survey is available, it will be possible to estimate c based on the ratio of the change in joint length ΔL to the original joint length L_o : $c = \Delta L / L_o$. In these cases, the accuracy of c will be directly related to the accuracy of the current and the original weld-to-weld lengths (i.e., $L_{current}$ and L_o). Based on the Geopig specification for weld-to-weld distance accuracy of ± 12.5 mm (about ± 0.5 inches), estimates of centerline extensional strain in a 40-foot long pipe joint are expected to be accurate only to within $\pm 0.1\%$ to $\pm 0.2\%$. Considering this level of accuracy, it may be worthwhile to develop an along-the-pipe profile plot of $\Delta L / L_o$ for each pipe joint across the study area as a basis for establishing $\text{sign}(c)$ as well as confirmation of the magnitude of c in the boundaries of the displaced section. As an illustration of this type of plot, Figure 4.1 presents a profile of the “exact” extensional strain (from State B of the preliminary fault crossing analysis case discussed in Section 3.2 and shown in Figure 3.4). The “stepped” joint average centerline strain profile is derived based on the amount of lengthening computed over designated 40-foot joints throughout the model (i.e. it represents $\Delta L / L_o$). The circular symbols at about ± 60 feet from the center of the fault profile designate the locations where the constant of integration “ c ” is defined. As shown, the extensional strain profile deduced from the PIPLIN curvature is constant in the exterior boundary sections of the model but varies between the circular symbols where the pipe curvatures become significant. Figure 4.1(a) provides a tightly zoomed in view of these profiles while Figure 4.1(b) presents the corresponding zoomed out view. It should be noted that the magnitude of c is expected to be fairly small and for cases with significant levels of strain (e.g., one or two percent strain) within the displaced section of the pipeline, the error associated with neglecting c is not expected to be significant (i.e., set $c=0$).

4.4 Assessment of Measurement Error

Because a geometry pig can only make measurements at discrete intervals, errors, aside from measurement inaccuracies, are inherently introduced when manipulating these data. For example, since the pipe curvature currently cannot be measured directly, it must be deduced by numerically differentiating the pipeline pitch or azimuth orientation with respect to the pipe distance; e.g., as depicted in Equations (4.1) and (4.2). Numerical differentiation is notoriously inaccurate if proper precautions in selecting a step size relative to a characteristic length and the type of difference approximation employed are not exercised.

In this section, theoretical error analyses of landslide-type and fault-type displacement functions are performed to establish a characterization of the relative error resulting from numerical differentiation and its dependence upon the ratio of gage length (step size) to characteristic feature length and the relative abruptness of the displacement. This analysis is followed by investigation of anticipated error associated with the employment of current geometry pig data by performing surrogate digital pig analyses of PIPLIN computations.

4.4.1 Theoretical Error Analysis

As demonstrated earlier, the total longitudinal strain in a displaced pipeline varies linearly with (nearly directly proportional to) its change in curvature. Therefore, estimates of the total longitudinal strain in a displaced pipeline can be established if its change in curvature can be determined. A geometry pig makes discrete measurements of the pipe orientation profile from which the pipeline centerline curvature can be estimated. The pig orientation measurements are made over the cup-to-cup length L_{pig} of the pig (see Figure 3.8) as the pig traverses the pipeline. When the gage length between measurement points used to deduce the curvature is equal to the pig length; i.e., $L_{gage} = L_{pig}$, the discretized form for the curvature is equivalent to a central difference approximation and from a mathematical point of view this approximation is optimal under these conditions. It is desirable to have an estimate for the error

associated with this algorithm for estimating the curvature since this error directly impacts the precision with which the total longitudinal strain in the displaced pipeline can be deduced. An estimate for the difference between the actual curvature and that deduced from the central difference approximation is provided in the following.

Essential to quantifying the expected error in the central difference approximation of the pipeline curvature is a realistic representation for the ground displacement. Although the pipeline displacement profile is not identical to the ground displacement profile, the ground displacement provides a reasonable basis for characterizing the pipeline displacement profile. Based upon observations of Japanese earthquakes, Reference [5] provides analytical ground displacement functions for both landslide-type ground movements and for fault-type ground movements. It can be shown that the ground displacement functions given in [5] can be expressed in the following general form:

$$y(x) = \delta - \delta \cos^n \lambda x; \quad \lambda = \frac{\pi}{2L} \quad (4.7)$$

For landslide-type displacements, $L = W_s$ (where $2W_s$ is the total width of the landslide) the equation applies over the range: $0 \leq x/W_s \leq 1$. For fault-type displacements, $L = W_f$ (where W_f is the width of the fault zone) the equation applies over the range: $0 \leq x/W_f \leq 1$.

In these displacement functions, W_s and W_f define the characteristic length of the distance perpendicular to the ground motion between the positions of minimum (zero) displacement and maximum displacement δ (or a measure of the ramp distance of the displacement). The exponent n governs the abruptness of the transition region of the displaced pipeline which increases with increasing n .

The linearized form of the curvature, valid when the square of the slope of the profile is negligible compared to unity, is:

$$\Psi(x) = \frac{d^2 y}{dx^2} \quad (4.8)$$

The introduction of Equation (4.7) into Equation (4.8) yields:

$$\Psi(x) = \delta \lambda^2 \left[n^2 \cos^n \lambda x - n(n-1) \cos^{n-2} \lambda x \right] \quad (4.9)$$

The maximum curvature, upon which the following error estimate will be based, occurs at $x=0$ and is

$$\Psi(0) = \delta n \lambda^2 \quad (4.10)$$

The central difference approximation for the curvature expressed in terms of the transverse displacement is:

$$\Psi_a = \frac{y_{i+1} - 2y_i + y_{i-1}}{\Delta x^2} \quad (4.11)$$

where $y_i = y(x_i)$, etc., and $\Delta x = x_{i+1} - x_i = x_i - x_{i-1}$. If symmetry of the displacements is assumed at $x = 0$, Equation (4.11) yields:

$$\Psi_a(0) = \frac{2y(\Delta x)}{\Delta x^2} \quad (4.12)$$

The introduction of Equation (4.7) into Equation (4.12) leads to:

$$\Psi_a(0) = 2\delta \frac{1 - \cos^n \lambda \Delta x}{\Delta x^2} \quad (4.13)$$

The Taylor series expansion of $\cos^n \lambda \Delta x$ about $\Delta x = 0$ is:

$$\cos^n \lambda \Delta x = 1 - \frac{n}{2!} (\lambda \Delta x)^2 - \frac{n(3n-4)}{4!} (\lambda \Delta x)^4 + \dots \quad (4.14)$$

Finally, the substitution of Equation (4.14) into Equation (4.13) yields:

$$\Psi_a(0) = \Psi(0) \left[1 - \frac{3n-2}{12} (\lambda \Delta x)^2 + \dots \right] \quad (4.15)$$

It is clear from Equation (4.15) that the central difference approximation for the curvature underestimates the actual curvature. The relative error between the actual curvature and the central difference approximation is:

$$E_r = \frac{3n-2}{12} (\lambda \Delta x)^2 \quad (4.16)$$

which for a slide-type displacement is:

$$E_r = \frac{3n-2}{12} \left(\frac{\pi \Delta x}{2 W_s} \right)^2 \quad (4.17)$$

and for a fault-type displacement is:

$$E_r = \frac{3n-2}{12} \left(\frac{\pi \Delta x}{2 W_f} \right)^2 \quad (4.18)$$

It is apparent from Equation (4.17) and Equation (4.18) that the gage length as represented by Δx must be sufficiently small compared to the characteristic length W_s or W_f of the slide or fault displacements, respectively, for the relative error to be less than an acceptable value. It is also apparent that as the

abruptness of the transition increases, as measured here by increasing value of the exponent n , the gage length must be further decreased in order to maintain the same relative error. An increased abruptness has the effect of reducing the characteristic length. For example, Equations (4.17) and (4.18) may be rewritten as:

$$E_r = \frac{1}{12} \left(\frac{\pi}{2} \frac{\Delta x}{L_{eff}} \right)^2 \quad (4.19)$$

in which $L_{eff} = W_s / \sqrt{3n-2}$ or $L_{eff} = W_f / \sqrt{3n-2}$, respectively, is the effective characteristic length which clearly depends upon the abruptness of the loading as measured in this case by the exponent n .

Since the gage length L_{gage} used in a geometry pig is practically limited to the length of the pig L_{pig} , then for a central difference approximation for the curvature, the length of the pig must be sufficiently small compared to effective characteristic length (e.g., the axial distance from the point of minimum pipe cross sectional rotation to maximum pipe cross section rotation) of the displaced pipeline in order that the error in the deduction of the curvature is within acceptable limits. While it may be possible to satisfy this condition for relatively gradual transitions, it may not be possible to do so for relative abrupt transitions where the effective length is relatively short compared to the pig length. In other words, the pig length may limit the minimum characteristic length for which the approach may be applied without introducing unacceptable errors. Conversely, the physical limitation on the length of the pig may introduce significant errors in regions of abrupt transitions.

Although the relative errors presented in Equations (4.17) and Equation (4.19) for the central difference approximation of the curvature depend upon the specific form selected for the displacement functions (i.e., the assumed ground displacement profiles), the relative errors for other displacement functions will, nevertheless, vary as the square of the ratio of the gage length to an effective characteristic length. Furthermore a similar dependence of the error on the square of this ratio would have been attained if the curvature had been evaluated at locations other than $x=0$.

The fact that the relative error varies as the square of the gage length for the central difference approximation for the curvature can be exploited to obtain an improved estimate for the curvature. Suppose the central difference approximation is used to compute the curvature at the same point for two different gage lengths Δx_1 and Δx_2 , then based upon Equation (4.15) it is permissible to write:

$$\begin{aligned} \Psi_{a1} &= \Psi(1 - E_{r1}) \\ \Psi_{a2} &= \Psi(1 - E_{r2}) \end{aligned} \quad (4.20)$$

where Ψ_{a1} and E_{r1} , and Ψ_{a2} and E_{r2} are the central difference approximation for the curvature and relative error for gage lengths Δx_1 and Δx_2 , respectively. These two equations can be combined to yield:

$$\frac{E_{r1}}{E_{r2}} = \left(\frac{\Delta x_1}{\Delta x_2} \right)^2 = \frac{\Psi - \Psi_{a1}}{\Psi - \Psi_{a2}} \quad (4.21)$$

from which an improved approximation for the curvature is:

$$\Psi = \frac{\Psi_{a1}\Delta x_2^2 - \Psi_{a2}\Delta x_1^2}{\Delta x_2^2 - \Delta x_1^2} \quad (4.22)$$

Because the selected gage lengths may not permit establishing the central difference approximation for the curvature at exactly the same point, linear interpolation of the difference approximations for the curvature for a given gage length may be used to establish it at the point of interest.

If L_{pig} does not equal L_{gage} , then the relative error is expected to be proportional to the Δx . It follows in a manner analogous to the development of Equation (4.22) that an improved estimate for the curvature is:

$$\Psi = \frac{\Psi_{a1}\Delta x_2 - \Psi_{a2}\Delta x_1}{\Delta x_2 - \Delta x_1} \quad (4.23)$$

4.4.2 Evaluation of Improved Strain Calculations

In order to evaluate the improved strain calculations embodied by the improved estimate for the curvature of Equation (4.23), the equation was applied to the matrix of PIPLIN analyses described in Chapter 3. For this evaluation, the deduced strains based on digital pigging for gage lengths of $L_{gage}=L_{pig}$ and $L_{gage}=3D$ were applied in the following equation:

$$\varepsilon_{improved} = \frac{\varepsilon_{L_{pig}} \cdot 3D - \varepsilon_{3D} \cdot L_{pig}}{3D - L_{pig}} \quad (4.24)$$

The bar charts in Figures 4.2 through 4.6 present the ratio of the improved strain to the exact strain for the 8-inch through 48-inch diameter cases, respectively. For reference, the bar charts also show the previously developed deduced strain to exact strain ratios. In these figures, the red bar represents the ratio of the algorithm strain deduced from the PIPLIN nodal curvature to the exact strain, the yellow bar represents the ratio of the algorithm strain deduced from the digital pig curvature using $L_{gage}=L_{pig}$ to the exact strain, the green bar represents the ratio of the algorithm strain deduced from the digital pig curvature using $L_{gage}=3D$ to the exact strain and the blue bar represents the ratio of the improved strain from Equation (4.24) to the exact strain. The top and bottom panels in these plots present the results for States A and B, respectively.

An initial observation is that the improved strain is always larger than the strains deduced by digital pigging using $L_{gage}=L_{pig}$ and $L_{gage}=3D$. As illustrated in Figures 4.2 through 4.6, for all cases where the strains deduced by digital pigging using $L_{gage}=L_{pig}$ and $L_{gage}=3D$ under-estimate the exact strain, the improved strain provides a more accurate estimate of the exact strain. However, for all cases where the strains deduced by digital pigging using $L_{gage}=L_{pig}$ and $L_{gage}=3D$ overestimate the exact strain, the improved strain provides a less accurate estimate of the exact strain. Based on Figures 4.2 through 4.6, the following observations can be made:

- For the 8-inch pipe cases, the improved strain matches the governing exact strain to within $\pm 10\%$ for 12 of the 26 (46%) pipe states evaluated and to within $\pm 20\%$ for 21 of the 26 (81%) pipe states evaluated.
- For the 16-inch pipe cases, the improved strain matches the governing exact strain to within $\pm 10\%$ for 30 of the 54 (56%) pipe states evaluated and to within $\pm 20\%$ for 44 of the 54 (81%) pipe states evaluated.

- For the 24-inch pipe cases, the improved strain matches the governing exact strain to within $\pm 10\%$ for 13 of the 26 (50%) pipe states evaluated and to within $\pm 20\%$ for 24 of the 26 (92%) pipe states evaluated.
- For the 36-inch pipe cases, the improved strain matches the governing exact strain to within $\pm 10\%$ for 4 of the 26 (15%) pipe states evaluated and to within $\pm 20\%$ for 15 of the 26 (58%) pipe states evaluated.
- For the 48-inch pipe cases, the improved strain matches the governing exact strain to within $\pm 10\%$ for 6 of the 26 (23%) pipe states evaluated and to within $\pm 20\%$ for 20 of the 26 (77%) pipe states evaluated.

Figure 4.7 presents a combined scatter diagram of the exact strain versus the improved strain for all cases/diameters--the top plot (a) presents the results for State A and the bottom plot (b) presents the results for State B. The dashed line with slope of unity represents the line of perfect correlation. A least squares fit trend line with a y -intercept of zero is also presented as well as lines corresponding to $\pm 20\%$ error. It is apparent from Figure 4.7 that the improved strain lies within $\pm 20\%$ of the exact strain for the vast majority of the cases that were investigated. It is worth noting that included in these data are those pipes whose loading is not predominantly transverse and therefore lie outside the restrictions imposed in the development of the algorithm. Since there is very little difference between the strains deduced by digital pigging using $L_{gage}=L_{pig}$ and $L_{gage}=3D$ for the 8-inch diameter pipe, the improved strain provides very little improvement for this pipe diameter. In this sense the results for the 8-inch pipe represent outliers and contribute to a larger scatter band. The slopes of the linear regression lines for both States A and B are slightly less than unity and there is close agreement between the regression lines and the Line of Perfect Agreement. The implication is that on average, the improved strain is very nearly equal to the exact strain and errs on the conservative side; i.e., is on average the improved strain over predicts the exact strain.

Figure 4.8 presents a plot of the slope of the regression line for States A and B as a function of the pipe diameter for the improved strains and the strains deduced using the PIPLIN nodal curvatures, and for the strains deduced by digital pigging using $L_{gage}=L_{pig}$ and $L_{gage}=3D$. With exception of the 8-inch diameter pipe, the slope of the regression line for the improved strain of the other diameters is approximately 10% larger than the slope of the regression line for strains deduced by digital pigging using $L_{gage}=L_{pig}$. The slope of the regression line for the improved strain agrees favorably with the slope of the regression line for strain deduced using the PIPLIN nodal curvature for the larger diameter pipes that were investigated. The implication is that the on average, the improved estimate of the curvature provided by Equation (4.23) agrees favorably with PIPLIN nodal curvature for these diameters.

It is noteworthy that for the 24-inch diameter pipe the improved strain overestimates the exact strain, i.e., yields a conservative prediction for the strain, for all cases investigated except for fault crossings at 100° and 110° for which the algorithm also underestimates the strain when the PIPLIN nodal curvatures are used. Consequently, the slope of the regression line for the 24-inch pipe is decreased and is responsible for the slight dip in the slope of regression line for the improved strain for State A in Figure 4.8(a). The analogous point for State B, in which there is an additional under prediction, is slightly less suppressed. For the 48-inch diameter pipe the improved strain overestimates the exact strain, i.e., yields a conservative prediction for the strain, for all cases investigated except for fault crossings at 100° and 110° , for both States A and B. Consequently, the slope of the regression line for the 48-inch pipe is slightly suppressed by these underestimates. If it were not for the under predictions for the cases noted, the curve of the slope of the regression lines for the improved strain would monotonically increase with pipe diameter and approach the curve deduced with PIPLIN nodal curvature. It appears that the improved estimate for the curvature of Equation (4.23) on average approaches the PIPLIN nodal curvature as the diameter of the pipe increases.

4.5 Discussion of Noise in Geometry Pig Data

As geometry pigs travel through a pipeline, they encounter a wide range of pipe imperfections and features which are basically deviations from a perfect cylinder. Typical pipe imperfections and features include expander marks, longitudinal weld seams, weld beads, minor offsets and misalignments at girth welds, etc. These features are recorded by the pig instruments and appear as “noise” in the gyroscope/accelerometer data. It should be noted that pipeline imperfection features actually tend to be quite repeatable from survey to survey. While these features are clearly not associated with real pipeline strains, they can have a significant influence on the pipeline curvature computed from the pipeline orientation data. The following discussion illustrates some effects of noise in geometry pig data.

Reference [7] provides several illustrations of noise in geometry pig surveys of a 48-inch diameter pipeline. The frequency content of the pitch profile across a section of the pipeline was examined by plotting its power spectral density spectrum. For a given frequency in the spectrum, the corresponding pitch wavelength is estimated by dividing the average pig speed by the frequency. The pitch spectrum plots showed the presence of a component of “pitch energy” centered at a frequency of about 8 Hz which at a speed of about 9 fps, corresponds to a feature length of about 13.5 inches. The noise in the pitch signal is attributed to the pig responding in a pitching motion as its front and back cups traverse small, periodic diameter changes (expander marks) in the pipe joints which result from the (UOE) pipe manufacturing process. Subsequent investigation of the noise, including examination of similar noise features in pipe joints from three different pipe manufacturers indicated that the noise features are repeatable and are different for different pipe manufacturers.

Clearly, these short wave length features in the pitch signal are not related to real pipe curvature/strain demand. As detailed in Reference [7], the pitch profile was processed to compute curvature profiles using four different gage lengths namely; 10 feet, 5.5 feet (which is equal to L_{pig}), 3 feet and 1 foot. Plots of the bending strain profiles showed that high-frequency (short wave length) oscillations are present in the computed curvature and that the amplitude of the noise increases with decreasing gage lengths (especially for gage lengths shorter than the length of the pig). It is apparent that the “noise” component has a significant effect on the computed bending strain profiles. It is obviously desirable to remove the noise from the bending strain profiles prior to making a pipeline structural integrity assessment. After a careful review of the data, a low-pass filter with a cut-off frequency of 1.5 Hz was applied to remove the high-frequency (short wave length) features. This cut-off frequency was selected because it is below the frequencies associated with low amplitude noise in the pitch spectrum and it corresponds to a wavelength that is close to the length of the pig. The effect of the filtering is very pronounced because it virtually eliminates the bothersome noise and provides a much clearer picture of the true pipe bending strain. For each gage length, the difference between the unfiltered and filtered bending strain profiles can be taken as the “noise profile”. Figure 4.9 presents a plot of the standard deviation, range and maximum/minimum values of the noise profile as a function of curvature calculation gage length. As shown, for gage lengths greater than or equal to the length of the pig, the statistical parameters of the noise profile are essentially constant while for shorter gage lengths, the magnitude of the noise measures increases significantly.

Figure 4.10 presents a similar plot of the standard deviation, range and maximum/minimum values of the noise profile as a function of curvature calculation gage length from a geometry pig survey of an unnamed 10-inch diameter pipeline. For this case, curvature calculation gage lengths of 20 feet, 12 feet, 5 feet, 2.6875 feet (3D), and 1.05 feet (12.625 inches which is equal to L_{pig}) were used. In this illustration, a low-pass filter with a cut-off frequency of 7.2 Hz was applied to remove the high-frequency (short wave length) features. This cut-off frequency was selected because it corresponds to a wavelength that is equal to the length of the pig.

Figures 4.9 and 4.10 provide examples of the characteristics of noise that may be present in geometry pig data. It should be noted that errors introduced due to noise in the geometry pig data would add to the theoretical error developed in Section 4.4.1. It is important to note that the data from geometry pig surveys should be reviewed on a case-by-case basis to make an assessment of the influence of noise. Special care and engineering judgment must be exercised to ensure that the calculated results are meaningful, especially in relation to filtering of the data and selection of the gage length for calculating curvature.

4.6 Importance of a Baseline Survey

All of the theoretical developments and the analytical processing described in this report are based on operating on *changes* in the pipeline geometry and in particular, changes in the pipeline curvature. In these analysis cases, the pipeline was originally perfectly straight such that the change in curvature is equal to the total curvature.

In long, straight sections of real pipelines remote from field and fabricated bends, the actual profile of the pipeline will not be perfectly straight due to inevitable variations in the trench profile which will result in modest amounts of elastic “roping” curvature over distances of say one to several pipe joint lengths. In addition to these “global” deviations from a perfectly straight pipeline profile, a geometry pig survey will undoubtedly highlight repeatable, low amplitude, short length noise features along the pipe profile (e.g., due expander marks, longitudinal weld seams, weld beads, minor offsets and misalignments at girth welds, etc.). Although all of these features of the “as-built” pipeline geometry can show up as curvature in the data from a geometry pig survey, none of these features are associated with pipeline curvature due to imposed ground displacements. Therefore, the ideal framework for applying the calculations developed in this report would include the execution of a baseline geometry pig survey of the pipeline soon after construction. The deduced strain calculations would then be performed on the *change* (i.e., the difference) between the current pipeline curvature profile and the “as-built” curvature profile. In pipelines for which an initial “as-built” geometry pig survey is not available, the most common way forward with the data is to assume that all curvature (excluding curvature due to field bends and fabricated bends) is due to ground movement. As previously noted, it will most likely be necessary to filter the data using a low-pass filter in order to remove the high-frequency, short wave length features not associated with real curvature.

For major new pipelines which incorporate strain based design concepts and a “monitor and maintain” design philosophy, it is common practice to perform a baseline geometry pig survey very soon after construction of the pipeline [6,12]. For these pipelines, the deduced strain calculations embodied in Equations (2.1) through (2.4) would be applied to the profile of curvature *change* (i.e., the difference) between the current pipeline curvature profile and the “as-built” curvature profile. Note that because the pipe distance coordinates from different surveys will be different (i.e., due to variations in pig travel speed), it will be necessary to interpolate the pipe geometry data sets to a common distance coordinate vector “*S*”. It is most common to use the geometry survey with the most closely spaced set of odometer readings as the common distance coordinate. Once the pipe geometry profiles from each survey are interpolated to a common “*S*” axis, the *differences* between the various quantities (e.g., elevation, pitch, curvature, etc.) from different surveys can be readily computed and plotted.

4.7 Survey to Survey Comparisons

As previously noted, most geometry pig vendors provide the client with a software package that will allow for viewing and printing user selected profiles of the pipeline geometry survey data at different locations along the alignment. This software also has the capability to develop overlay profile plots of pipeline geometry data from different surveys as well as profiles of *differences* between geometry data

from different surveys (e.g., vertical curvature or resultant curvature). Most vendor software packages also have the capability of exporting user selected sections of the data to external files for additional processing using different software packages. Reference [12] provides an illustration of different types of plots that can be used to compare data from different geometry pig surveys and highlight changes in the pipe geometry. Plots of this sort provide a useful basis for assessing locations where ground movement induced pipeline displacement may have occurred.

5. CONCLUSIONS

An algorithm for deducing the longitudinal strain induced in laterally displaced pipelines was developed for situations where the loading is predominantly transverse and the magnitude of the maximum longitudinal strain exceeds the yield strain. This algorithm may be applied to data from in-line inspection tools (geometry pigs) that will permit the direct determination of the longitudinal strain in laterally displaced pipelines. Such direct determinations preclude the need for detailed pipe-soil interaction analyses which require sophisticated numerical modeling and computations, and pipe and soil material property data that are not generally available. This longitudinal strain can be combined with the operational strains to establish the total strain demand which, when compared with the strain capacity, permits establishing the margin of safety of the displaced pipeline.

The induced strain is found to depend upon the pipe curvature. PIPLIN computations were performed for a variety of lateral pipeline displacements due to block subsidence, block landslides intersecting the pipeline at varying angles, and fault crossings at different angles, different pipe geometries and loading states. The computed nodal curvatures were treated as surrogate measured pipeline curvatures and used in the algorithm to compute the extensional and longitudinal strains which were compared with the PIPLIN computed strains to validate the algorithm. With the exception of fault crossing scenarios with tensile crossing angles, the deduced extensional strains overestimated the actual strains; i.e., the algorithm generally provided a conservative estimate for the actual strain. The agreement between the deduced and the actual strains improved with increased plastic yielding. The algorithm failed to provide reliable estimates of the longitudinal strain for block landslides running along the axis of the pipeline (i.e., a 0° crossing angle) because the loading in this case is predominantly axial and the accompanying curvature is relatively small. Of course, this predominantly axial loading violates the restriction/assumption of predominantly transverse loading required by the algorithm. Interestingly, when the crossing angle of the landslide relative to the pipeline axis increased to as little as 7.5°, the algorithm once again overestimates the actual strain. Except for this singular case, the close agreement between the actual strains and those estimated from the strain algorithm provides validation of the algorithm.

Key to establishing a reliable estimate for the total longitudinal strain is developing a dependable approximation for the curvature from the measured centerline orientation of the displaced pipeline. The fact that the deduced strain from digitally pigged curvature profiles underestimates the PIPLIN strain indicates that the numerical differentiation underestimates the curvature for curvature calculation gage lengths as small as L_{pig} . The often favorable agreement between the deduced strain and the exact strain or improved strain is the result of compensating errors; i.e., the typical over prediction by the longitudinal strain algorithm is offset by the underestimate for the curvature. To the extent such favorable comparisons exist for loadings not considered in this investigation, the deduced strain or the improved strain may provide an adequate estimate for the exact strain. The exception to this postulation is the 8-inch pipe for which the deduced strain can significantly underestimate the exact strain.

An error analysis for a central difference approximation of the curvature with curvature calculation gage length equal to the pig length indicates the relative error varies as the square of the ratio of the gage length to the length of the characteristic deformation feature of interest which in this case corresponds to length over which there is a rapid change in pitch or azimuth of the pipeline. The length of the characteristic feature length is dependent upon the abruptness of the lateral displacement—the greater the abruptness, the shorter the feature length and for the same gage length the greater the error in deducing the curvature and, hence, the longitudinal strain. For gage lengths not equal to the pig length, the relative error is proportional to the gage length. This property was exploited to provide an improved estimate for the curvature and, hence, the total longitudinal strain when the curvature was estimated using two different gage lengths (L_{pig} and $3D$). This refinement resulted in an enhancement over the deduced strain with $L_{gage} = L_{pig}$ of approximately 10 percent for all cases excluding the 8-inch diameter pipe. Only minor improvement was

obtained for the 8-inch pipe because small differences in the estimated curvature for L_{gage} equal to L_{pig} and $3D$. The large errors in the digitally pigged curvatures for the 8-inch line are believed to be related to the shortness of the feature lengths relative to the pig length and the curvature calculation gage length.

Current geometry pig measurements of the pitch and azimuth for estimating the curvature can contain a significant level of noise. Frequently, the gage length used in computing the curvature is adjusted so as to act as a filter—a larger gage length providing greater filtering or smoothing of the curvature signal. The gage length cannot be made arbitrarily long to enhance the filtering or smoothing operation, but must remain small compared to the characteristic feature length to ensure reliable estimates for the curvature. For example, digital pigging of the PIPLIN results with a gage length of $3D$ produced estimates for the longitudinal strain that are significantly less than the strain based upon PIPLIN nodal curvature for the smaller pipe diameters, but the disparity decreased with increasing pipe diameter. Selecting a gage length suitable for the purpose of filtering and at the same time leading to an acceptable estimate for the curvature may be a challenge. In this case it may be appropriate to utilize a low-pass filter to smooth out the noise in the curvature profile.

Because using difference approximations for performing numerical differentiation for establishing the curvature can produce significant errors in a region where the gradient of the pipeline orientation is large, it would be advantageous to be able to measure the curvature directly without the need for differentiation. Such a capability does not currently exist and could be a topic for future research.

The most sophisticated method of monitoring *in situ* pipeline geometry is through the use of instrumented in-line inspection tools equipped with odometer wheels, mechanical calipers, accelerometers and gyroscopes (referred to herein as geometry pigs). As a geometry pig travels through a pipeline, the instruments are sampled at a rate which provides profiles of closely-spaced, essentially continuous, pipe geometry measures, including derived estimates of the pipeline curvature. Smart geometry pigs are viewed as the most promising basis for interfacing with the pipeline strain calculations developed in this report which rely on accurate curvature profiles.

Most geometry pig vendors provide a software package that allows for viewing and printing user selected profiles of the pipeline geometry survey data at different locations along the alignment. Given the software capabilities available for viewing and processing data from geometry pig surveys, extension of the software to include the deduced total strain calculations embodied in Equations (2.1) through (2.4) should be relatively straightforward. The main requirements are (a) addition of Equation (2.4) to estimate the extensional strain term, (b) determination of the constant of integration c , and (c) the ability to combine the bending and extensional strains using Equation (2.1). The capability to compute “improved strains” using curvatures computed from two different gage lengths Equation (4.23) should also be easily programmable. The software should allow for curvature/bending strain calculations based on a user-specified gage length and should include the capability to filter the resulting profiles for example using low-pass filtering to remove high frequency (short wavelength) noise features.

A key feature of the deduced total strain calculations presented herein is that they must be applied to the *change* in curvature due to ground movement. Therefore, the ideal framework for applying the calculations would include the execution of a baseline geometry pig survey of the pipeline soon after construction. For major new pipelines which incorporate strain based design concepts and a “monitor and maintain” design philosophy, it is common practice to perform a baseline geometry pig survey very soon after construction [6, 12]. For these pipelines, the deduced strain calculations embodied in Equations (2.1) through (2.4) would be applied to the profile of curvature *change* (i.e., the difference) between the current pipeline curvature profile and the “as-built” curvature profile. Therefore, the vendor software should be able to calculate the difference between the current curvature profile and the curvature profile corresponding to an initial baseline survey of the pipeline.

6. RECOMMENDED FUTURE RESEARCH

It is recommended that future research be directed at incorporating the developed technology into in-line inspection tool data processing to enable the deduction of the induced longitudinal strain in laterally displaced pipelines. It will be necessary to interface the longitudinal strain algorithm with ILI monitoring technology. Crucial to the determination of the induced strain is a reliable measurement of the curvature of the pipeline in the presence of geometry pig noise. Emphasis should be placed upon how best to filter the noise and at the same time minimize the error in deducing the curvature. If the filtering is to be done by adjusting the gage length, the incremental step size when numerically performing a differentiation of a measurement signal, then the optimal gage length must be determined that will effectively filter the noise but at the same time minimize the error in deducing the curvature. To avoid the pitfalls of numerical differentiation, research should focus on instrumentation that would permit direct determination of the curvature.

7. REFERENCES

- [1] SSD, Inc., "*PIPLIN: Stress and Deformation Analysis of Pipelines*", Version 4.56, User Reference and Theoretical Manual, Reno, Nevada, March, 2007.
- [2] ASCE, "*Guidelines for the Seismic Design of Oil and Gas Pipeline Systems*", Committee on Gas and Liquid Fuel Lifelines, 1984.
- [3] ASCE American Lifelines Alliance, "*Guidelines for the Design of Buried Steel Pipe*", Published by the ASCE American Lifelines Alliance, www.americanlifelinesalliance.org, July 2001.
- [4] Mroz, Z., "*On the Description of Anisotropic Work-Hardening*", Journal of Mechanics, Physics and Solids, Vol. 15, pp. 163-175, 1967.
- [5] D.G. Honegger and D.J. Nyman, "Guidelines for the Seismic Design and Assessment of Natural Gas and Liquid Hydrocarbon Pipelines," PRCI Report PR-268-9823, October 1, 2004.
- [6] Hart, J.D., Zulfiqar, N., Moore, D.H., and Swank, G.R., "*Digital Pigging as a Basis for Improved Pipeline Structural Integrity Evaluations*", IPC06-10349, Proceedings of the International Pipeline Conference, Calgary, Alberta, Canada, September 25-29, 2006.
- [7] Hart, J.D., Powell, G. H., Hackney, D., and Zulfiqar, N., "*Geometry Monitoring of the Trans-Alaska Pipeline*", Proceedings of the ASCE Cold Regions Conference, Anchorage, Alaska, May 20-22, 2002.
- [8] Simmons, G.G., and Alto, J.V., "*Pipeline Curvature by Polynomial Approximation*", Proceedings of the Conference on Pipeline Infrastructure, ASCE Pipeline Division, Boston, Massachusetts, June 6-7, 1988.
- [9] Czyz, J.A. and Wainselboin, S.E., "*Monitoring Pipeline Movement and its Effect on Pipe Integrity Using Inertial/Caliper In-Line Inspection*", Paper IBP575_03, Rio Pipeline Conference & Exposition 2003.
- [10] Aue, H., Paeper, S., Brown, B., Humphreys, M. and Sutherland, J., "*High Quality Geometry Module for Pipeline Strain Analysis*," Pigging Products and Services Association, 2007.
- [11] Short, G. and Ogunjimi, P., "*Out-of-Straightness Detection, Assessment, and Monitoring using the SAAM Pipeline Inspection Tool*", Proceedings of the Pipeline Pigging, Integrity Assessment, and Repair Conference, Houston, Texas, February, 2001.
- [12] Hart, J.D., Zulfiqar, N., and Erikson, T.H., "*3rd Party Review of Geometry Pig Inertial Survey Data at the Colville River HDD*", Paper IPC08-64306, Proceedings of the International Pipeline Conference, Calgary, Alberta, Canada, September 29-October 3, 2008.

TABLES

Table 3.1: Pipe-Soil Interaction Analysis Cases and Results - NPS8 Pipe

Case Number	Model Description	Diameter (inches)	Wall Thickness (inches)	Pressure (psi)	Cover Depth (feet)	State A Ground Disp. (feet)	State A Feature Length (feet)	Exact Strain (%)	State A Deduced Strains From:			State B Ground Disp. (feet)	State B Feature Length (feet)	Exact Strain (%)	State B Deduced Strains From:		
									PIPLIN (%)	$L_{gage} = 3D$ (%)	$L_{gage} = L_{pig}$ (%)				PIPLIN (%)	$L_{gage} = 3D$ (%)	$L_{gage} = L_{pig}$ (%)
2	200' Block Subsidence	8.625	0.322	1500	4	2.5	3.5	1.77	2.39	1.58	1.62	4.5	3.3	2.80	3.40	2.14	2.18
1	100' Block Subsidence	8.625	0.322	1500	6	1.5	3.1	1.73	2.43	1.43	1.47	2.0	2.8	2.74	3.60	1.90	1.97
72	100' Block Subsidence, Ramp=20'	8.625	0.322	1500	6	2.25	3.7	1.71	2.19	1.37	1.41	2.75	3.3	2.87	3.43	1.81	1.86
73	100' Block Subsidence, Ramp=40'	8.625	0.322	1500	6	4.25	4.0	1.58	1.80	1.24	1.27	5.25	3.5	2.80	2.94	1.67	1.71
8	100' Block Landslide, 90 deg	8.625	0.322	1500	6	1.75	3.8	1.67	2.19	1.74	1.77	2.75	4.2	2.23	2.70	2.16	2.19
9	100' Block Landslide, 45 deg	8.625	0.322	1500	6	2.25	3.5	1.52	2.22	1.73	1.78	3.5	3.7	2.29	3.08	2.35	2.39
3	Right Lateral Fault, $\beta = 70$ deg	8.625	0.322	1500	3	1.15	3.8	-1.36	-1.54	-1.23	-1.26	1.3	3.2	-2.74	-3.00	-1.70	-1.76
4	Right Lateral Fault, $\beta = 80$ deg	8.625	0.322	1500	3	1.1	3.2	-1.61	-1.89	-1.48	-1.52	1.3	2.5	-2.92	-3.40	-2.14	-2.23
5	Right Lateral Fault, $\beta = 90$ deg	8.625	0.322	1500	6	1.5	3.6	1.83	2.61	1.65	1.70	3.0	4.1	2.80	3.41	2.27	2.29
61	Right Lateral Fault, $\beta = 90$ deg, Ramp=20'	8.625	0.322	1500	6	6.0	6.0	2.33	2.60	2.16	2.18	9.0	10.4	2.27	2.34	1.93	1.95
62	Right Lateral Fault, $\beta = 90$ deg, Ramp=40'	8.625	0.322	1500	6	6.0	4.8	1.57	1.76	1.43	1.46	9.0	5.6	1.87	1.96	1.69	1.70
6	Right Lateral Fault, $\beta = 100$ deg	8.625	0.322	1500	6	1.25	4.3	1.28	1.50	1.16	1.18	2.5	4.6	2.03	2.15	1.75	1.76
7	Right Lateral Fault, $\beta = 110$ deg	8.625	0.322	1500	6	1.5	4.2	1.48	1.54	1.30	1.32	3.0	5.8	1.83	1.77	1.49	1.50

Table 3.2: Pipe-Soil Interaction Analysis Cases and Results – NPS16 Pipe

Case Number	Model Description	Diameter (inches)	Wall Thickness (inches)	Pressure (psi)	Cover Depth (feet)	State A Ground Disp. (feet)	State A Feature Length (feet)	Exact Strain (%)	State A Deduced Strains From:			State B Ground Disp. (feet)	State B Feature Length (feet)	Exact Strain (%)	State B Deduced Strains From:		
									PIPLIN (%)	$L_{gage} = 3D$ (%)	$L_{gage} = L_{pig}$ (%)				PIPLIN (%)	$L_{gage} = 3D$ (%)	$L_{gage} = L_{pig}$ (%)
11	200' Block Subsidence	16.0	0.375	725	4	4.0	4.9	2.36	2.98	1.79	2.10	6.0	4.4	3.36	3.94	2.40	2.74
10	100' Block Subsidence	16.0	0.375	725	6	2.25	4.6	1.98	2.67	1.50	1.79	4.0	3.6	4.08	4.86	2.63	3.21
56	100' Block Subsidence, n=20	16.0	0.375	725	6	4.0	3.8	3.50	4.08	2.54	3.05	7.0	3.6	4.91	5.33	3.54	4.10
57	100' Block Subsidence, n=10	16.0	0.375	725	6	4.0	4.5	2.83	3.29	2.29	2.62	7.0	4.1	4.16	4.45	3.24	3.63
58	100' Block Subsidence, n=4	16.0	0.375	725	6	4.0	6.4	1.56	1.81	1.60	1.70	7.0	5.7	2.53	2.63	2.31	2.41
74	100' Block Subsidence, Ramp=20'	16.0	0.375	725	6	2.5	4.1	1.94	2.52	1.59	1.86	4.25	3.5	3.99	4.60	2.74	3.32
75	100' Block Subsidence, Ramp=40'	16.0	0.375	725	6	4.25	5.7	1.94	2.25	1.54	1.75	6.5	4.2	3.98	4.14	2.72	3.16
17	100' Block Landslide, 90 deg	16.0	0.375	725	6	6.0	8.4	2.65	2.98	2.45	2.56	9.0	12.3	2.62	2.70	2.24	2.34
18	100' Block Landslide, 45 deg	16.0	0.375	725	6	6.0	6.3	2.65	3.22	2.63	2.85	9.0	8.4	2.73	3.24	2.67	2.83
53	100' Block Landslide, 45 deg, n=20	16.0	0.375	725	6	6.0	6.7	2.51	3.03	2.64	2.85	9.0	8.7	2.62	3.08	2.67	2.85
54	100' Block Landslide, 45 deg, n=10	16.0	0.375	725	6	6.0	6.0	2.53	3.01	2.54	2.74	9.0	8.1	2.78	3.18	2.67	2.86
55	100' Block Landslide, 45 deg, n=4	16.0	0.375	725	6	6.0	7.8	1.50	1.69	1.53	1.59	9.0	7.7	2.47	2.59	2.30	2.37
19	100' Block Landslide, 30 deg	16.0	0.375	725	6	6.0	5.7	2.10	2.73	2.22	2.49	9.0	6.5	2.70	3.26	2.71	2.93
20	200' Block Landslide, 15 deg	16.0	0.375	725	6	6.0	6.1	0.86	1.46	1.16	1.29	9.0	4.9	1.65	2.67	2.03	2.33
21	400' Block Landslide, 7.5 deg	16.0	0.375	725	7	6.0	7.6	0.43	0.66	0.60	0.60	9.0	6.6	0.87	1.61	1.18	1.18
22	1000' Block Landslide, 0 deg	16.0	0.375	725	7	2.0	5.7	0.53	0.13	0.06	0.06	5.0	5.7	0.53	0.13	0.06	0.06

Table 3.2: Pipe-Soil Interaction Analysis Cases and Results – NPS16 Pipe (Continued)

Case Number	Model Description	Diameter (inches)	Wall Thickness (inches)	Pressure (psi)	Cover Depth (feet)	State A Ground Disp. (feet)	State A Feature Length (feet)	Exact Strain (%)	State A Deduced Strains From:			State B Ground Disp. (feet)	State B Feature Length (feet)	Exact Strain (%)	State B Deduced Strains From:		
									PIPLIN (%)	$L_{gage} = 3D$ (%)	$L_{gage} = L_{pig}$ (%)				PIPLIN (%)	$L_{gage} = 3D$ (%)	$L_{gage} = L_{pig}$ (%)
12	Right Lateral Fault, $\beta = 70$ deg	16.0	0.375	725	3	1.0	8.5	-0.43	-0.53	-0.52	-0.53	2.0	4.5	-3.18	-3.33	-2.07	-2.41
13	Right Lateral Fault, $\beta = 80$ deg	16.0	0.375	725	3	2.0	6.3	-1.57	-1.86	-1.34	-1.45	3.0	4.1	-4.82	-5.71	-3.06	-3.67
50	Right Lateral Fault, $\beta=80$ deg, $W_f=30'$, $n=10$	16.0	0.375	725	3	2.0	6.3	-1.49	-1.76	-1.34	-1.45	3.0	4.0	-4.57	-5.39	-3.00	-3.58
51	Right Lateral Fault, $\beta=80$ deg, $W_f=40'$, $n=10$	16.0	0.375	725	3	2.0	6.4	-1.40	-1.66	-1.32	-1.43	3.0	3.9	-4.18	-4.89	-2.91	-3.50
52	Right Lateral Fault, $\beta=80$ deg, $W_f=50'$, $n=10$	16.0	0.375	725	3	2.0	6.8	-1.11	-1.32	-1.13	-1.22	3.0	4.5	-3.54	-4.04	-2.55	-3.04
71	Right Lateral Fault, $\beta=80$ deg, $W_f=70'$, $n=10$	16.0	0.375	725	3	2.0	9.1	-0.59	-0.73	-0.69	-0.71	3.0	6.7	-1.56	-1.78	-1.45	-1.59
14	Right Lateral Fault, $\beta=90$ deg	16.0	0.375	725	6	6.0	7.5	3.06	3.58	2.67	2.81	9.0	10.8	3.02	3.45	2.54	2.67
63	Right Lateral Fault, $\beta=90$ deg, Ramp=20'	16.0	0.375	725	6	6.0	7.1	3.07	3.49	2.77	2.93	9.0	10.4	3.04	3.37	2.65	2.80
64	Right Lateral Fault, $\beta=90$ deg, Ramp=40'	16.0	0.375	725	6	6.0	7.4	1.86	2.11	1.71	1.85	9.0	8.2	2.73	2.84	2.21	2.32
15	Right Lateral Fault, $\beta=100$ deg	16.0	0.375	725	6	5.0	8.4	2.39	2.33	1.99	2.03	8.0	12.5	2.38	2.25	1.98	2.04
16	Right Lateral Fault, $\beta=110$ deg	16.0	0.375	725	6	2.0	6.5	1.53	1.54	1.37	1.44	3.5	7.6	2.16	2.02	1.76	1.80

Table 3.3: Pipe-Soil Interaction Analysis Cases and Results - NPS24 Pipe

Case Number	Model Description	Diameter (inches)	Wall Thickness (inches)	Pressure (psi)	Cover Depth (feet)	State A Ground Disp. (feet)	State A Feature Length (feet)	Exact Strain (%)	State A Deduced Strains From:			State B Ground Disp. (feet)	State B Feature Length (feet)	Exact Strain (%)	State B Deduced Strains From:		
									PIPLIN (%)	$L_{gage} = 3D$ (%)	$L_{gage} = L_{pig}$ (%)				PIPLIN (%)	$L_{gage} = 3D$ (%)	$L_{gage} = L_{pig}$ (%)
24	200' Block Subsidence	24.0	0.562	725	4	4.00	10.0	0.94	1.30	1.03	1.15	7.0	7.2	2.37	2.83	1.88	2.24
23	100' Block Subsidence	24.0	0.562	725	6	4.00	6.0	2.36	2.99	1.81	2.20	7.0	5.5	3.20	3.84	2.26	2.81
76	100' Block Subsidence, Ramp=20'	24.0	0.562	725	6	4.00	6.3	2.50	3.14	1.82	2.24	7.0	5.9	2.97	3.62	2.13	2.58
77	100' Block Subsidence, Ramp=40'	24.0	0.562	725	6	4.00	7.4	1.70	2.16	1.50	1.74	7.0	6.4	2.31	2.80	1.98	2.32
30	100' Block Landslide, 90 deg	24.0	0.562	725	6	6.00	9.7	2.33	2.68	2.25	2.39	9.0	13.0	2.35	2.62	2.23	2.31
31	100' Block Landslide, 45 deg	24.0	0.562	725	6	6.00	8.4	1.80	2.26	1.95	2.12	9.0	9.5	2.39	2.78	2.38	2.52
25	Right Lateral Fault, $\beta = 70$ deg	24.0	0.562	725	3	2.00	10.4	-0.90	-1.02	-0.88	-0.94	3.0	6.3	-3.46	-3.58	-2.28	-2.73
26	Right Lateral Fault, $\beta = 80$ deg	24.0	0.562	725	3	4.00	6.3	-3.30	-3.86	-2.63	-3.12	5.0	5.1	-5.06	-6.05	-3.76	-4.56
27	Right Lateral Fault, $\beta = 90$ deg	24.0	0.562	725	6	6.00	8.9	2.48	2.98	2.45	2.59	9.0	11.5	2.61	3.01	2.53	2.63
28	Right Lateral Fault, $\beta = 100$ deg,	24.0	0.562	725	6	6.00	11.5	2.11	2.09	1.85	1.87	9.0	16.0	2.10	2.09	1.85	1.86
29	Right Lateral Fault, $\beta = 110$ deg	24.0	0.562	725	6	6.00	13.4	2.04	1.95	1.72	1.76	9.0	18.1	2.41	2.18	1.94	1.95
65	Right Lateral Fault, $\beta = 110$ deg, Ramp=20'	24.0	0.562	725	6	6.00	13.4	2.09	2.02	1.73	1.75	9.0	17.9	2.31	2.19	1.92	1.93
66	Right Lateral Fault, $\beta = 110$ deg, Ramp=40'	24.0	0.562	725	6	6.00	11.8	2.03	1.94	1.57	1.61	9.0	15.2	2.30	2.28	1.87	1.89

Table 3.4: Pipe-Soil Interaction Analysis Cases and Results - NPS36 Pipe

Case Number	Model Description	Diameter (inches)	Wall Thickness (inches)	Pressure (psi)	Cover Depth (feet)	State A Ground Disp. (feet)	State A Feature Length (feet)	Exact Strain (%)	State A Deduced Strains From:			State B Ground Disp. (feet)	State B Feature Length (feet)	Exact Strain (%)	State B Deduced Strains From:		
									PIPLIN (%)	$L_{gage} = 3D$ (%)	$L_{gage} = L_{pig}$ (%)				PIPLIN (%)	$L_{gage} = 3D$ (%)	$L_{gage} = L_{pig}$ (%)
33	200' Block Subsidence	36.0	0.500	1000	4	4.0	11.2	1.06	1.54	1.06	1.33	7.0	7.6	2.79	3.47	2.03	2.79
32	100' Block Subsidence	36.0	0.500	1000	6	3.0	8.4	1.58	2.27	1.31	1.76	4.0	6.8	2.52	3.39	1.83	2.60
78	100' Block Subsidence, Ramp=20'	36.0	0.500	1000	6	3.0	8.5	1.58	2.27	1.32	1.77	4.0	7.6	2.08	2.86	1.61	2.24
79	100' Block Subsidence, Ramp=40'	36.0	0.500	1000	6	3.0	10.0	1.05	1.53	1.13	1.43	4.0	8.7	1.47	2.05	1.42	1.93
39	100' Block Landslide, 90 deg	36.0	0.500	1000	6	6.0	9.0	3.36	4.00	3.20	3.84	9.0	11.2	3.87	4.39	3.66	4.14
40	100' Block Landslide, 45 deg	36.0	0.500	1000	6	6.0	8.2	2.49	3.33	2.52	3.21	9.0	8.9	3.55	4.34	3.42	4.17
34	Right Lateral Fault, $\beta = 70$ deg	36.0	0.500	1000	3	2.0	9.3	-1.66	-1.66	-1.31	-1.60	2.5	7.2	-3.23	-3.13	-2.08	-2.81
35	Right Lateral Fault, $\beta = 80$ deg	36.0	0.500	1000	3	3.0	8.1	-2.78	-2.96	-2.02	-2.69	4.0	6.2	-4.57	-4.87	-3.17	-4.43
36	Right Lateral Fault, $\beta = 90$ deg	36.0	0.500	1000	6	6.0	8.3	3.50	4.41	3.31	3.96	9.0	10.5	4.09	4.85	3.86	4.30
37	Right Lateral Fault, $\beta = 100$ deg	36.0	0.500	1000	6	6.0	10.9	3.36	3.25	2.73	2.92	9.0	15.1	3.47	3.35	2.84	2.94
67	Right Lateral Fault, $\beta = 100$ deg, Ramp=20'	36.0	0.500	1000	6	6.0	10.8	3.42	3.31	2.75	2.91	9.0	14.9	3.47	3.36	2.85	2.90
68	Right Lateral Fault, $\beta = 100$ deg, Ramp=40'	36.0	0.500	1000	6	6.0	10.9	2.88	2.73	2.24	2.50	9.0	13.4	3.44	3.23	2.74	2.86
38	Right Lateral Fault, $\beta = 110$ deg	36.0	0.500	1000	6	6.0	12.8	3.25	3.00	2.57	2.66	9.0	17.0	3.74	3.36	3.06	3.19

Table 3.5: Pipe-Soil Interaction Analysis Cases and Results - NPS48 Pipe

Case Number	Model Description	Diameter (inches)	Wall Thickness (inches)	Pressure (psi)	Cover Depth (feet)	State A Ground Disp. (feet)	State A Feature Length (feet)	Exact Strain (%)	State A Deduced Strains From:			State B Ground Disp. (feet)	State B Feature Length (feet)	Exact Strain (%)	State B Deduced Strains From:		
									PIPLIN (%)	$L_{gage} = 3D$ (%)	$L_{gage} = L_{pig}$ (%)				PIPLIN (%)	$L_{gage} = 3D$ (%)	$L_{gage} = L_{pig}$ (%)
42	200' Block Subsidence	48.0	0.562	1000	4	6.0	11.0	1.97	2.62	1.48	1.93	9.0	9.1	3.14	3.86	2.14	2.93
80	200' Block Subsidence, Ramp=20'	48.0	0.562	1000	4	6.0	11.1	1.95	2.59	1.49	1.94	9.0	9.2	3.04	3.75	2.07	2.78
81	200' Block Subsidence, Ramp=40'	48.0	0.562	1000	4	6.0	11.1	1.94	2.58	1.48	1.93	9.0	9.4	2.94	3.64	2.04	2.78
41	100' Block Subsidence	48.0	0.562	1000	6	6.0	17.3	0.33	0.53	0.52	0.53	9.0	17.3	0.33	0.53	0.52	0.53
48	100' Block Landslide, 90 deg	48.0	0.562	1000	6	6.0	10.0	3.16	3.90	2.96	3.65	9.0	11.4	4.19	4.81	3.85	4.49
49	100' Block Landslide, 45 deg	48.0	0.562	1000	6	6.0	10.4	2.11	3.01	2.17	2.71	9.0	10.3	3.29	4.28	3.20	3.98
43	Right Lateral Fault, $\beta = 70$ deg	48.0	0.562	1000	3	2.0	12.8	-1.19	-1.22	-1.00	-1.14	3.0	8.3	-3.51	-3.37	-2.25	-2.99
44	Right Lateral Fault, $\beta = 80$ deg	48.0	0.562	1000	3	3.0	11.4	-1.95	-2.08	-1.51	-1.83	5.0	7.3	-5.13	-5.44	-3.37	-4.62
45	Right Lateral Fault, $\beta = 90$ deg	48.0	0.562	1000	6	6.0	9.4	3.30	4.29	3.01	3.69	9.0	10.7	4.32	5.21	3.97	4.52
46	Right Lateral Fault, $\beta = 100$ deg	48.0	0.562	1000	6	6.0	12.0	3.47	3.38	2.71	2.95	9.0	15.6	3.89	3.68	3.06	3.17
69	Right Lateral Fault, $\beta = 100$ deg, Ramp=20'	48.0	0.562	1000	6	6.0	11.9	3.45	3.36	2.73	2.97	9.0	15.5	3.83	3.62	3.06	3.14
70	Right Lateral Fault, $\beta = 100$ deg, Ramp=40'	48.0	0.562	1000	6	6.0	12.0	3.26	3.13	2.41	2.76	9.0	14.7	4.03	3.73	3.03	3.27
47	Right Lateral Fault, $\beta = 110$ deg	48.0	0.562	1000	6	6.0	13.5	3.50	3.18	2.69	2.83	9.0	18.1	3.64	3.29	2.89	2.98

Table 3.6: Pipe-Soil Interaction Analysis Cases and Results – NPS10 Pipe

Case Number	Model Description	Diameter (inches)	Wall Thickness (inches)	Pressure (psi)	Cover Depth (feet)	State A Ground Disp. (feet)	State A Feature Length (feet)	Exact Strain (%)	State A Deduced Strains From:			State B Ground Disp. (feet)	State B Feature Length (feet)	Exact Strain (%)	State B Deduced Strains From:		
									PIPLIN (%)	$L_{gage} = 3D$ (%)	$L_{gage} = L_{pig}$ (%)				PIPLIN (%)	$L_{gage} = 3D$ (%)	$L_{gage} = L_{pig}$ (%)
59	Block Subsidence High Side of Riser	10.75	0.594	1480	3	6	5.6	1.26	2.33	1.97	2.19	9	4.7	2.14	3.88	3.25	3.62
60	Block Subsidence Low Side of Riser	10.75	0.594	1480	3	6	5.0	1.60	2.60	2.22	2.47	9	3.8	2.72	4.46	3.86	4.27

FIGURES

Figure 3.1: Pipe Strain Profiles for State A: 4' of Subsidence over 100' Long Block Profile, D=16", 6' of Sand Cover

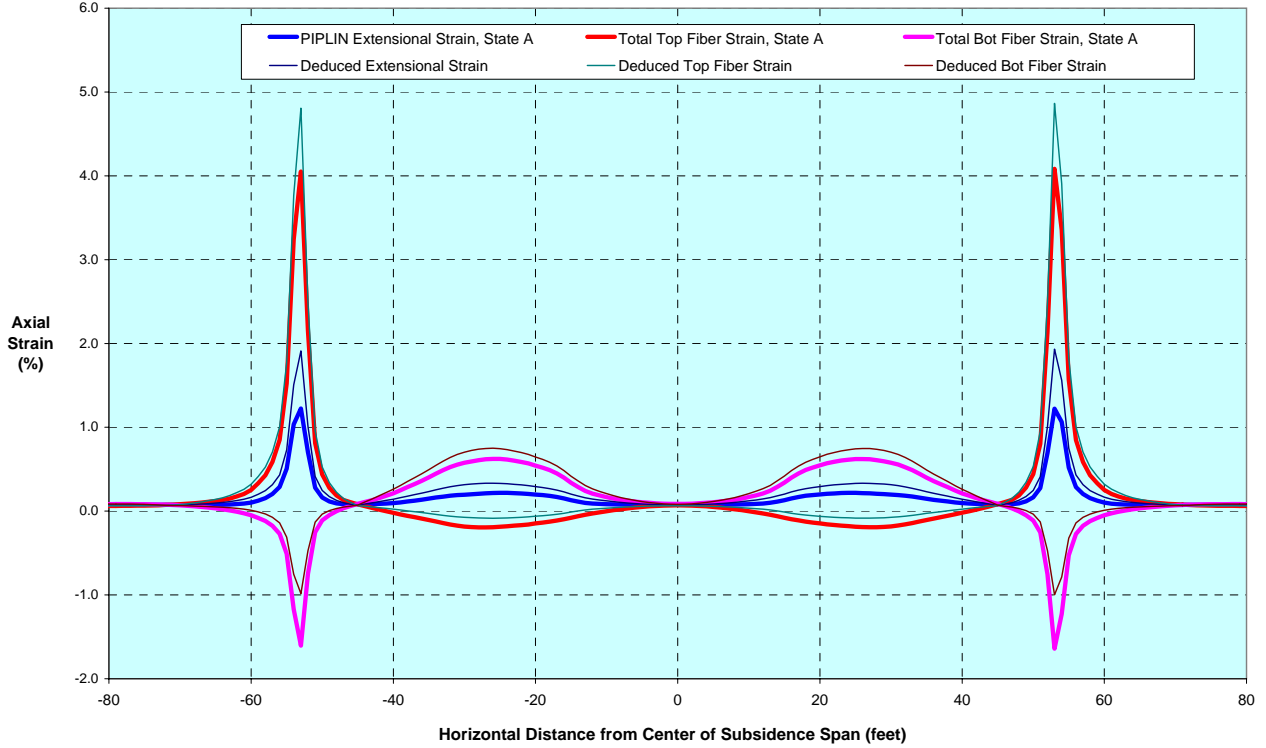
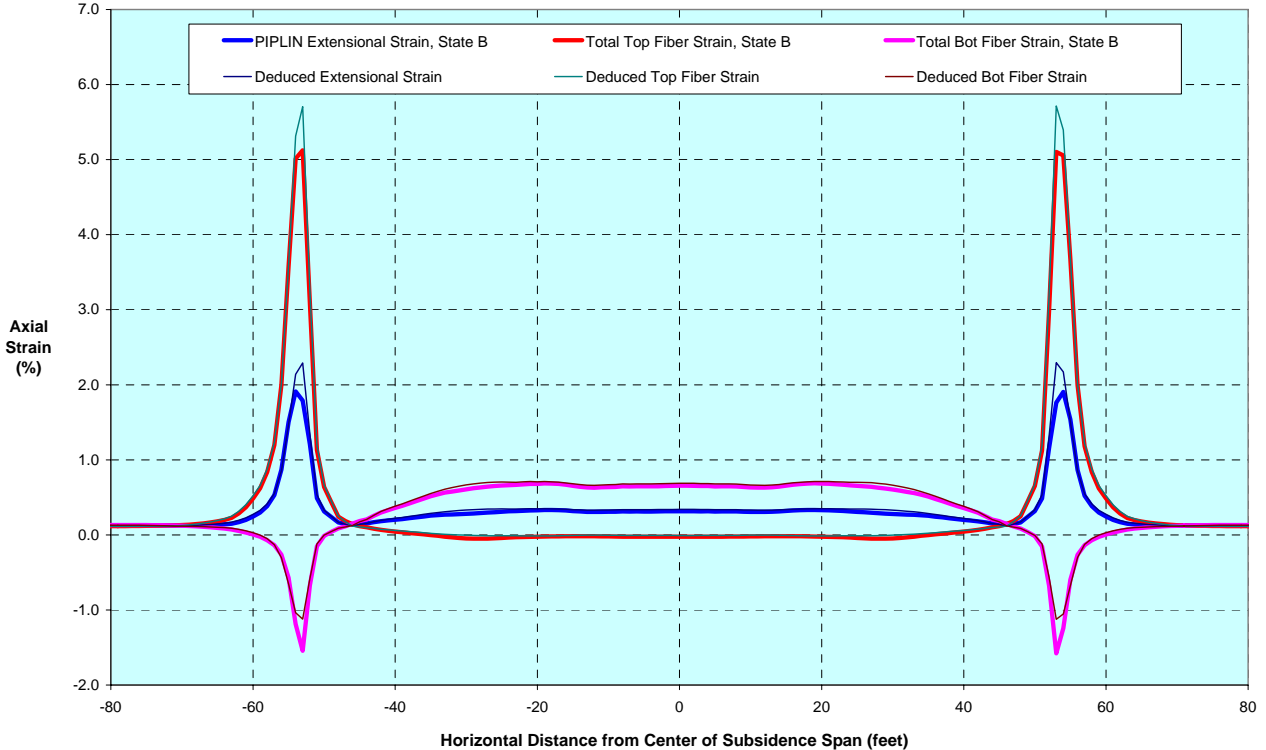
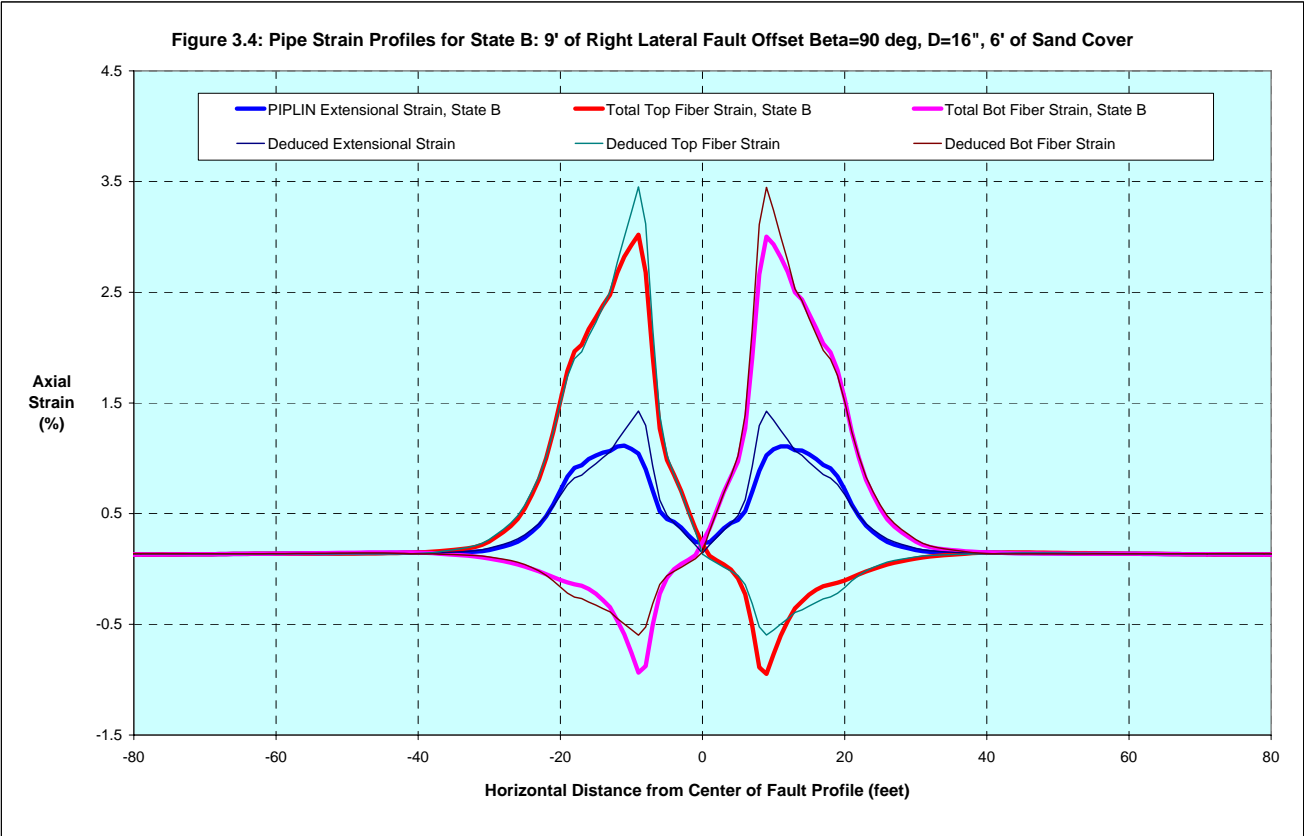
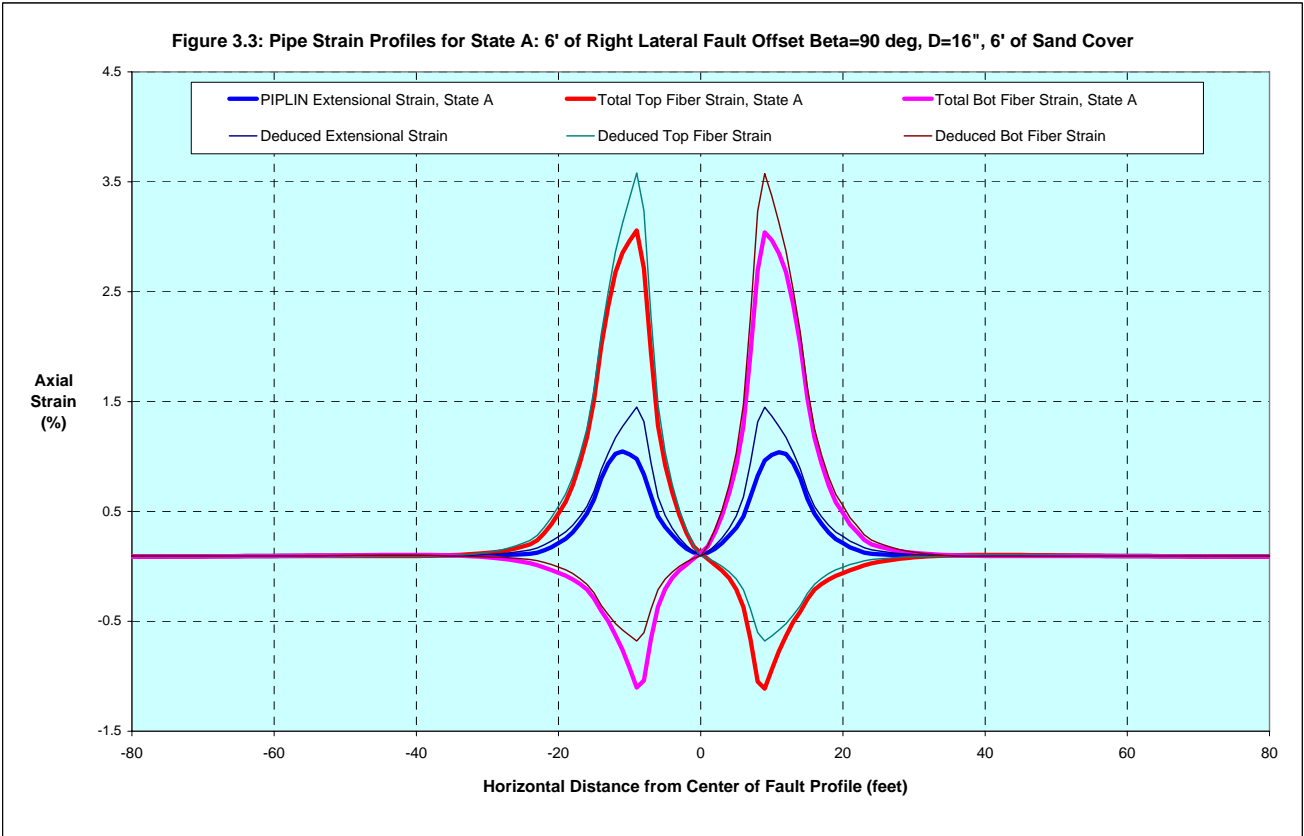


Figure 3.2: Pipe Strain Profiles for State B: 7' of Subsidence over 100' Long Block Profile, D=16", 6' of Sand Cover





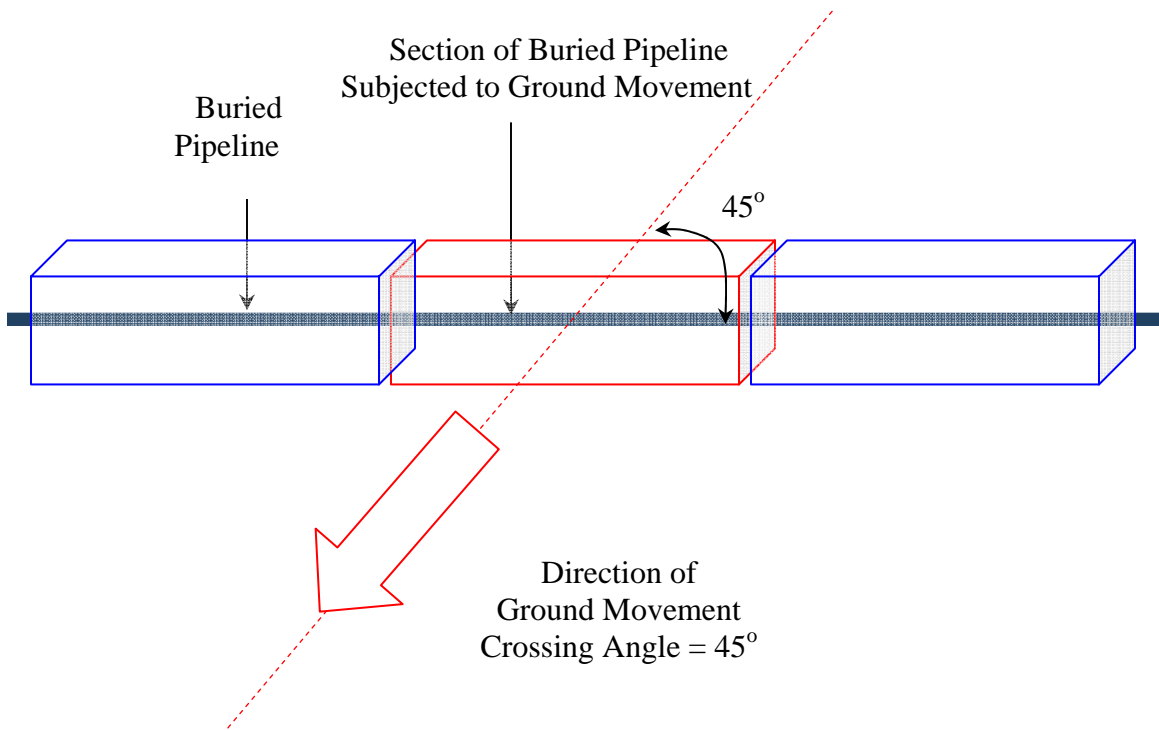
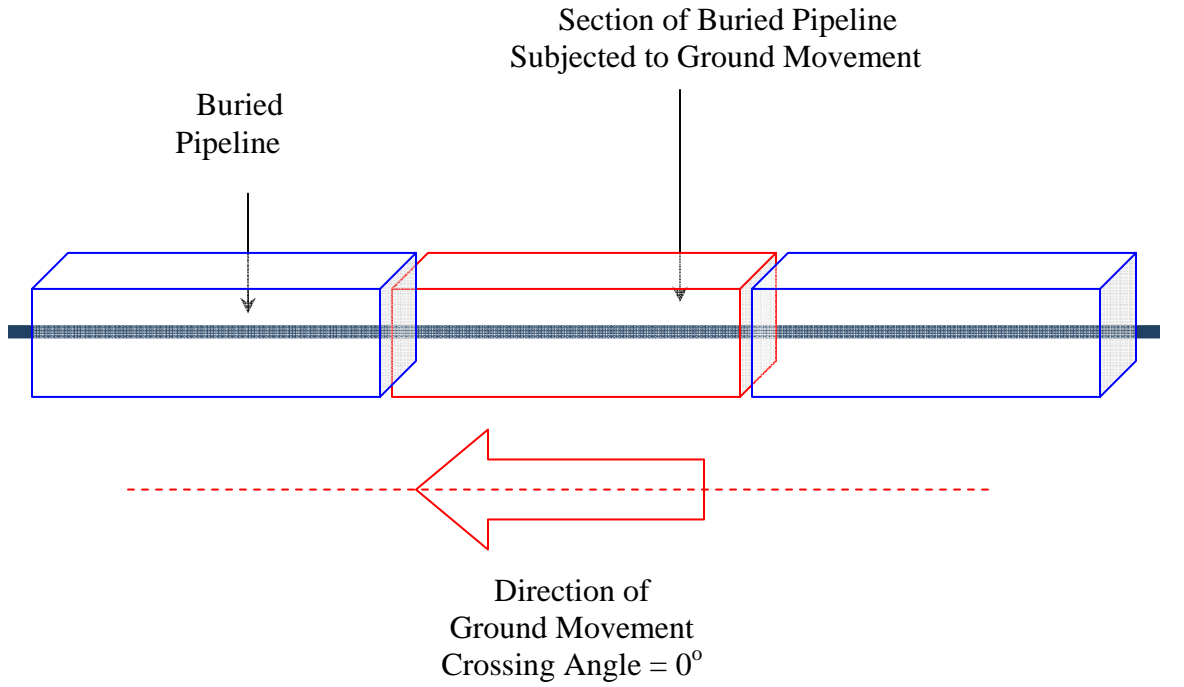
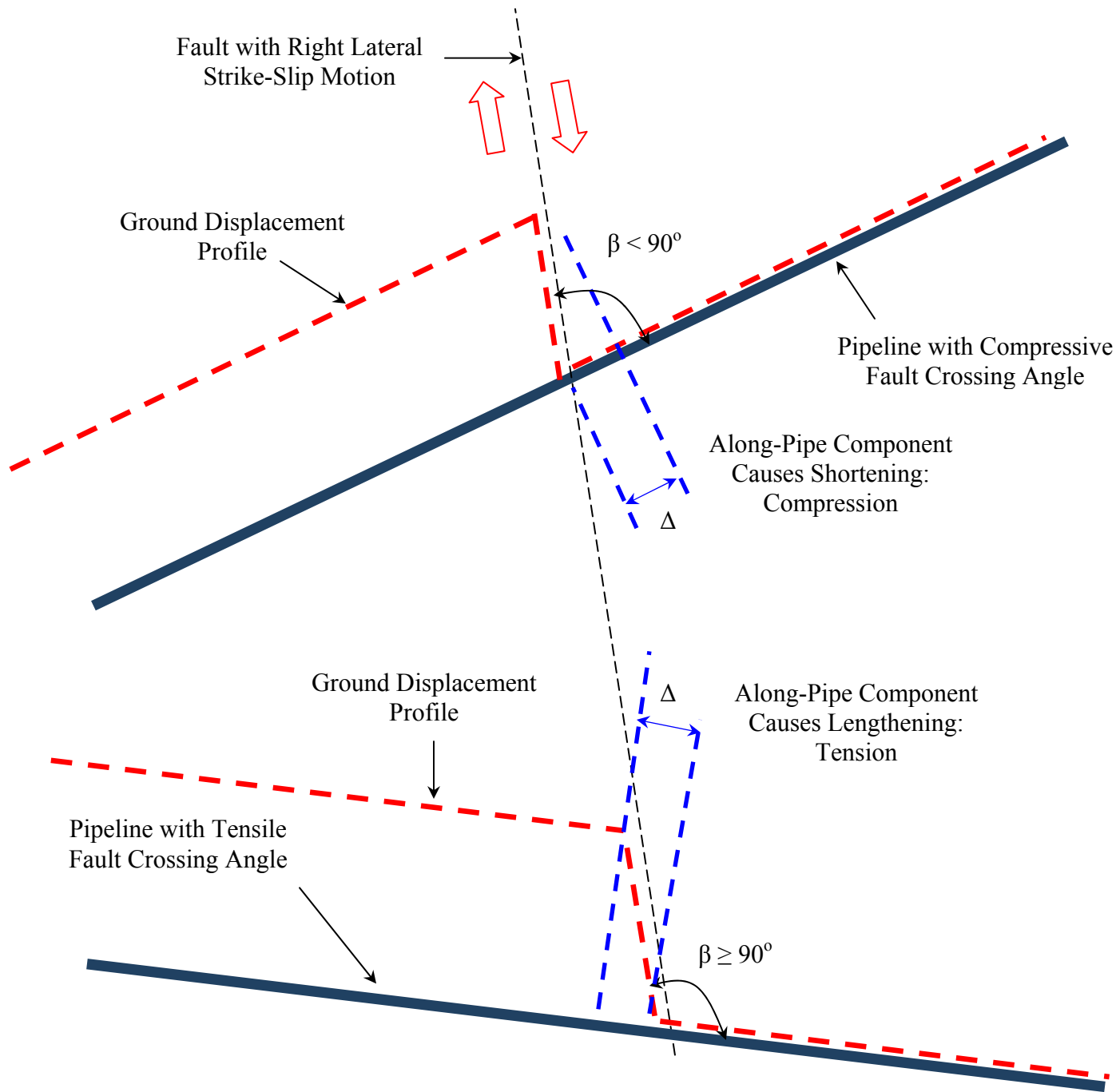
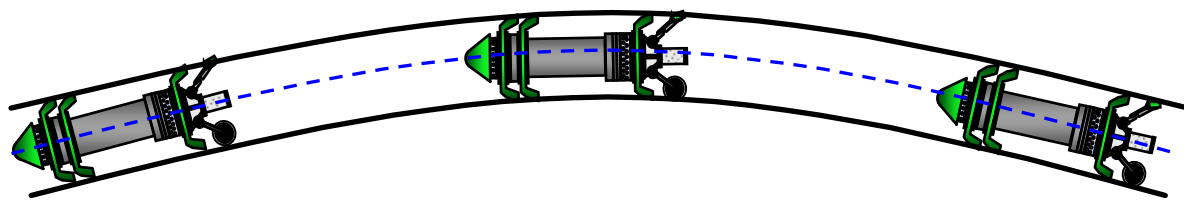


Figure 3.5: Plan View of Pipeline Crossing a Horizontal Landslide: Schematic Illustration of Different Crossing Angles

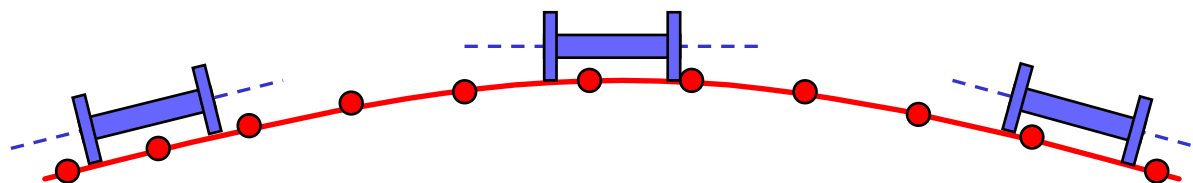


$$\begin{aligned} \text{Fault Offset} &= \Delta \\ \text{Transverse-to-Pipe Component} &= \Delta \cdot \sin \beta \\ \text{Along-Pipe Component} &= \Delta \cdot \cos \beta \end{aligned}$$

Figure 3.6: Plan View of Pipelines Crossing a Right Lateral, Strike-Slip Fault Schematic Illustration of Effect of Pipeline Fault Crossing Angle β



Geometry Pig Traversing Real Pipeline Profile



Digital Pig Traversing Analytical Pipeline Profile

Figure 3.7: Overview of Digital Pigging Concept

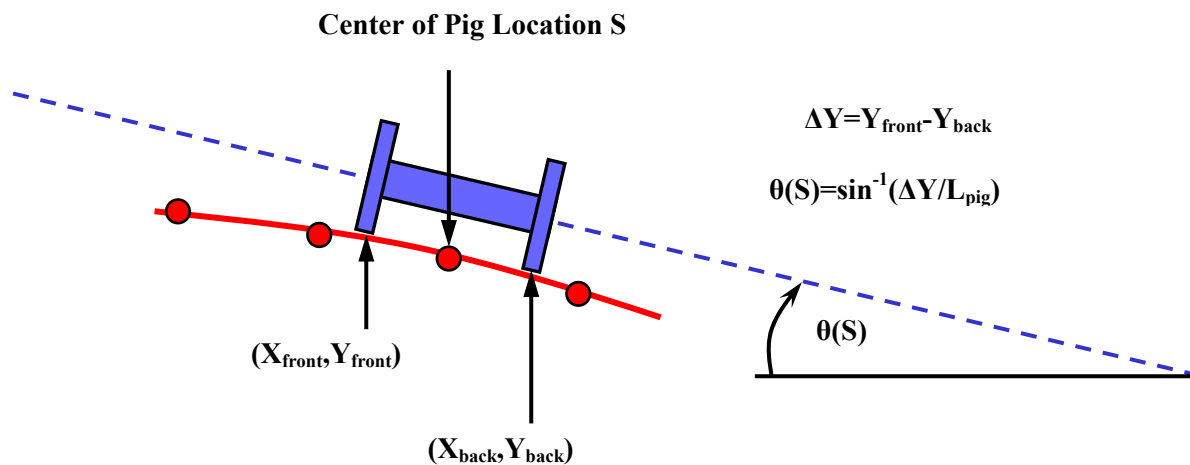


Figure 3.8: First Pass Calculations to Compute Profile of Pig Pitch Angle $\theta(S)$ Based on Elevation Change (ΔY) Over Length of Pig

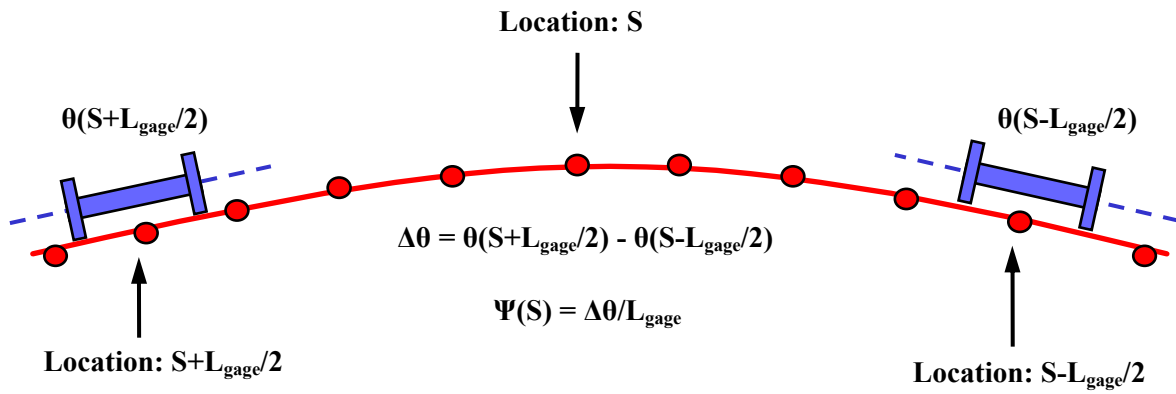


Figure 3.9: Second Pass Calculations to Compute Profile of Vertical Curvature $\Psi(S)$ Based on Pitch Angle Change ($\Delta\theta$) Over Gage Length

Figure 3.10 (a): 8-inch Pipe: Comparison of Governing Normalized Strains - State A

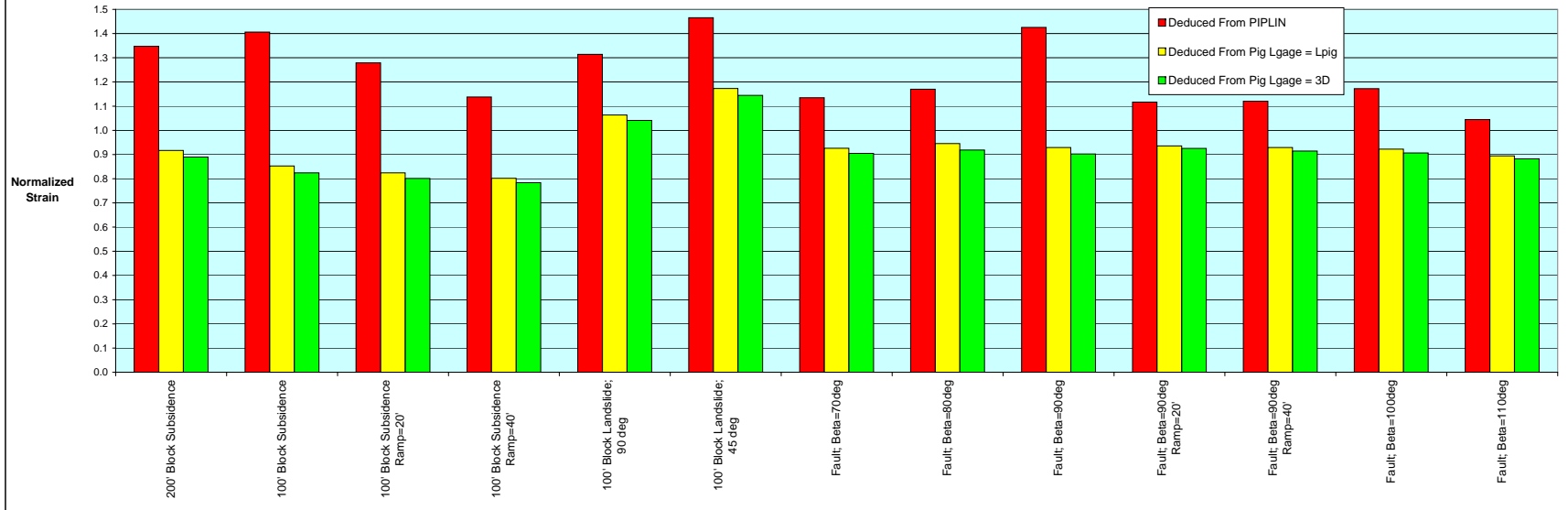


Figure 3.10 (b): 8-inch Pipe: Comparison of Governing Normalized Strains - State B

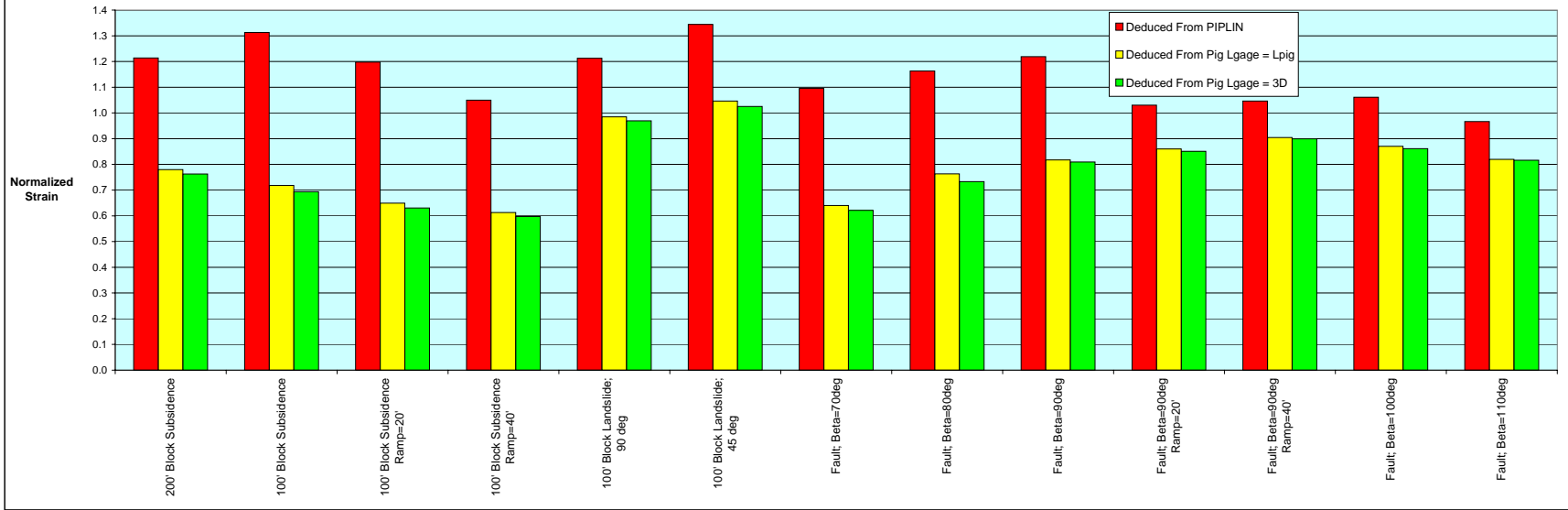


Figure 3.11 (a): 16-inch Pipe: Comparison of Governing Normalized Strains - State A

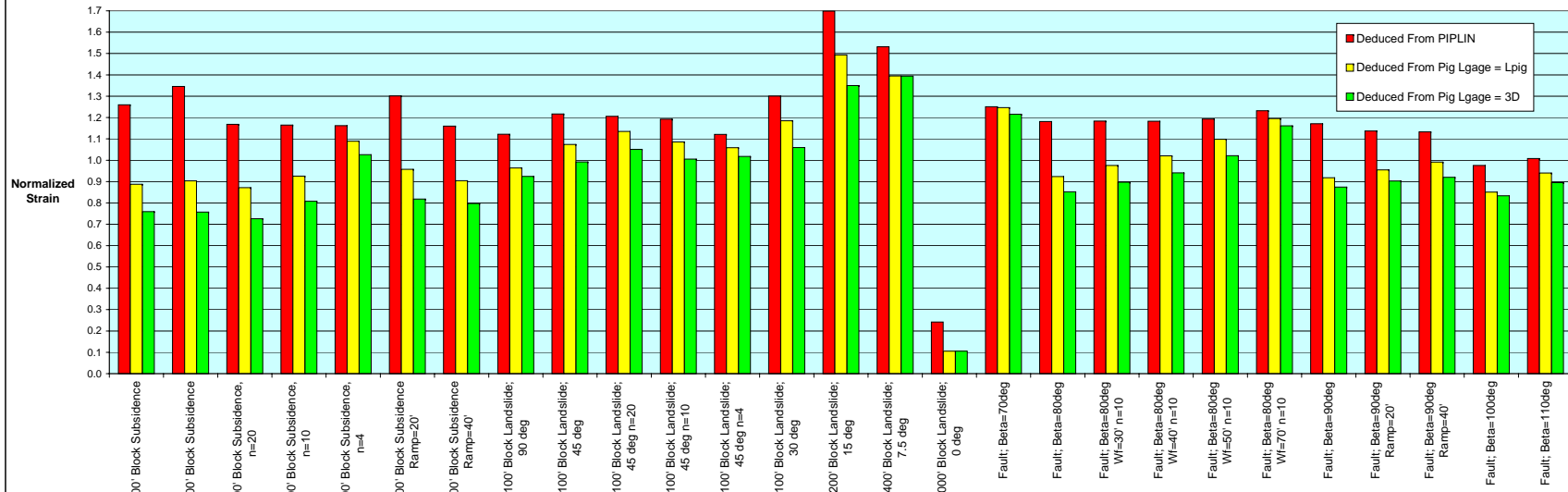


Figure 3.11 (b): 16-inch Pipe: Comparison of Governing Normalized Strains - State B

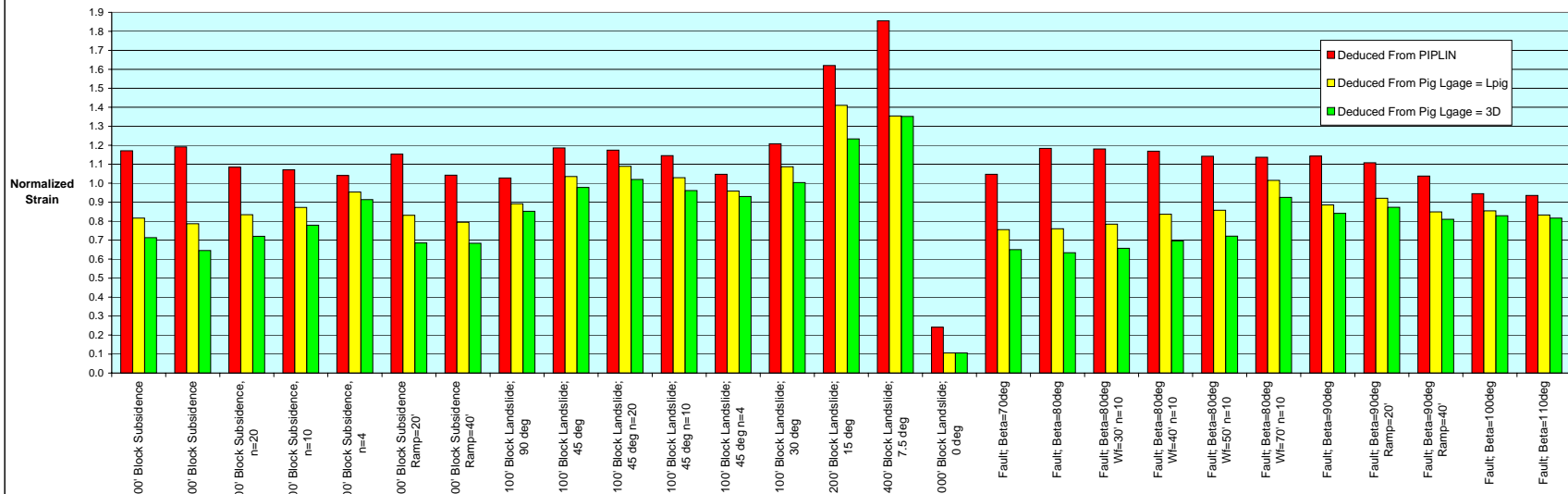


Figure 3.12 (a): 24-inch Pipe: Comparison of Governing Normalized Strains - State A

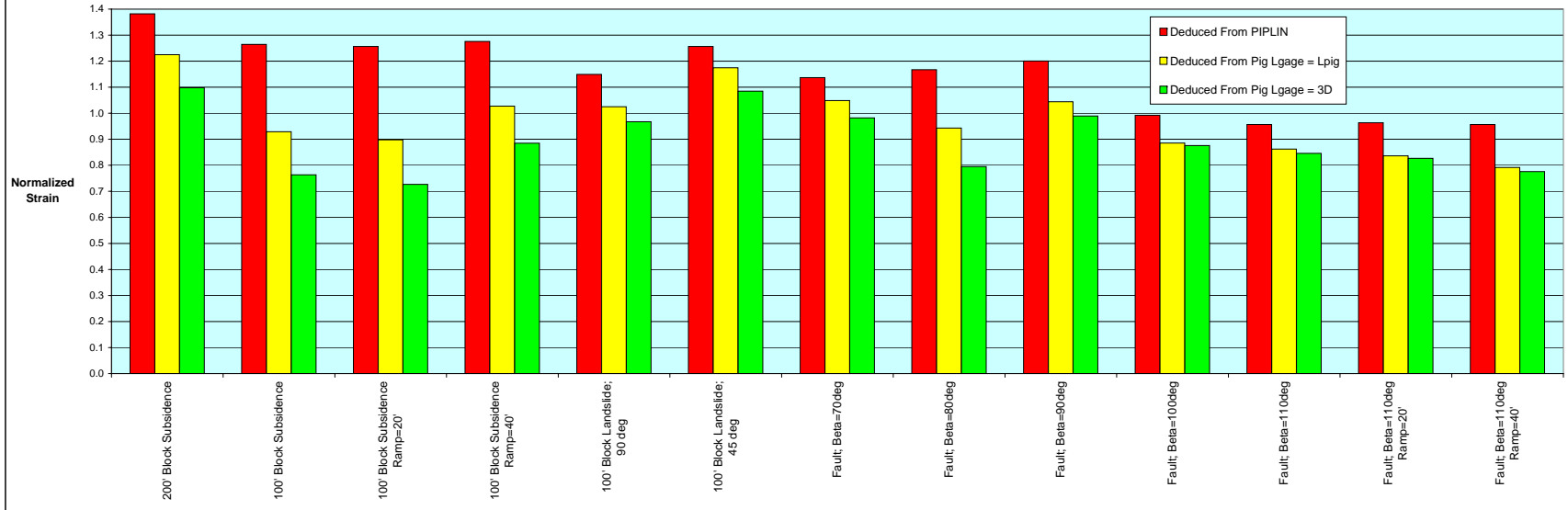


Figure 3.12 (b): 24-inch Pipe: Comparison of Governing Normalized Strains - State B

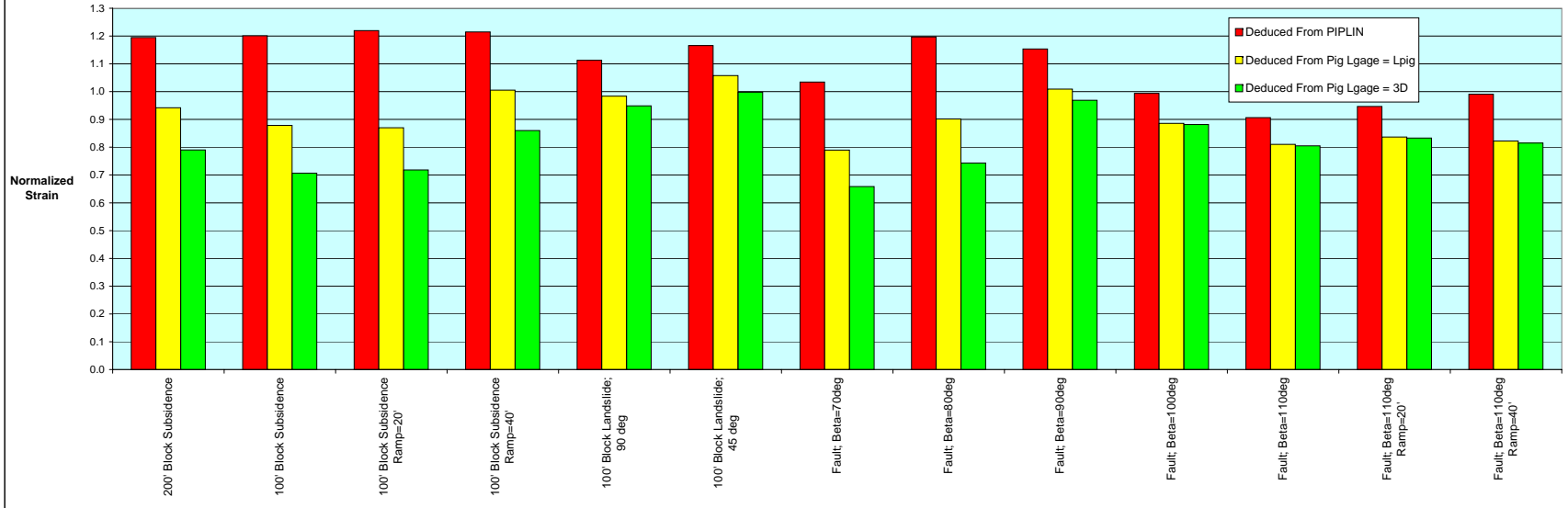


Figure 3.13 (a): 36-inch Pipe: Comparison of Governing Normalized Strains - State A

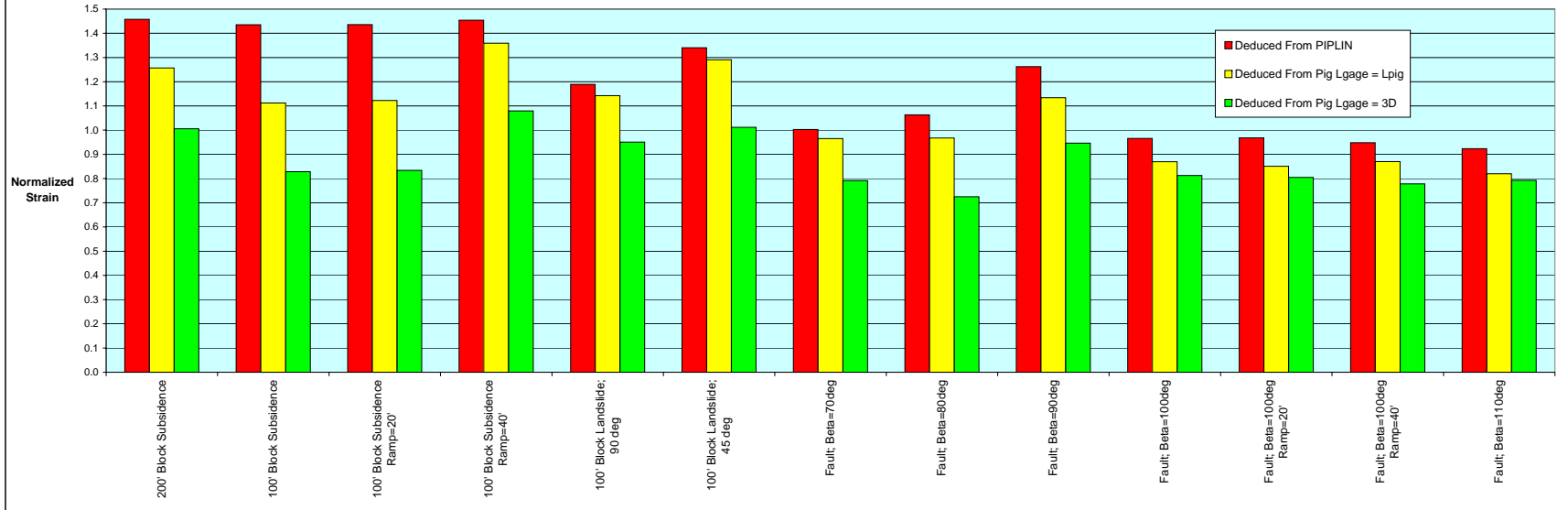


Figure 3.13 (b): 36-inch Pipe: Comparison of Governing Normalized Strains - State B

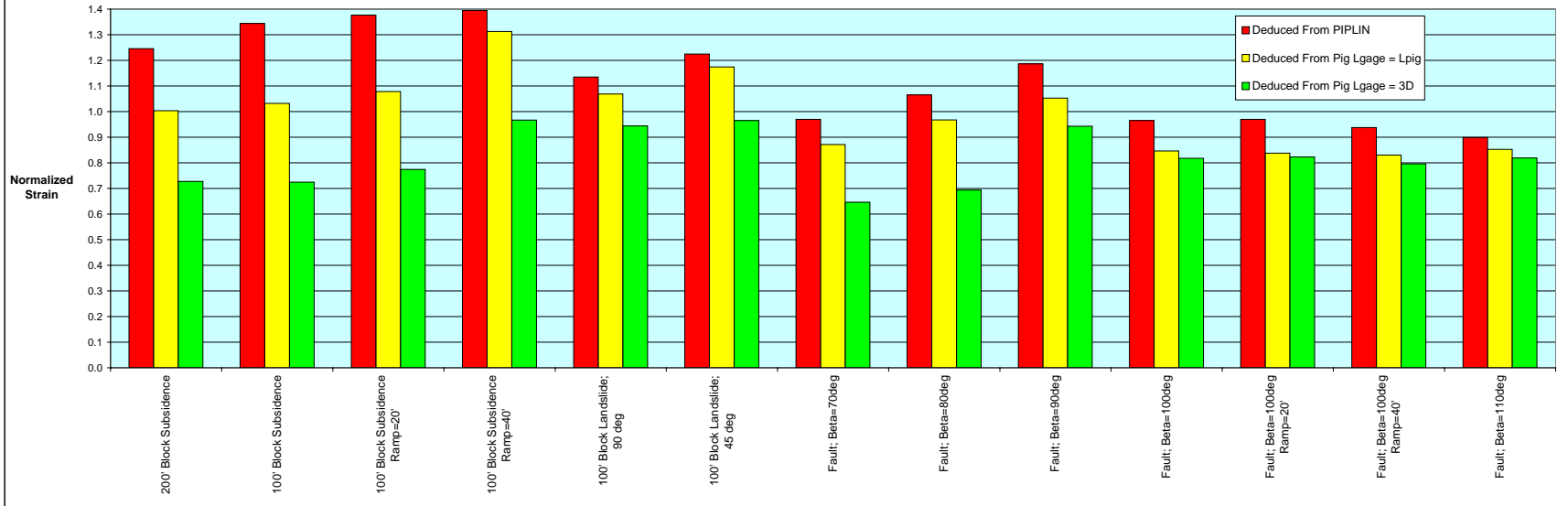


Figure 3.14 (a): 48-inch Pipe: Comparison of Governing Normalized Strains - State A

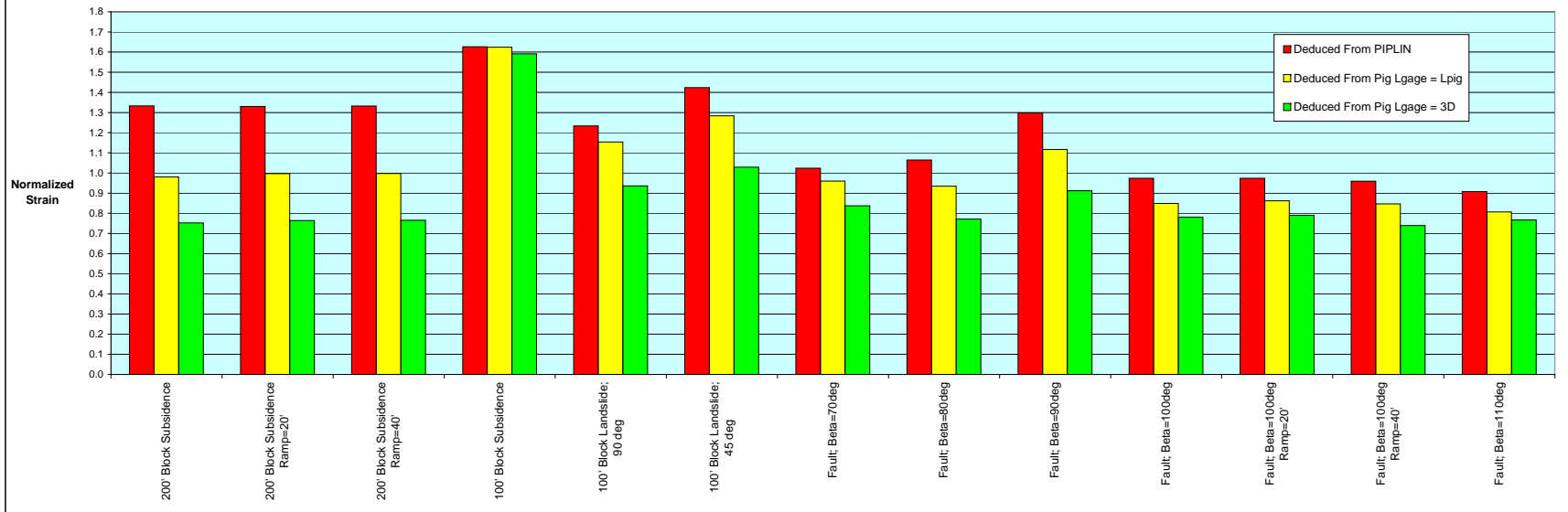


Figure 3.14 (b): 48-inch Pipe: Comparison of Governing Normalized Strains - State B

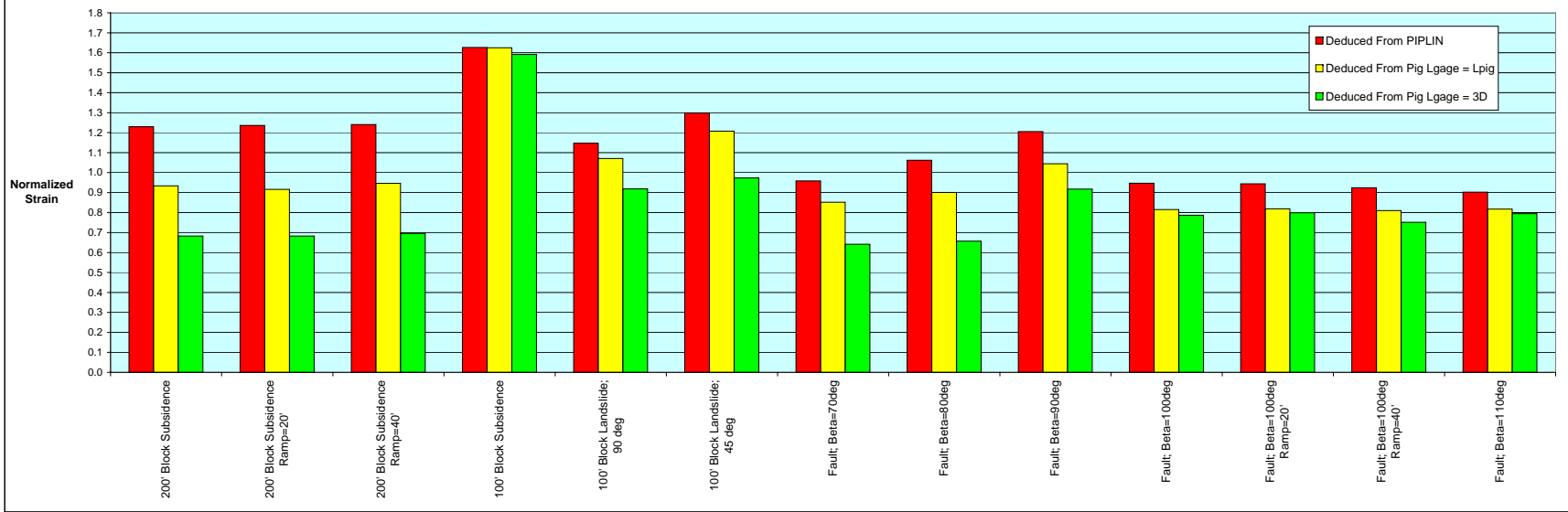


Figure 3.15 (a): NPS 8 Cases, Exact vs. Deduced with Lgage = Lpig

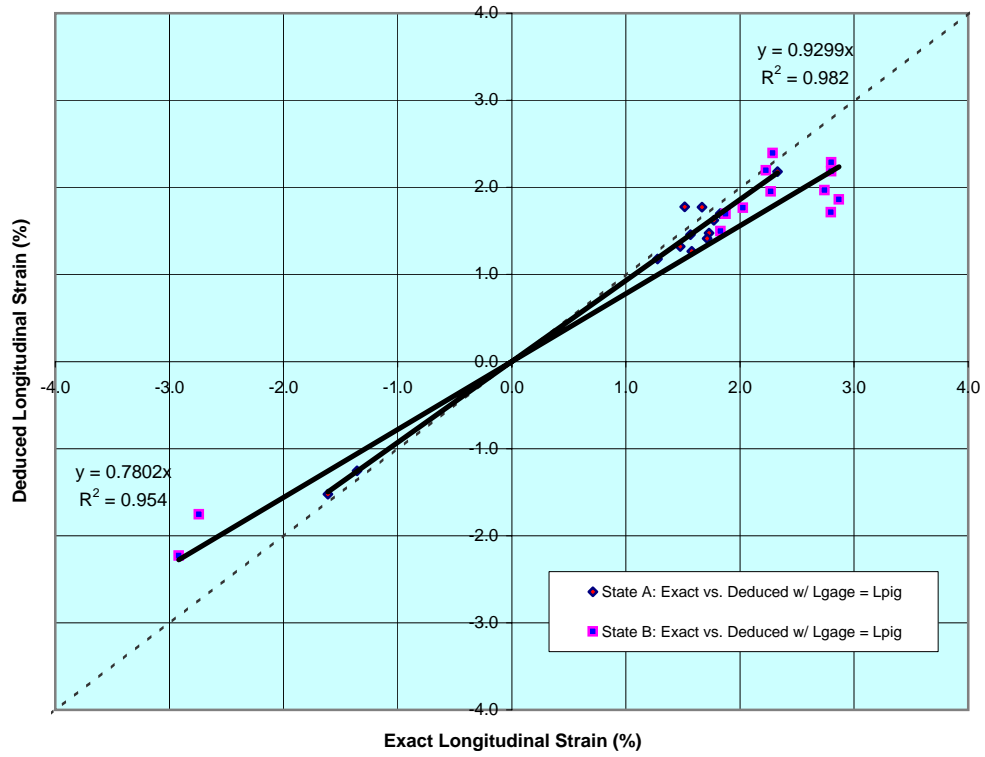


Figure 3.15 (b): NPS 8 Cases, Exact vs. Deduced with Lgage = 3D

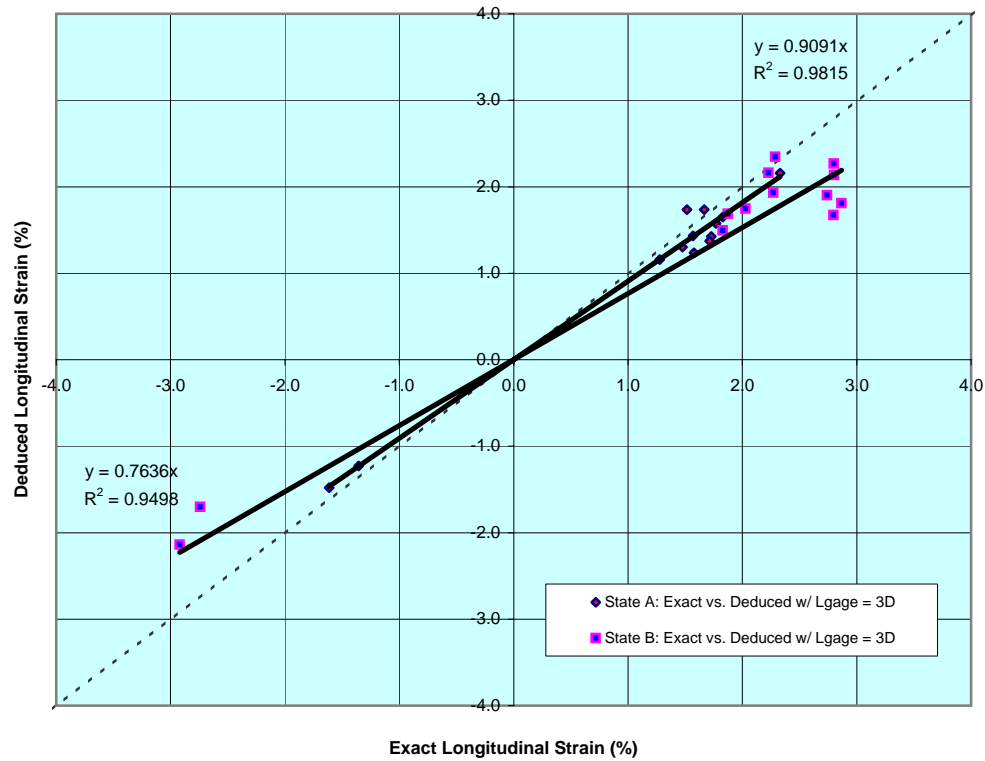


Figure 3.16 (a): NPS 16 Cases, Exact vs. Deduced with Lgage = Lpig

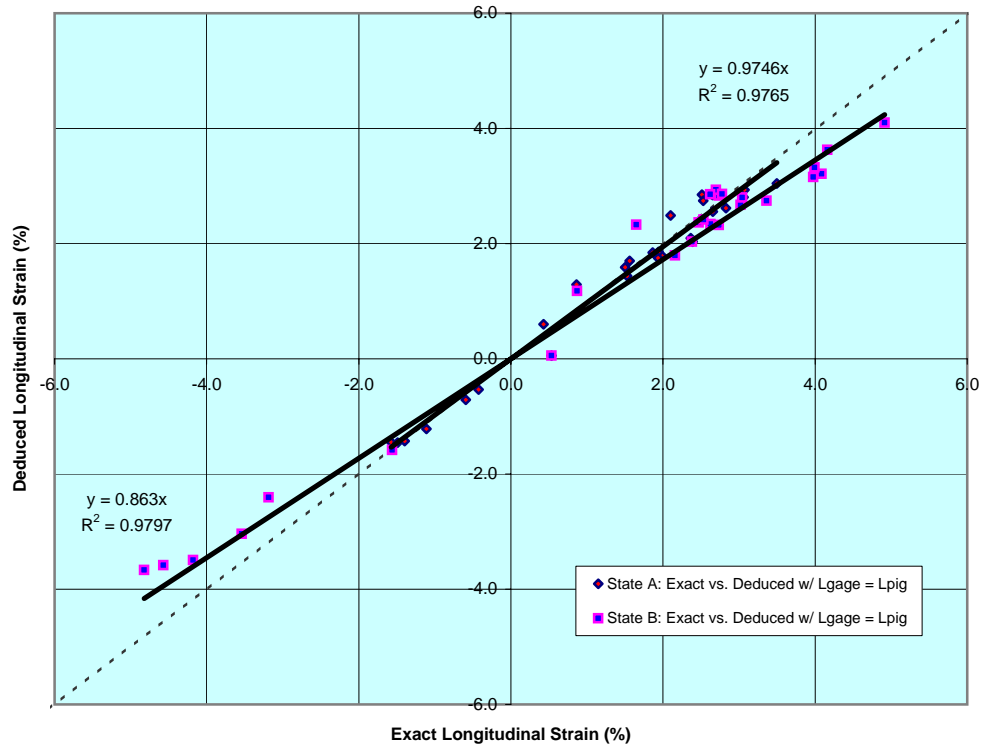


Figure 3.16 (b): NPS 16 Cases, Exact vs. Deduced with Lgage = 3D

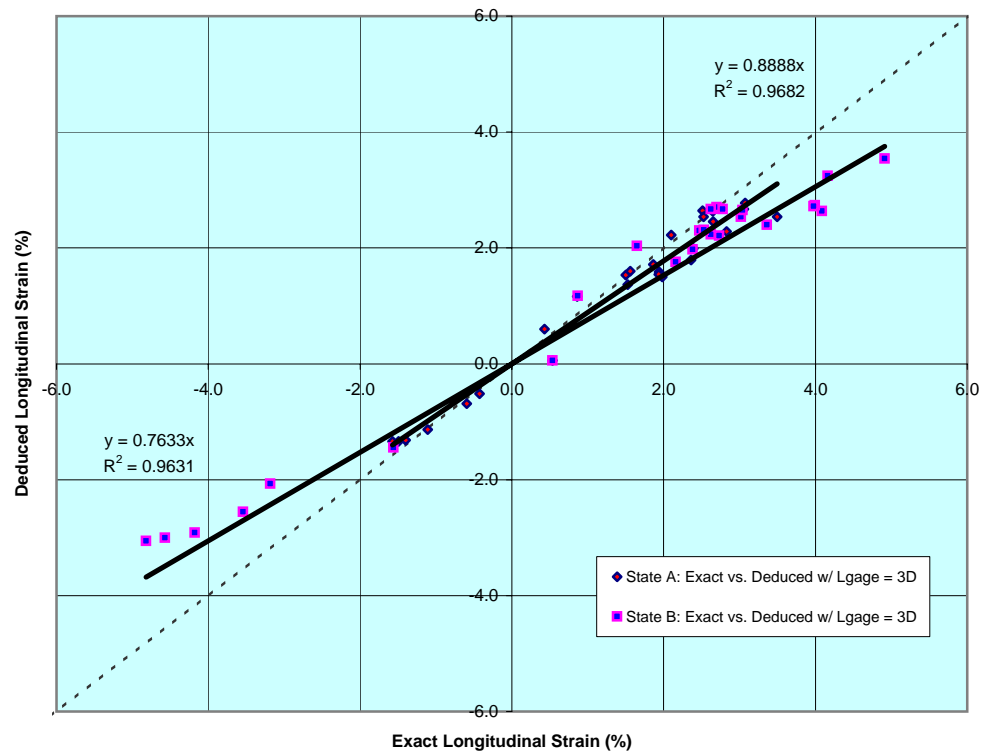


Figure 3.17 (a): NPS 24 Cases, Exact vs. Deduced with Lgage = Lpig

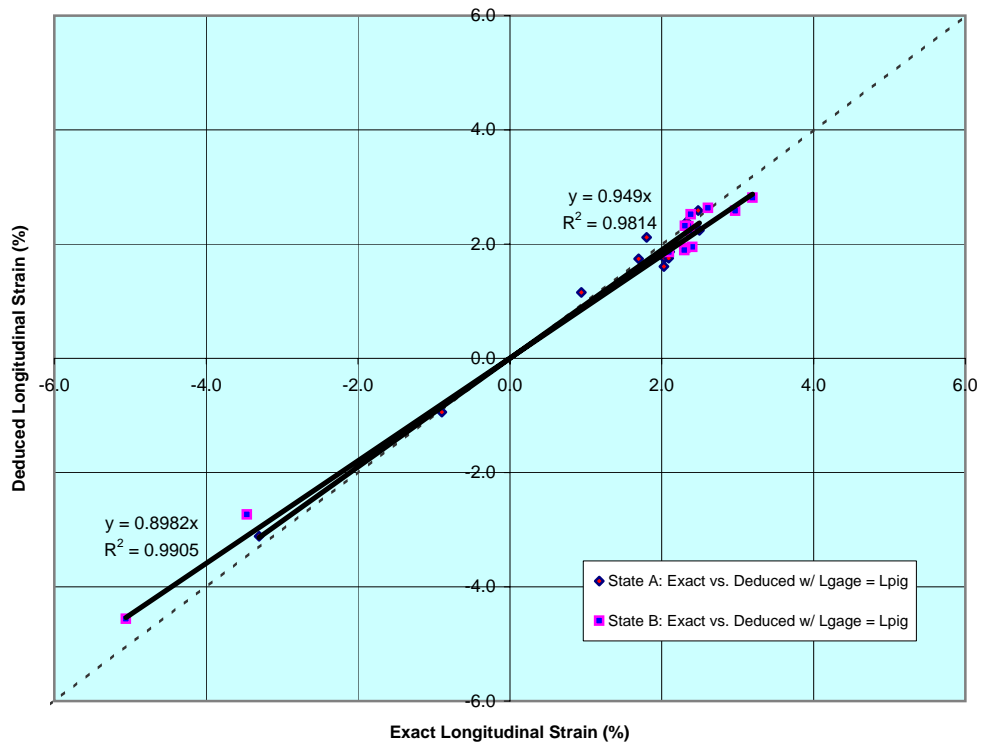


Figure 3.17 (b): NPS 24 Cases, Exact vs. Deduced with Lgage = 3D

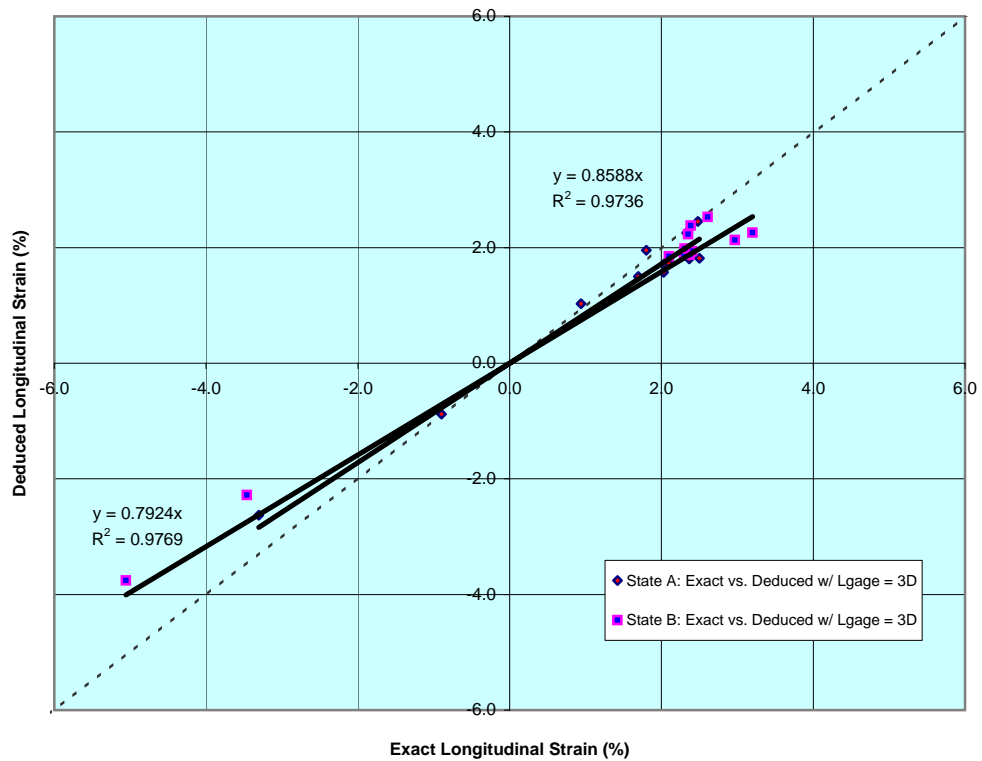


Figure 3.18 (a): NPS 36 Cases, Exact vs. Deduced with Lgage = Lpig

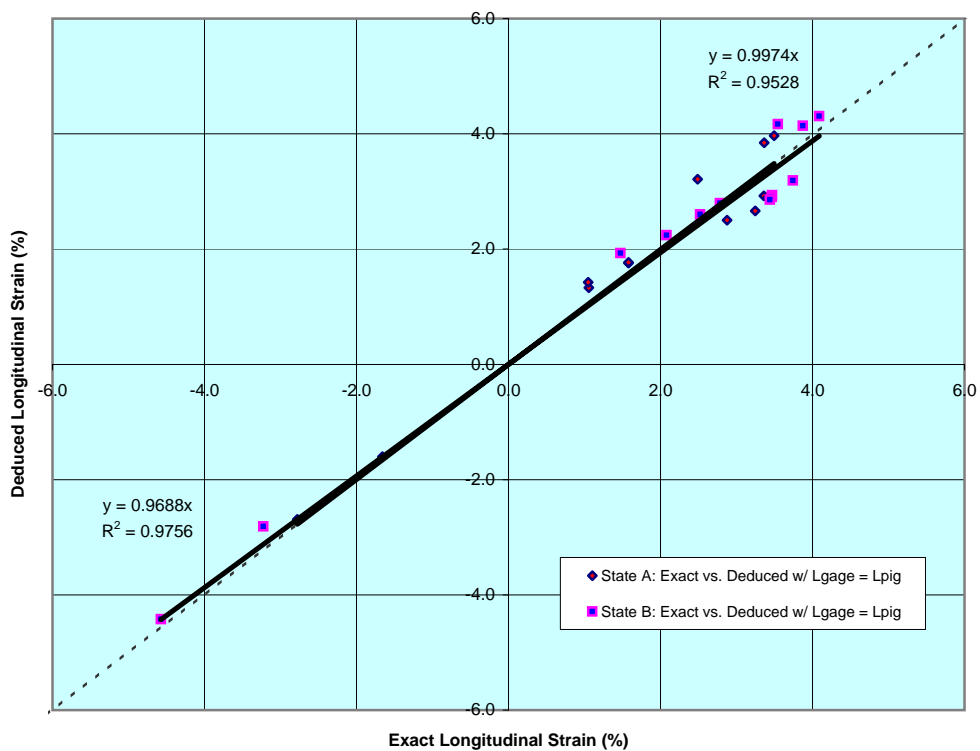


Figure 3.18 (b): NPS 36 Cases, Exact vs. Deduced with Lgage = 3D

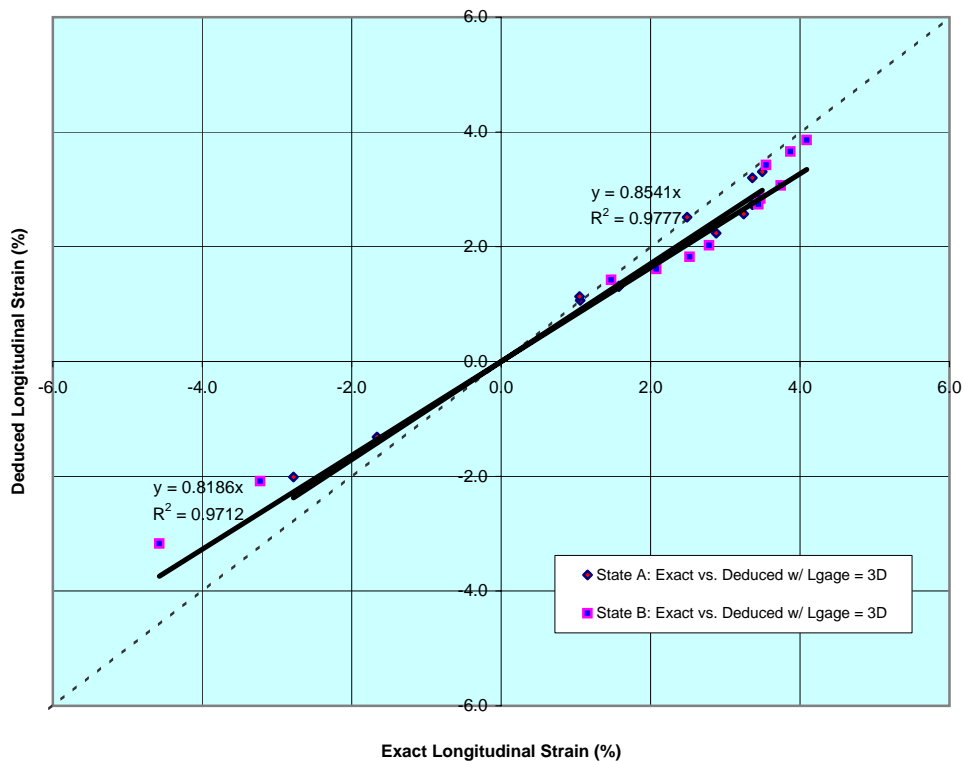


Figure 3.19 (a): NPS 48 Cases, Exact vs. Deduced with Lgage = Lpig

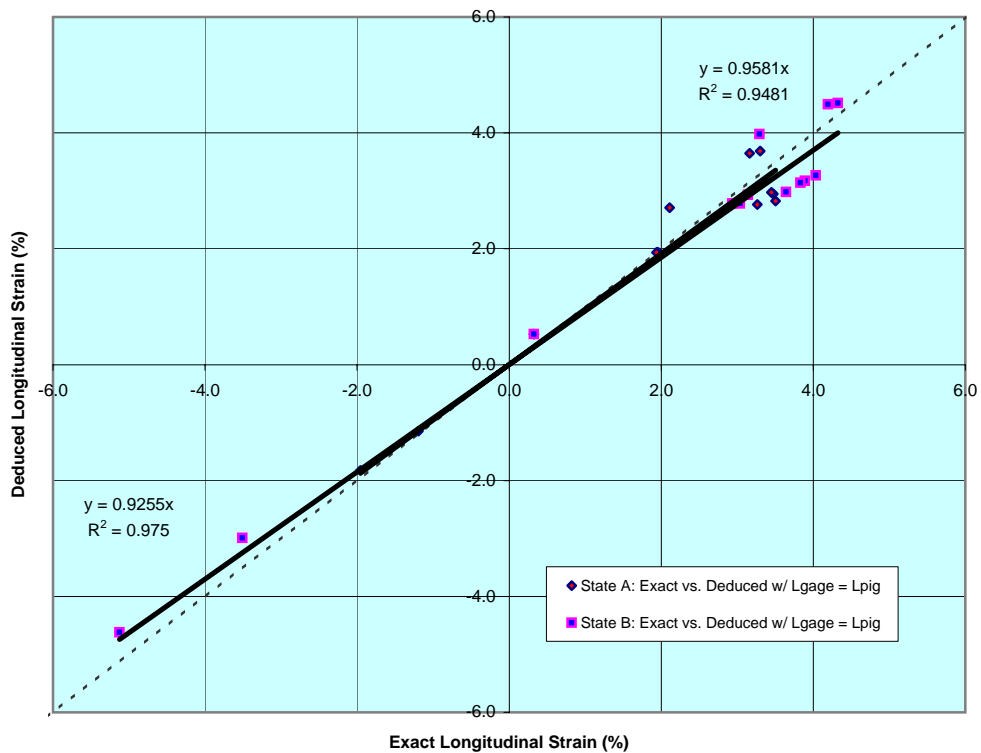


Figure 3.19 (b): NPS 48 Cases, Exact vs. Deduced with Lgage = 3D

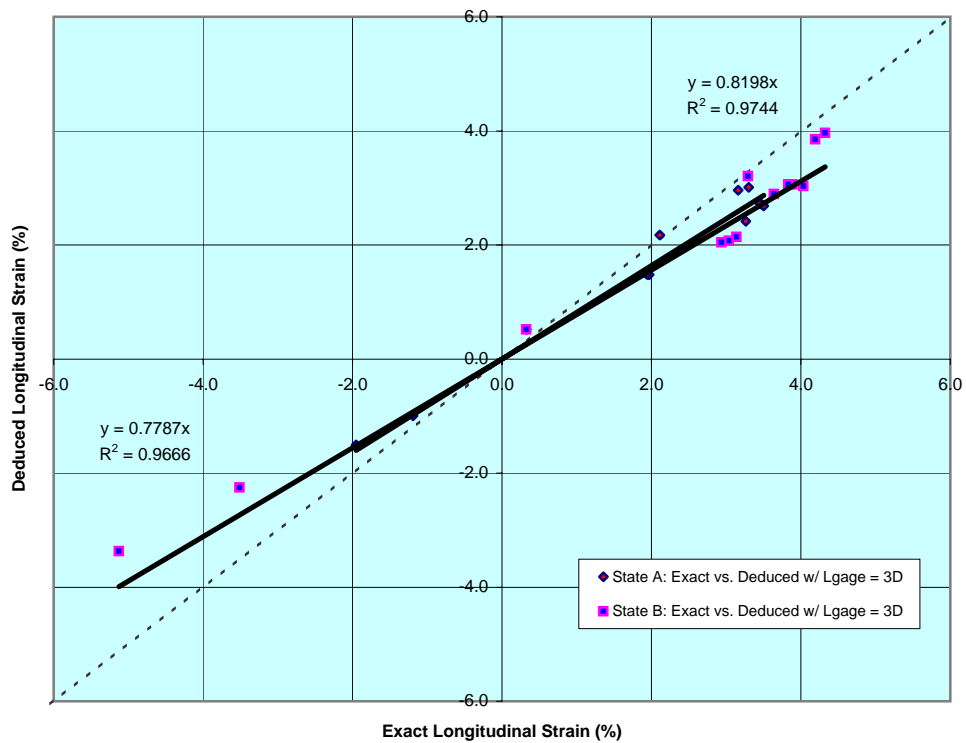


Figure 3.20 (a): Slope of Regression Line with Zero Intercept, State A

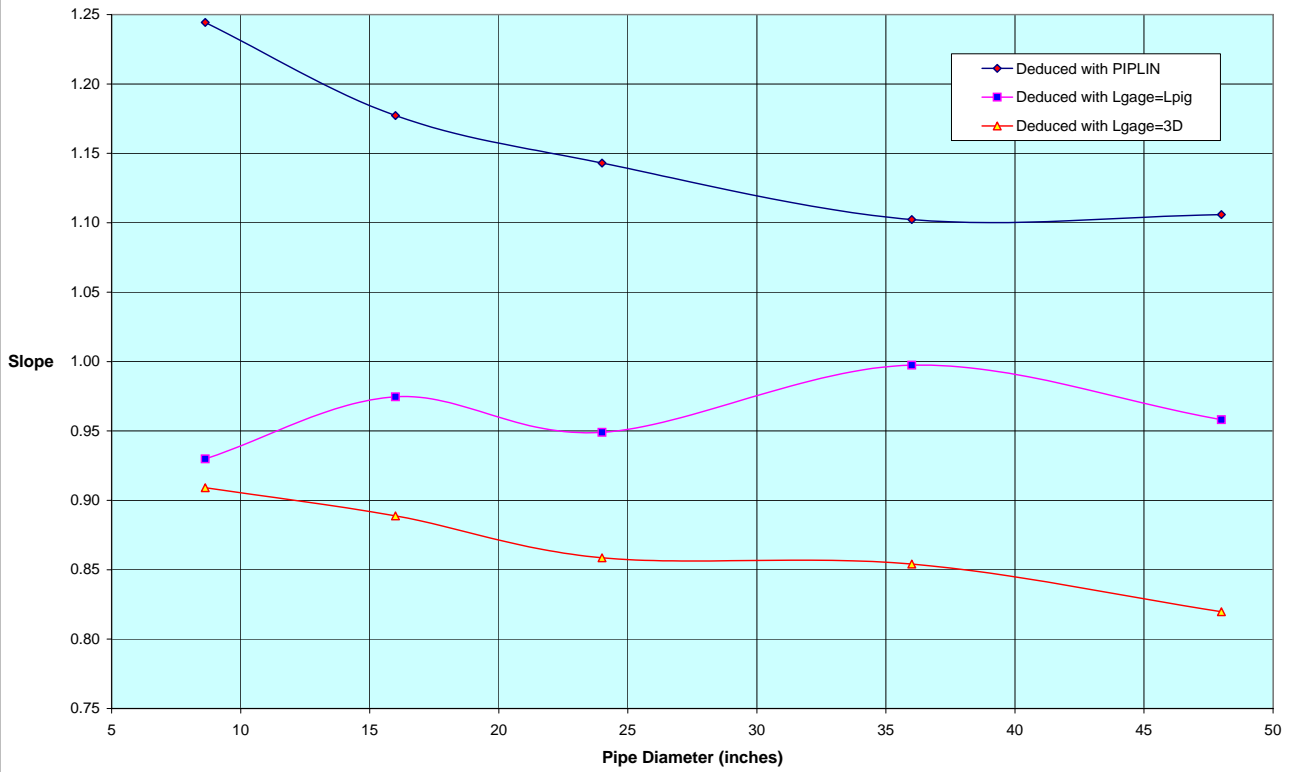


Figure 3.20 (b): Slope of Regression Line with Zero Intercept, State B

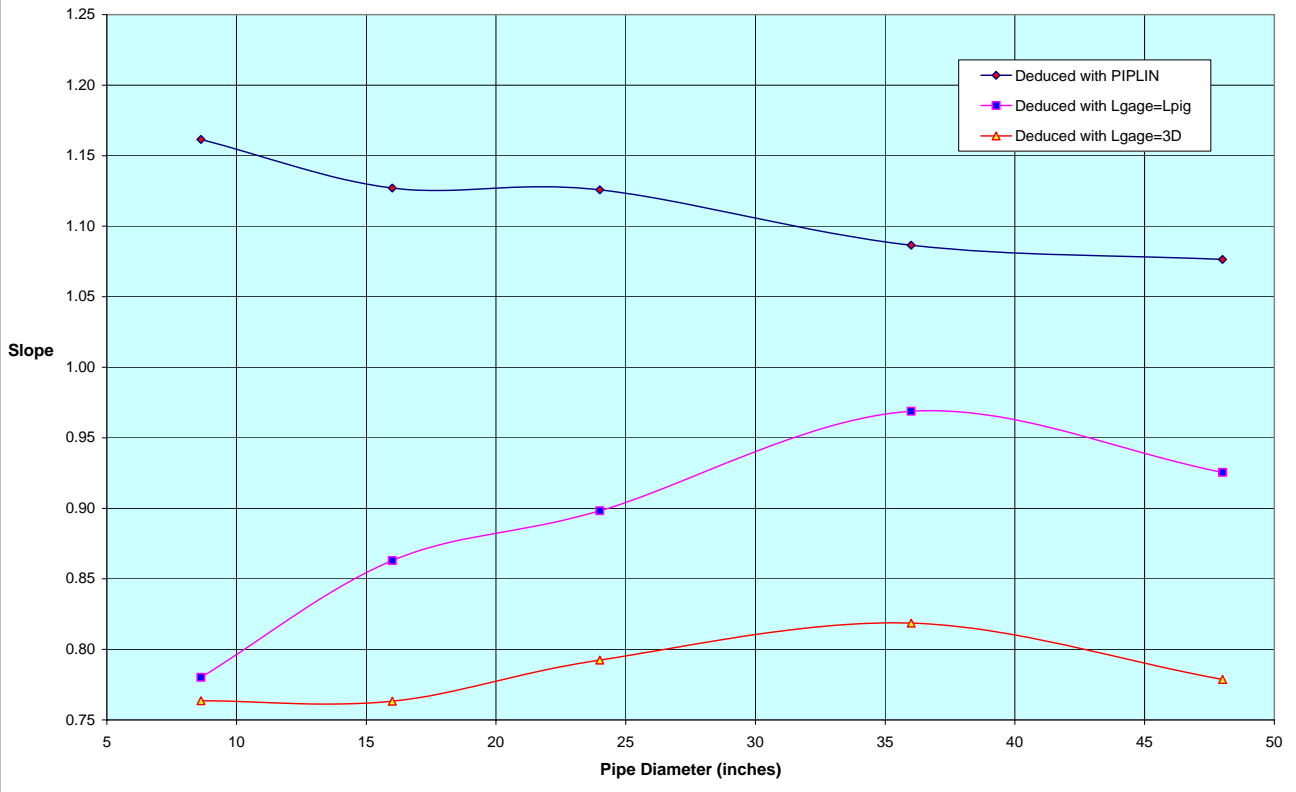


Figure 3.21: Feature Length vs. Pipe Diameter

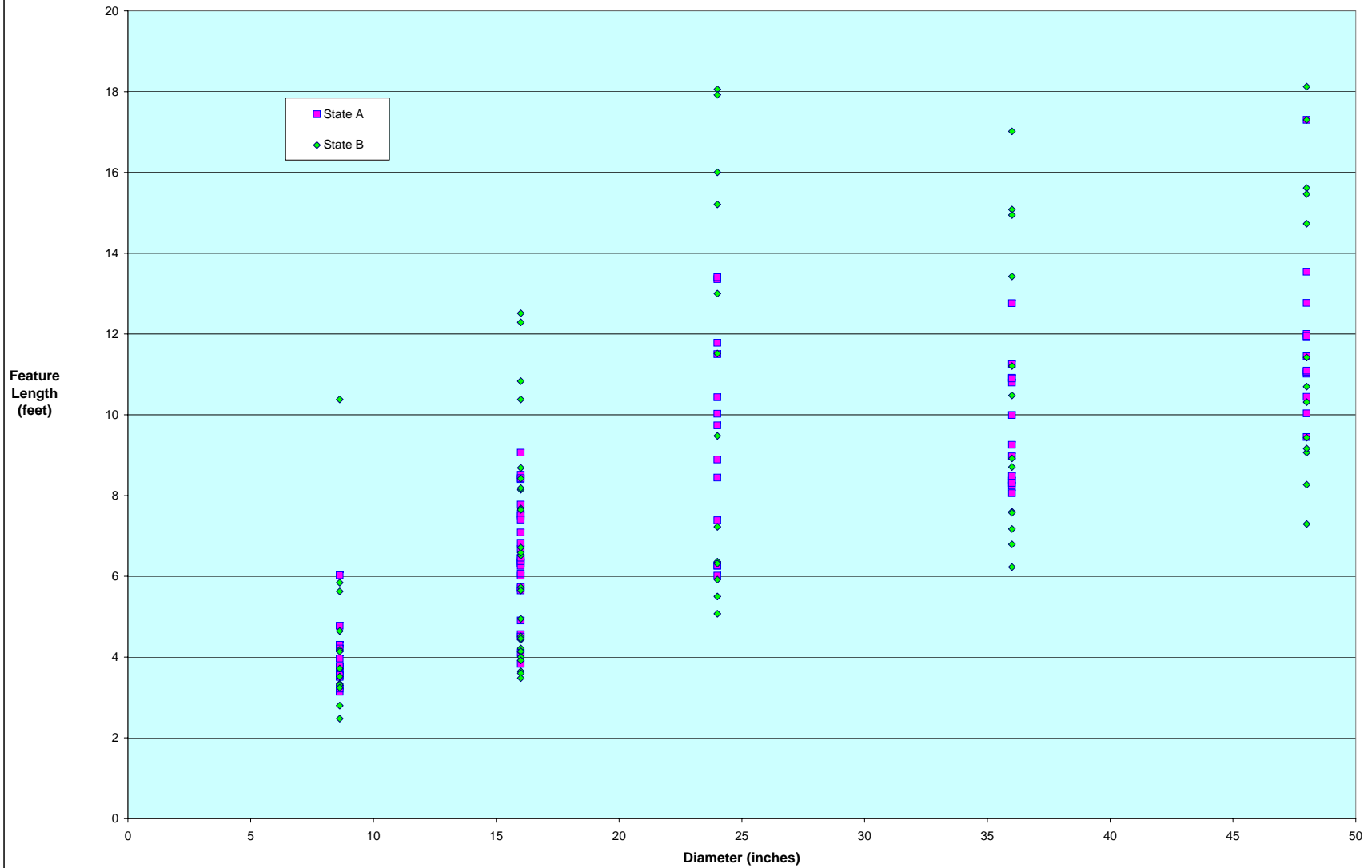


Figure 4.1 (a): Extensional Strain Profiles for State B: 9' of Right Lateral Fault Offset Beta=90 deg, D=16", 6' of Sand Cover

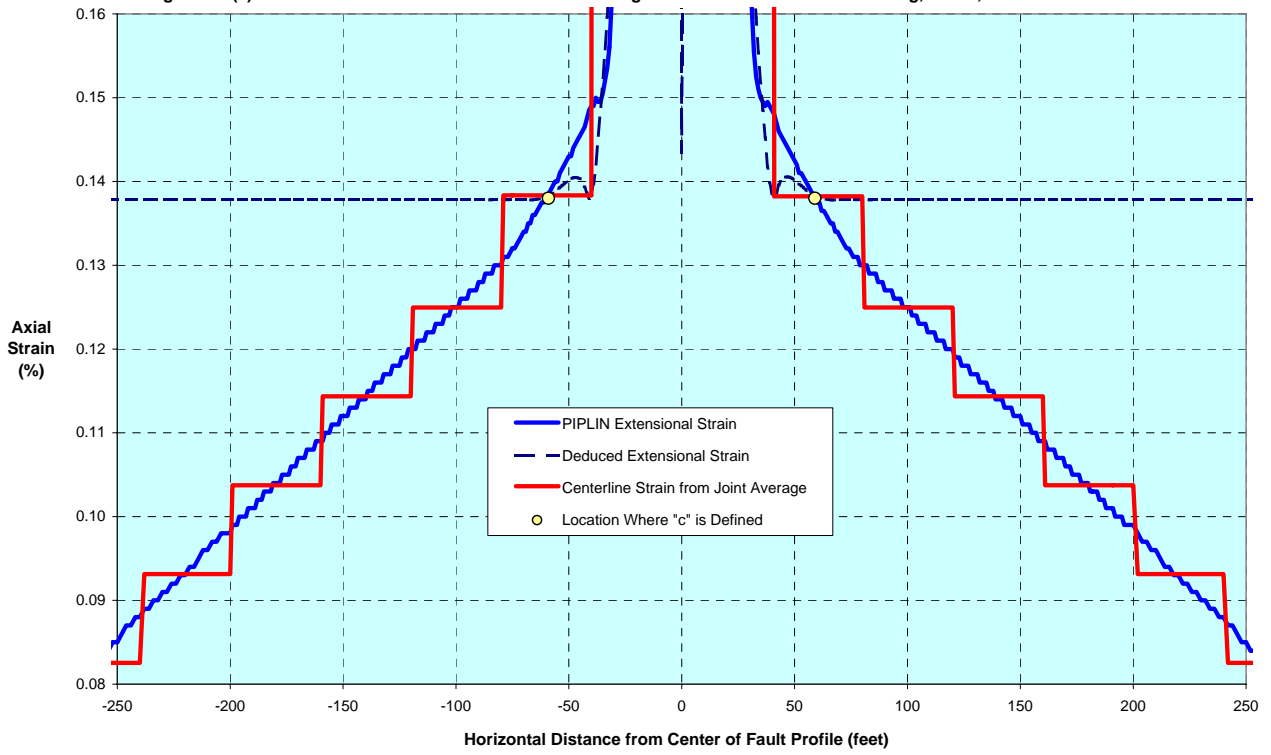


Figure 4.1 (b): Extensional Strain Profiles for State B: 9' of Right Lateral Fault Offset Beta=90 deg, D=16", 6' of Sand Cover

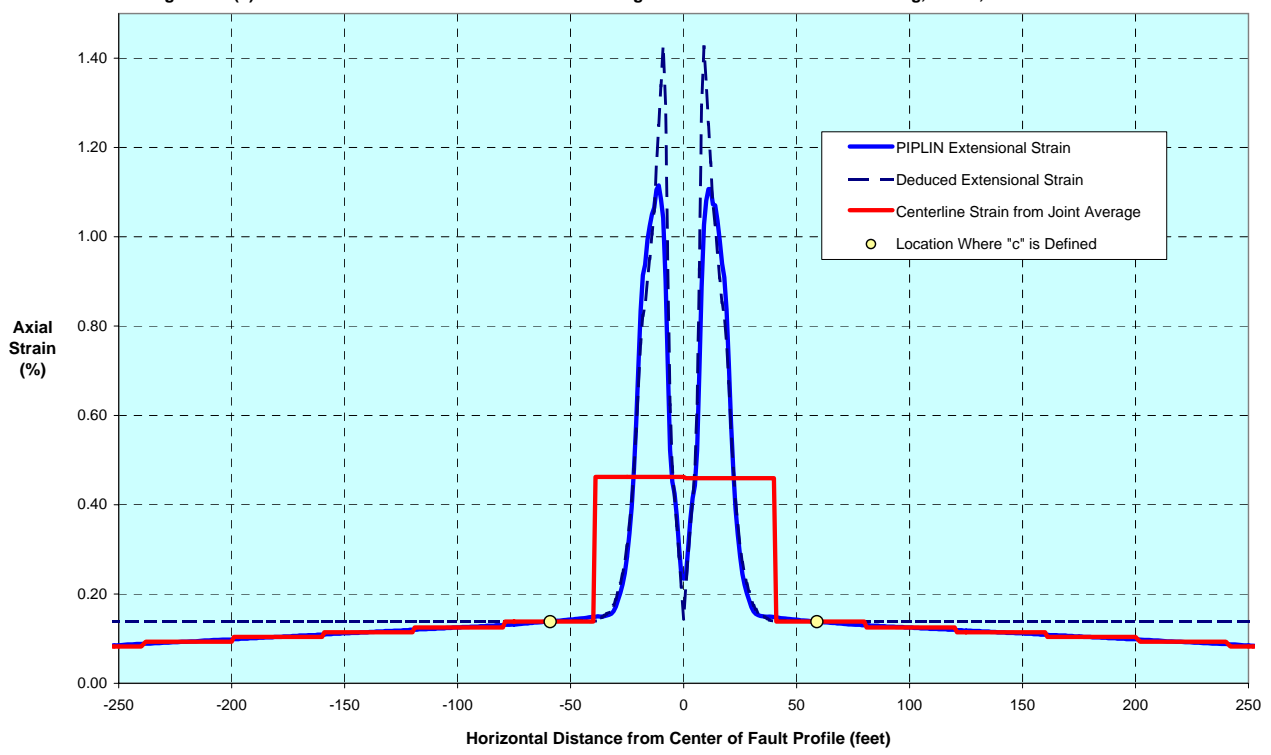


Figure 4.2 (a): 8-inch Pipe: Comparison of Governing Normalized Strains - State A

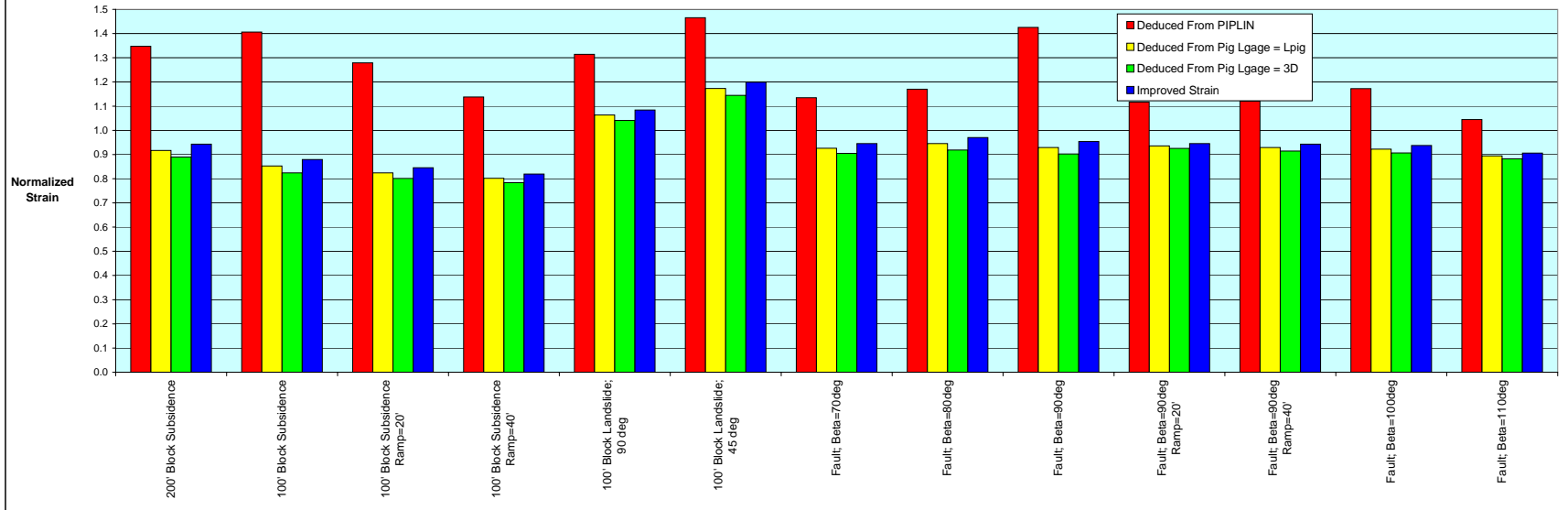


Figure 4.2 (b): 8-inch Pipe: Comparison of Governing Normalized Strains - State B

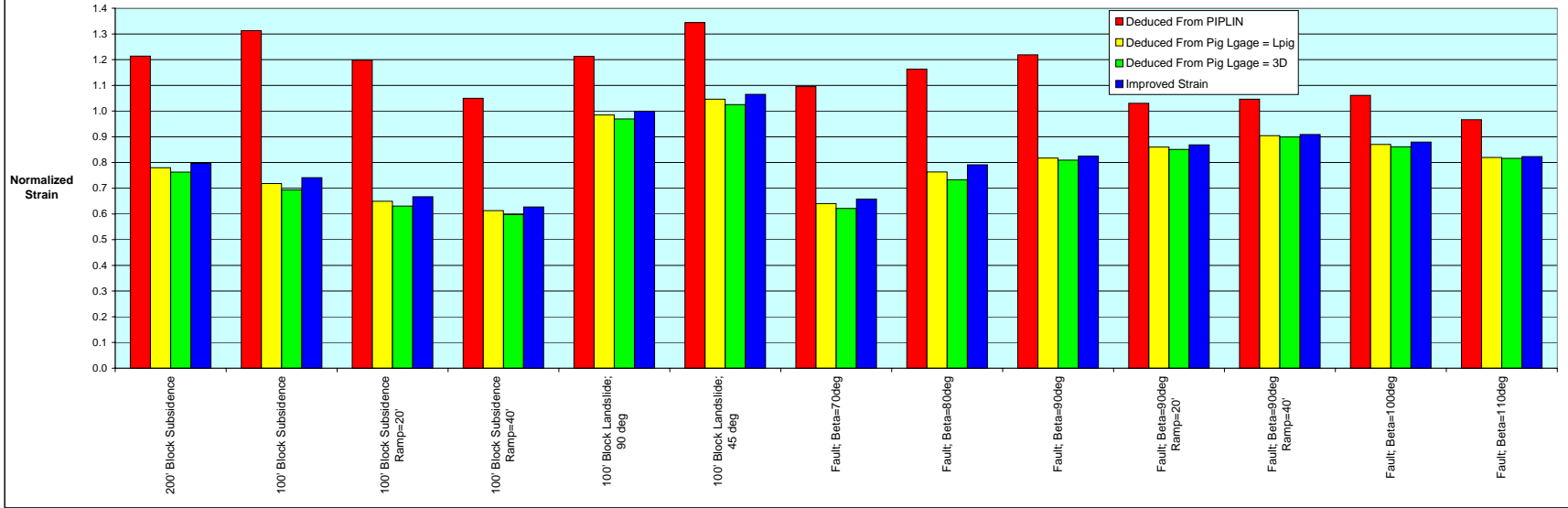


Figure 4.3 (a): 16-inch Pipe: Comparison of Governing Normalized Strains - State A

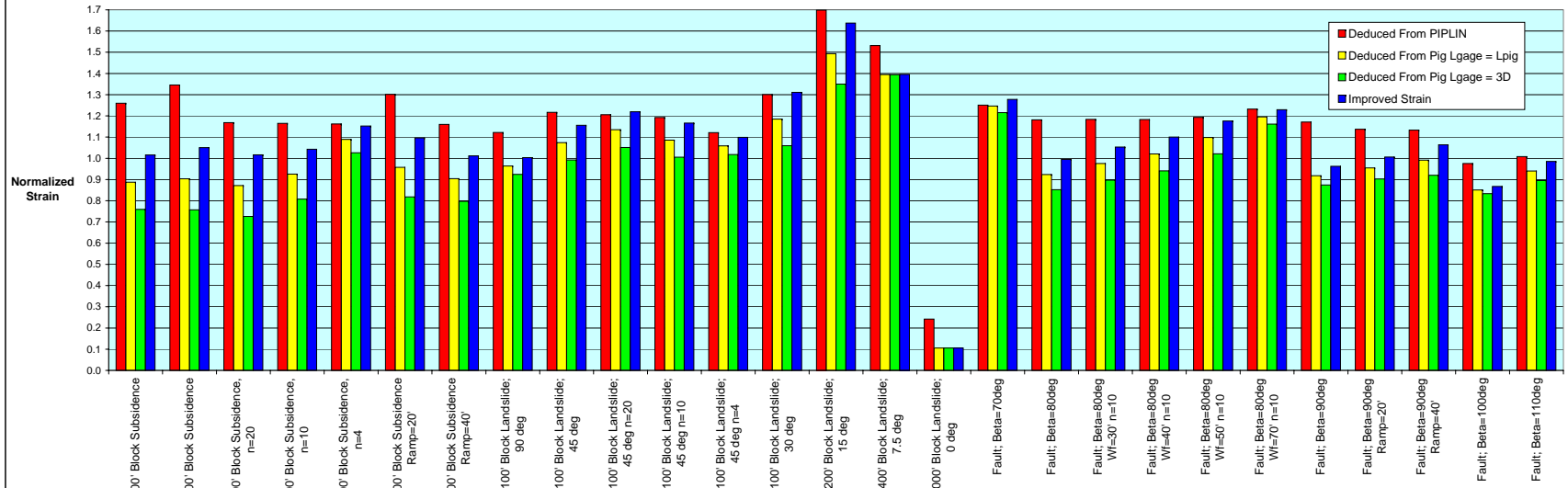


Figure 4.3 (b): 16-inch Pipe: Comparison of Governing Normalized Strains - State B

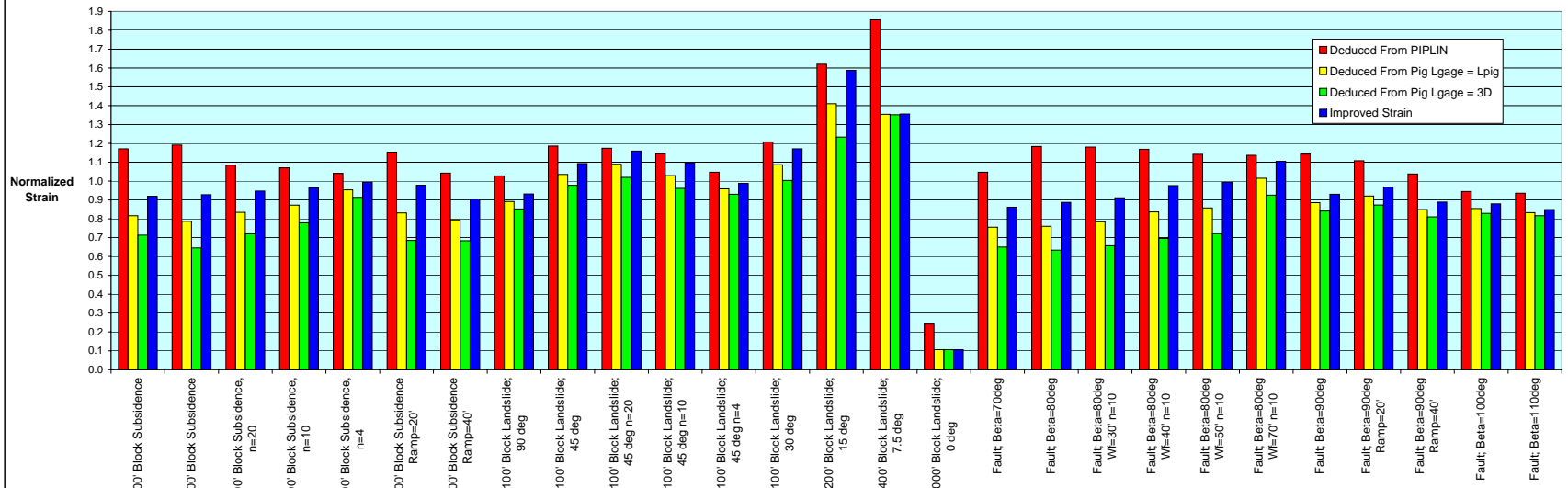


Figure 4.4 (a): 24-inch Pipe: Comparison of Governing Normalized Strains - State A

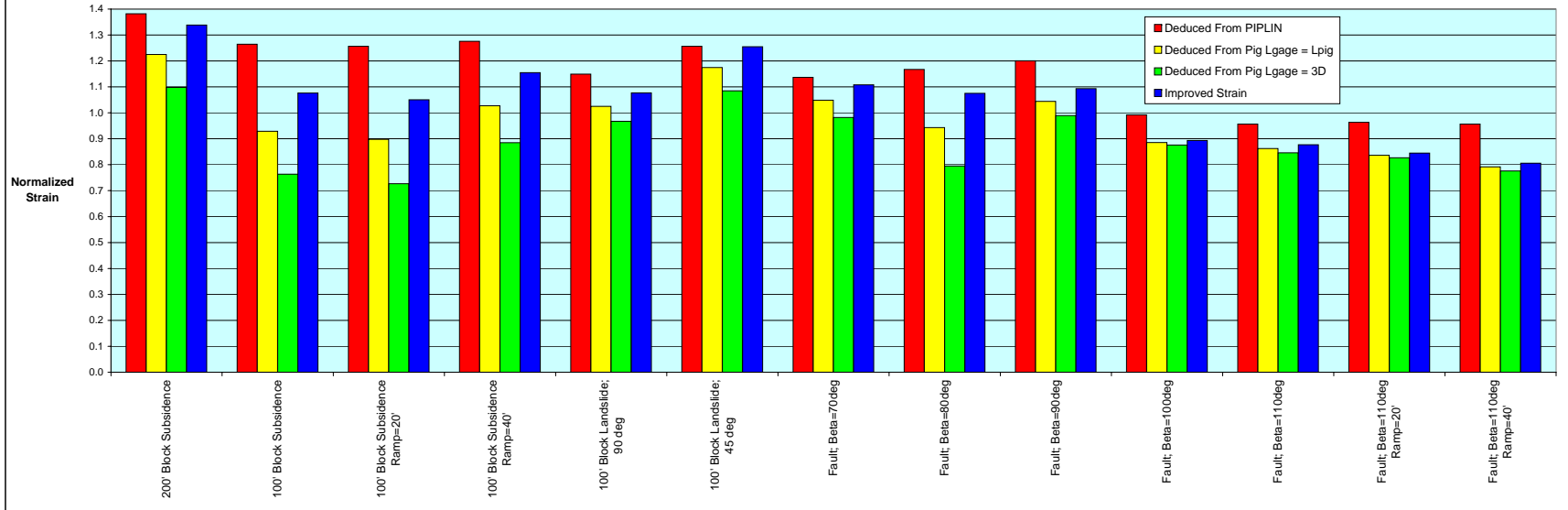


Figure 4.4 (b): 24-inch Pipe: Comparison of Governing Normalized Strains - State B

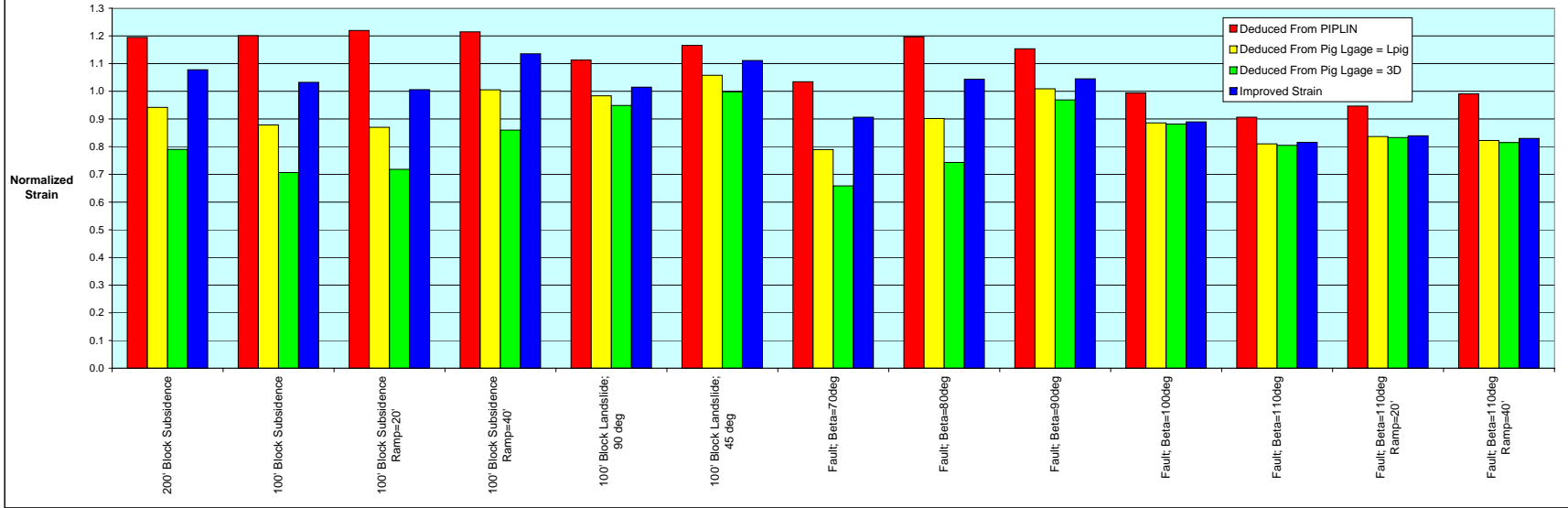


Figure 4.5 (a): 36-inch Pipe: Comparison of Governing Normalized Strains - State A

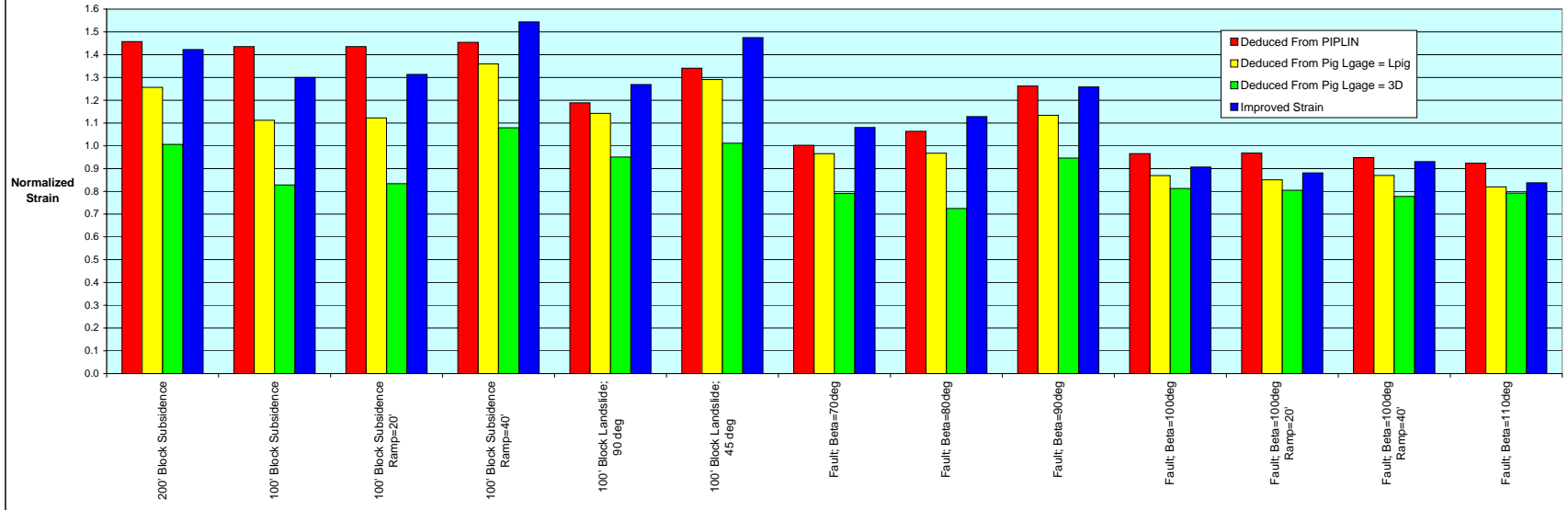


Figure 4.5 (b): 36-inch Pipe: Comparison of Governing Normalized Strains - State B

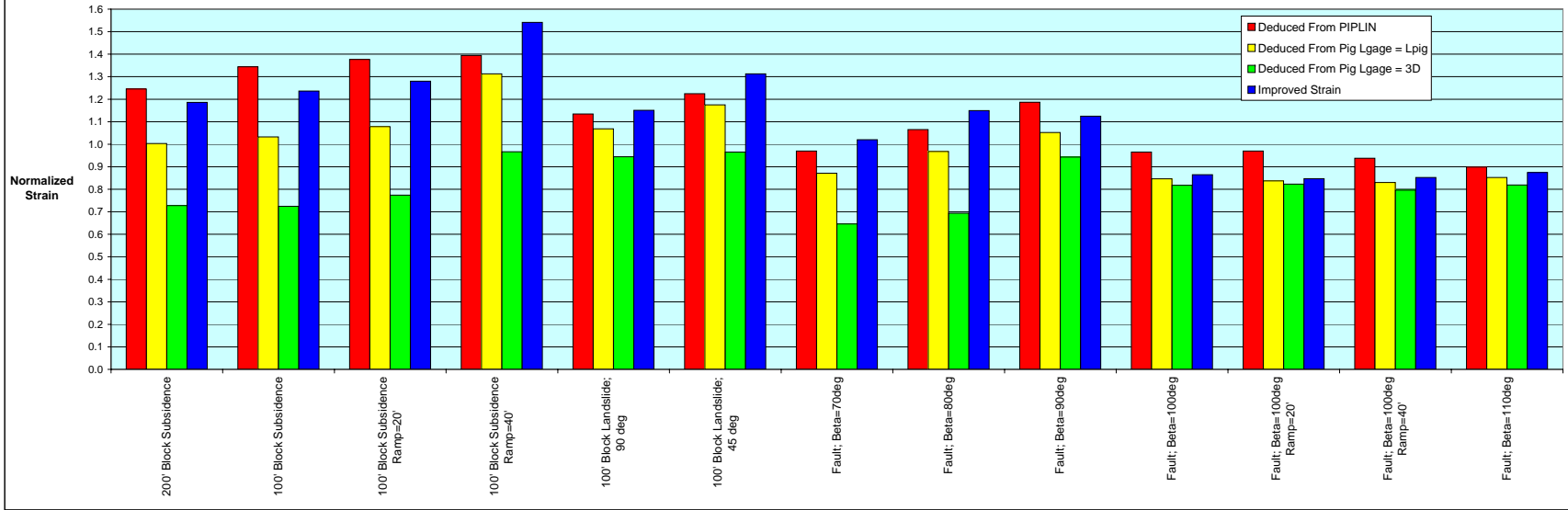


Figure 4.6 (a): 48-inch Pipe: Comparison of Governing Normalized Strains - State A

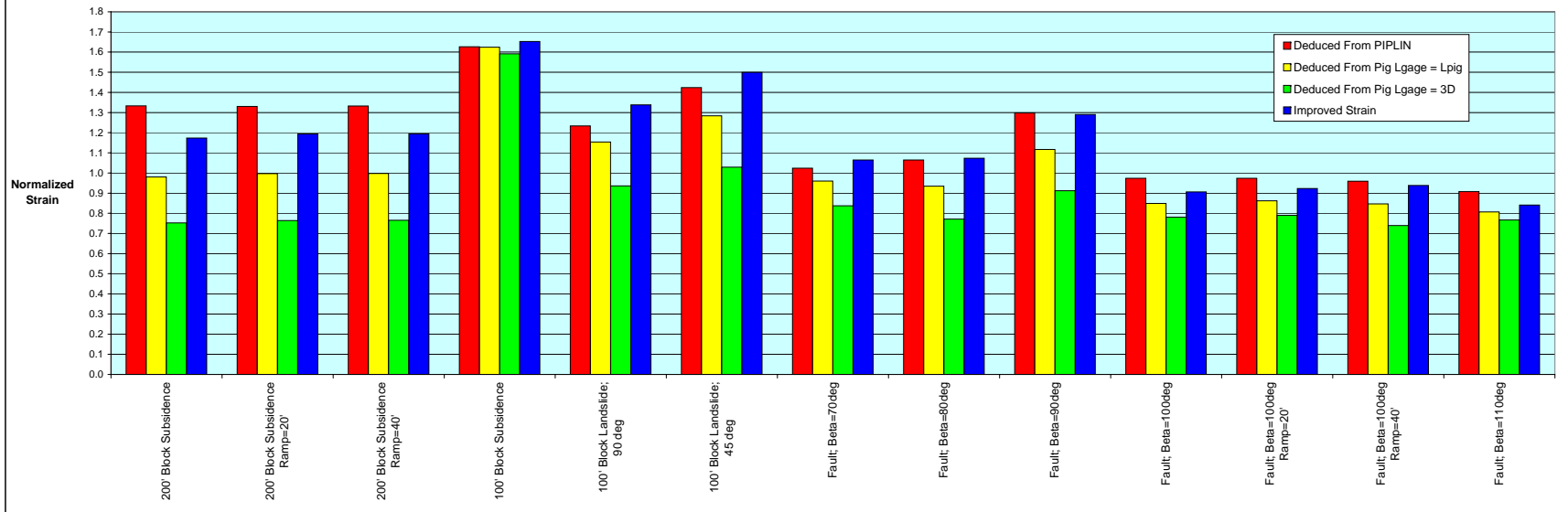


Figure 4.6 (b): 48-inch Pipe: Comparison of Governing Normalized Strains - State B

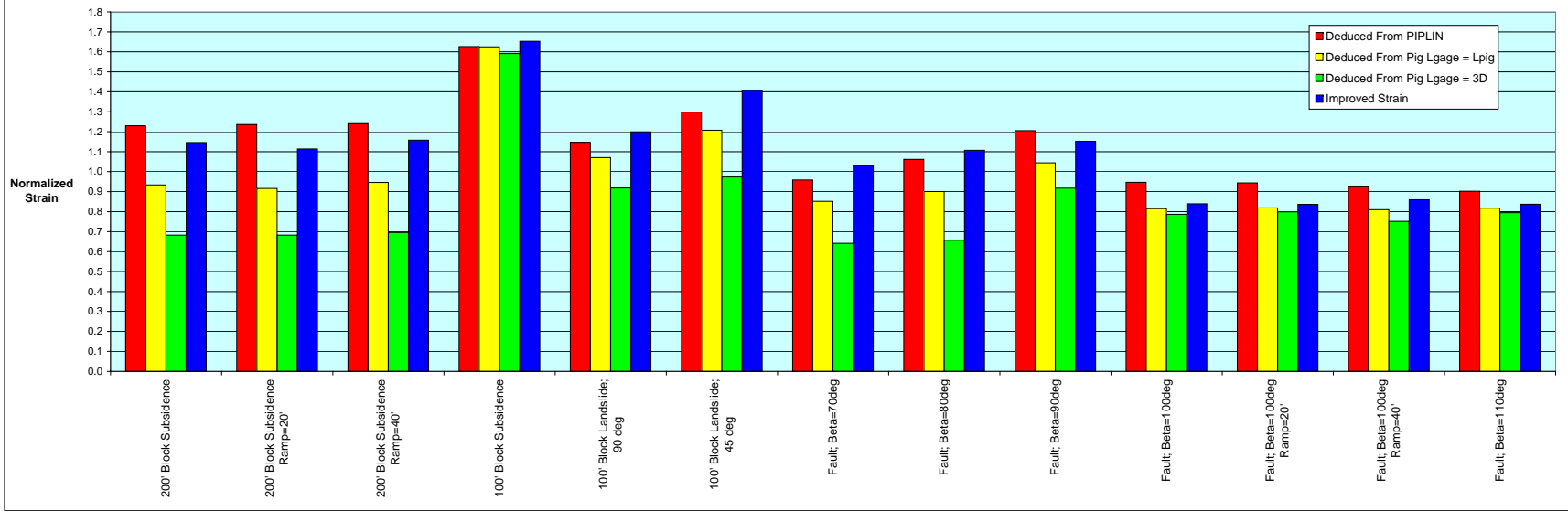


Figure 4.7 (a): Exact Strain Versus Improved Strain State A

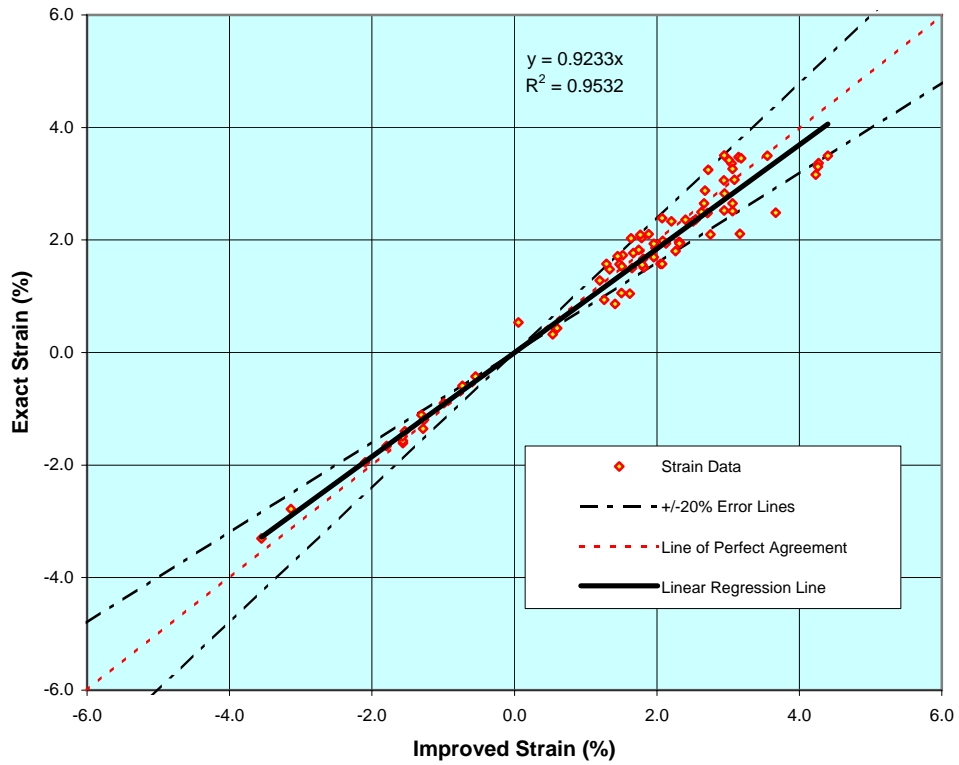


Figure 4.7 (b): Exact Strain Versus Improved Strain State B

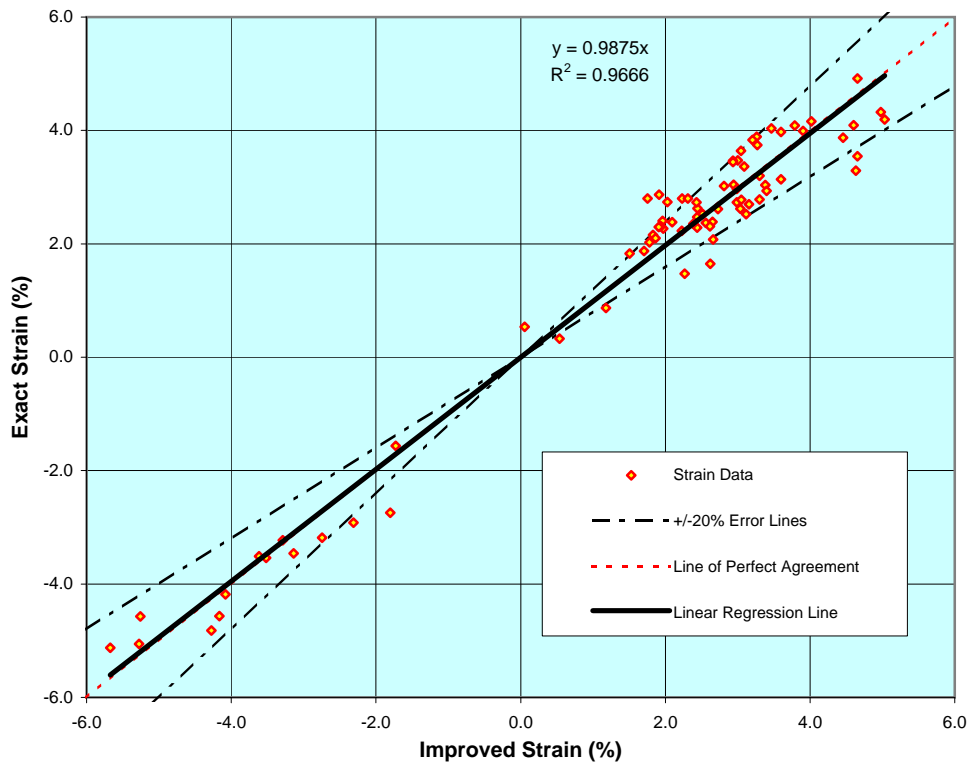


Figure 4.8 (a): Slope of Regression Line with Zero Intercept, State A

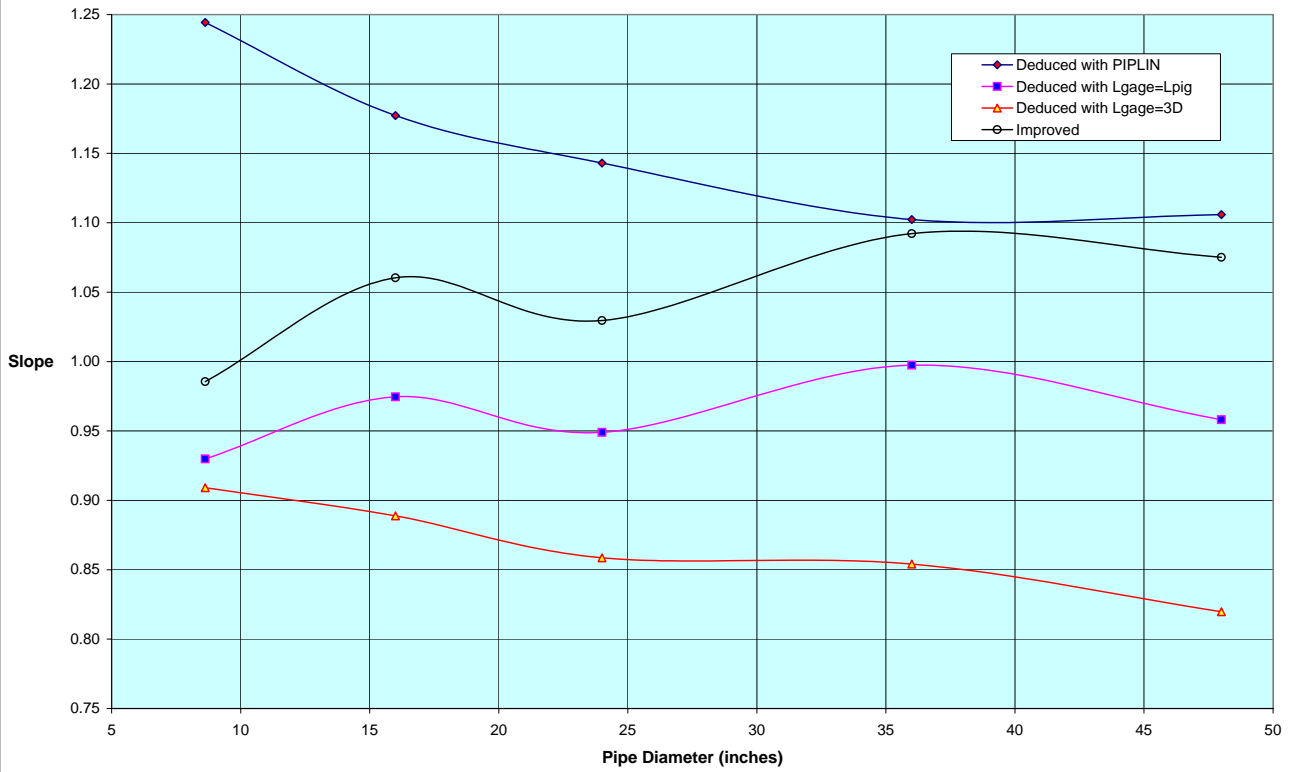


Figure 4.8 (b): Slope of Regression Line with Zero Intercept, State B

